
COMPUTATION OF MEDIAL SETS IN RIEMANNIAN MANIFOLDS

Von der Fakultät für Elektrotechnik und Informatik
der Gottfried Wilhelm Leibniz Universität Hannover
zur Erlangung des Grades eines

DOKTORS DER NATURWISSENSCHAFTEN

Dr. rer. nat.

genehmigte Dissertation von

Dipl.-Math. Henning Naß

geboren am 14. September 1975 in Wildeshausen

2007

Referent: Prof. Dr. Franz-Erich Wolter
Institut für Mensch-Maschine-Kommunikation
Gottfried Wilhelm Leibniz Universität Hannover

Koreferent: Dr.-Ing habil. Peter Milbradt
Institut für Bauinformatik
Gottfried Wilhelm Leibniz Universität Hannover

Tag der Promotion: 13. September 2007

Zusammenfassung

Die Riemannsche Geometrie ist ein klassisches Feld der Differentialgeometrie, das einige wesentliche Ideen für eine Verallgemeinerung des Cut-Locus-Konzepts beherbergt. Falls z.B. (M, d) eine Riemannsche Mannigfaltigkeit darstellt mit induzierter Metrik d , dann lautet eine mögliche Definition des Cut-Locus C_A einer Referenzmenge A folgendermaßen: C_A besteht aus dem Abschluß der Menge aller Punkte außerhalb A , wo die Distanzfunktion d_A nicht differenzierbar ist. Dieses Konzept des Cut Locus ist eng verwandt mit den Konzepten medialer Mengen.

Das vorliegende Dokument dient als Beitrag für berechnende Geometrien von medialen Mengen auf Riemannschen Mannigfaltigkeiten. Diese Arbeit setzt sich insoweit von bestehenden Arbeiten ab, als dass sie davon ausgeht, dass alle vorkommenden Objekte parametrisiert sind. Für die Berechnung von medialen Mengen werden wir im Wesentlichen mit den medialen Differentialgleichungen operieren, wobei es sich um ein gewöhnliches implizites Differentialgleichungssystem handelt. Ursprünglich wurde diese Idee schon in früheren Arbeiten benutzt. Allerdings bezogen sich diese Arbeiten auf Flächen der Dimension 2. Daher wird in dieser Arbeit ein großer Wert auf die Verallgemeinerung der entsprechenden Ergebnisse auf höher-dimensionale Mannigfaltigkeiten gelegt sowie auf verbesserte numerische Verfahren.

Die topologische Vielfalt von medialen Mengen kann hier nicht in vollem Umfang berücksichtigt werden. Vielmehr geht es in dieser Arbeit um die Betrachtung von Situationen, die in Anwendungen der realen Welt zum Tragen kommen. Einige der präsentierten Ideen stammen aus bestehenden Arbeiten, die sich mit dem Verhalten von medialen Mengen in euklidischen Räumen beschäftigen. Es gibt tatsächlich sehr viele Analogien zu diesem Fall.

Die wesentlichen Neuerungen im Vergleich zu bestehenden Arbeiten liegen hauptsächlich in der Entwicklung von Homotopieverfahren, mit denen es z.B. möglich ist das Problem der kürzesten Wege hinreichend genau zu lösen. Ebenso gehört auch der geodätische mediale Modellierer zu einer dieser Neuerungen, für dessen Implementation vor allem auf eine natürlichere Gestaltung von Freiformflächen Wert gelegt wurde. Die mediale Achse ist ein hervorragender Ansatz für die Parzellierung von dreidimensionalen Objekten, die dann z.B. für die Finite Elemente Simulationen benutzt werden können. Diese Arbeit enthält Beispiele für Berechnungen von medialen Flächen und von Voronoi-Diagrammen, um die theoretischen Grundlagen zu erhärten.

Keywords: Geodätische Mediale Achse, Mediale Differentialgleichungen, Geodätisches Voronoi-Diagramm

Abstract

Riemannian geometry is a classical field of differentiable geometry that provides some important ideas being useful for the generalisation of the cut locus concepts. If for example (M, d) is a Riemannian manifold with the induced intrinsic metric d , then the definition of the cut locus C_A of a reference set A could be as follows: The cut locus C_A is the closure of all points in $M \setminus A$ where the distance function d_A is not differentiable. This definition is equivalent to some other definitions that will be explained throughout this thesis.

The present document serves as a contribution to the computational geometry of medial sets and the cut locus in Riemannian manifolds. This approach is mainly based on the fact that every occurring object is given in parametric representation which provides the reason why this work differs heavily from existing works. For the computation of medial sets we will employ the so called medial differential equations which is a linear system of implicit ordinary differential equations. Originally this idea was already presented in earlier works in case of two-dimensional Riemannian manifolds. Therefore, this work mainly focuses on the generalisation of the aforementioned concepts to the higher dimensional cases and an improved numerical analysis.

The topological variety of medial sets can not be discussed here to the full extent since this would go beyond the scope of this thesis. This work is rather interested in situations that are typical in the context of real world applications. Some of the ideas presented refer to existing works that treat the behaviour of medial sets in Euclidean spaces and in fact there are many analogies to this case.

The essential innovation of this work in comparison to other works lies mainly in the development of homotopy methods that make it possible to accurately solve the shortest join problem on hypersurfaces. In addition, the geodesic modeller was one of the improvements of this work that differs from other modelling tools by the fact that the construction of freeform surface has become more natural. The medial axis of solids is a powerful approach for the construction of tessellations that can be used for example as a coarse grid in Finite Element applications. This thesis includes some examples of computations of medial surfaces and of Voronoi diagrams to illuminate the obtained results.

Keywords: Geodesic Medial Axis, Geodesic Voronoi Diagram, Medial Differential Equations

Acknowledgements

The present document is a product of studies over the past three years at the Gottfried Wilhelm Leibniz Universität Hannover. At the beginning of that time I applied for a scholarship at the Graduiertenkolleg 615. Prof. Dr. E. Stephan being the speaker of the Graduiertenkolleg 615 admitted me as a member of the Graduiertenkolleg. I acknowledge him for the chance of having that membership. I would also like to thank my adviser Prof. Wolter for inviting me to join the Graduiertenkolleg and for his willingness to support me and to give me helpful advice in every respect. Prof. Wolter made arrangements that I obtained an invitation to a research visit at MIT in Summer 06 where I could pursue research of my thesis project leading to substantial results in a creative and stimulating environment. I acknowledge Tobias Pick who accompanied me for his open ears and his assistance with regard to the organisational problems that arose at the beginning of that trip. I acknowledge my co-adviser PD Dr.-Ing. habil. Peter Milbradt for revising my thesis and his help to accomplish this work.

I would like to thank the whole Welfenlab research group for the support and especially Cem Doğan and Hannes Thielhelm for accomplishing their master thesis and diploma thesis under my supervision. This work would not have been possible without them. I thank Prof. Wolter for revising my thesis.

I acknowledge my family and especially my mother, my brother and my sister-in-law for supporting me all along. Although they could not support me in technical terms they kept me grounded in times when my progress with this thesis was slow. I thank my girlfriend Andrea Hohnhorst for her frankness and her patience she has exercised during that time. Finally, I would like to acknowledge Henrik Löhren for revising the final version of my PhD thesis.

Henning Naß, Hannover, August 2007

Contents

| | | |
|----------|---|-----------|
| 1 | Introduction | 3 |
| 2 | Preliminaries | 8 |
| 2.1 | A First Example | 8 |
| 2.2 | Central Difference Quotients | 11 |
| 2.3 | Boundary Value Problems | 16 |
| 2.4 | Homotopy Methods | 19 |
| 2.4.1 | Bifurcation Theory | 21 |
| 3 | Elements Of Differential Geometry | 23 |
| 3.1 | Manifolds | 23 |
| 3.2 | Riemannian Geometry | 24 |
| 3.2.1 | The Curvature Tensor | 31 |
| 3.2.2 | Jacobi Fields | 31 |
| 3.3 | The Notion Of Tubes And Fermi Coordinates | 32 |
| 3.4 | Applications | 34 |
| 4 | Offsets And Offset Functions | 36 |
| 4.1 | Difference Between Offsets And Offset Functions | 36 |
| 4.2 | Offsets On 2-dimensional Manifolds | 37 |
| 4.2.1 | Point Offsets | 37 |
| 4.2.2 | Offsets of Curves | 38 |
| 4.3 | Offsets On 3-dimensional Manifolds | 40 |
| 4.3.1 | Offsets of Points | 40 |
| 4.3.2 | Offsets of Curves | 40 |
| 4.3.3 | Offsets of Surfaces | 41 |
| 4.4 | Focal Sets | 42 |
| 4.4.1 | Curvature Computations Of Euclidean Tubes | 44 |
| 4.4.2 | Equations Of Riccati Type | 46 |
| 4.4.3 | Computation Of Focal Sets | 47 |
| 4.5 | Approximation Of Offset Functions | 49 |
| 5 | Medial Axis Inverse Transformation | 50 |
| 5.1 | 2D Medial Axis Inverse Transform | 53 |
| 5.1.1 | Geodesic Curvature Computation Of Envelope Points | 55 |
| 5.2 | 3D Medial Axis Inverse Transform | 57 |
| 5.2.1 | The Set A_1 | 58 |

| | | |
|----------|---|------------|
| 5.2.2 | The Set A_2 | 59 |
| 5.2.3 | The Set A_3 | 60 |
| 5.2.4 | A Proper Reconstruction Scheme | 61 |
| 5.3 | The Geodesic Medial Modeller | 61 |
| 6 | Medial Axis Transformation | 63 |
| 6.1 | Basics | 64 |
| 6.2 | Medial Differential Equations | 66 |
| 6.3 | Initial Values Of The Medial Differential Equations | 71 |
| 6.3.1 | Convex Homotopy Method | 71 |
| 6.3.2 | Nelder-Mead Method | 74 |
| 6.4 | Example | 75 |
| 7 | Geodesic Voronoi Diagrams | 77 |
| 7.1 | Definition Of Voronoi Diagrams And Examples | 78 |
| 7.2 | Properties Of Geodesic Voronoi Diagrams | 80 |
| 7.3 | Geometric Transformation | 84 |
| 7.4 | Minimal Joins | 86 |
| 7.4.1 | The Curve-Tracking-Method | 86 |
| 7.4.2 | The Method Of Single Coordinate Charts | 88 |
| 7.4.3 | The Implicit Method | 92 |
| 7.4.4 | Remarks On Singular Points | 94 |
| 7.5 | Distance Spheres, Voronoi Edges And Bisectors | 96 |
| 7.6 | Randomised Incremental Construction Of Voronoi Diagrams | 100 |
| 7.6.1 | The Algorithm | 101 |
| 7.7 | Examples | 105 |
| 8 | Outlook | 108 |
| | List of Tables | 111 |
| | List of Figures | 112 |
| | Index | 117 |

1 Introduction

Since the works of Harry Blum in the late sixties and the early seventies of the last century the medial axis has been subject of research in the scientific community of computational geometry. From that time on diverse strategies have been developed that are useful for a better understanding of the medial axis transform and the medial axis inverse transform. The big variety of approaches cannot be discussed to the full extent, but in short it can be stated that for discrete geometric models there have been established techniques stemming from major research projects pursued by many researchers in computational geometry. The **Power Crust algorithm** may be regarded as an important tool resulting from the aforementioned research. For the planar case it can be described as follows:

Consider a subset Ω of \mathbb{R}^2 with smooth boundary curve

$$\alpha : \begin{cases} [0, 2\pi] & \rightarrow \mathbb{R}^2 \\ t & \mapsto \alpha(t) \end{cases} .$$

The discrete point set $S = \{\alpha(t_0), \dots, \alpha(t_N)\}$, where $0 = t_0 < t_1 < \dots < t_N = 2\pi$, can be used to approximate the boundary curve α . Referring to figure 1.1 the points $\alpha(t_i)$ are labelled in black, whereas α is indicated in blue colour. Define for example the curve

$$\beta(t) = \begin{cases} [0, 2\pi] & \rightarrow \mathbb{R}^2 \\ t & \mapsto \beta(t) \end{cases} ,$$

as approximation for α where

$$\beta(t) = \alpha(t_i) + \frac{t - t_i}{t_{i+1} - t_i}(\alpha(t_{i+1}) - \alpha(t_i))$$

for $t_i \leq t < t_{i+1}$. β is a piecewise linear function that interpolates α in the given point set S . An approximation of the medial axis being defined as the **closure of all centres of maximal inscribed discs of Ω** can be achieved with reasonable effort:

Consider the Voronoi diagram of the points in S . In fact, only a subset of the Voronoi vertices (red points) that we will call **poles** will approximate the medial axis. Assign to every pole its corresponding **polar radius** $r^2(p)$, that is

$$r(p) = \sup\{r \geq 0; B(p, r) \cap S = \emptyset\}.$$

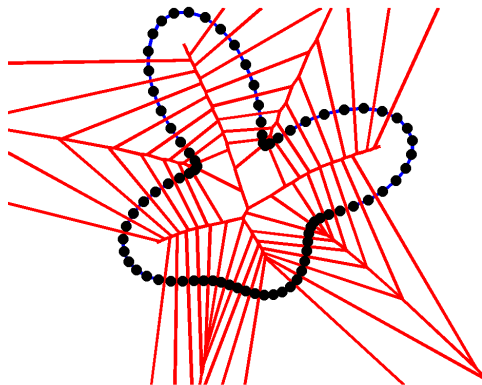


Figure 1.1: Power Crust Algorithm

Finally, we need the **power diagram** of the poles. This is a kind of Voronoi diagram with the significant difference that the distance to a pole p is not measured with the Euclidean metric but with the metric

$$d_{\text{pow}}(x, p) = d_{\text{Eucl.}}^2(x, p) - r^2(p).$$

Only those cells will be taken into account that are inside the domain Ω and the boundary of the union of those cells is called power crust. Note that in figure 1.1 only those Voronoi regions with finite area are shown.

The last example already contains a definition of the medial axis. This definition makes sense in a generalised context. Let for example (M, d) be a metric space. A ball B is a subset of M such that there exists $p \in M$ and $r > 0$ with

$$B = B(p, r) = \{x \in M; d(x, p) \leq r\}.$$

The medial axis of a set is defined to be the closure of all centres of maximal inscribed balls. This definition coincides with the definition of the medial axis in the Euclidean space.

From the point of view of Computer Graphics, Engineering, Physics etc. it is usually not necessary to think of such abstract metrics. A short example will explain that it is quite natural to treat such abstract metric spaces and that there exists an infinite number of such spaces.

Example 1.0.1

The medial axis $MA(\Omega)$ of a compact set $\Omega \subset \mathbb{R}^2$ with respect to the Euclidean metric can be seen as the limit set of a family of sets P^t , $t \geq 0$, which all share the same property. Every P^t constitutes a medial set of Ω with respect to a dedicated metric d^t . Consider a sphere M^t with centre $(0, 0, \frac{t}{2})$ and radius t . M^t together with the metric d^t that measures the distance of points on the sphere as the length of the minimal join

between these points is a metric space. We will use the stereographic projection ϕ^t that identifies points in the Euclidean plane with points on the sphere M^t . One can apply the definition of the medial axis in this special situation for the set $\phi^t(\Omega) = \Omega^t$ and the space (M^t, d^t) . Let then $MA^t(\Omega)$ be the medial axis of Ω^t on the sphere M^t . Reprojection of the sets $MA^t(\Omega)$ will lead to sets

$$P^t = (\phi^t)^{-1}(MA^t(\Omega))$$

that converge to $MA(\Omega)$, if t tends to infinity.

The main goal of this thesis is to take up the challenging task to present concepts showing that in any Riemannian 3-Space M the computation of the geodesic medial axis transform and Voronoi diagram respectively of a solid S and some sites $\{p_1, \dots, p_n\}$ respectively, that has been resistant so far against computational attempts, is feasible. We also show that it is possible to introduce a natural inverse of the medial axis transform of a solid by constructing for a given medial axis transform in Riemannian 3-Space the boundary of a solid. According to our knowledge all these computational endeavours appear to be completely new. We believe that this thesis will open up new avenues of research as we can demonstrate that even with moderate computing power geodesic medial axis and geodesic Voronoi diagrams computation become feasible in higher dimensional Riemannian spaces.

Some of the tools needed for the reliable and accurate computations of medial sets will be presented in the **Preliminary** section of this thesis. At first glance the introduction of central difference quotients does not appear to be completely new. This is true, but it will be helpful for a rapid computation of both the medial axis and the Voronoi diagram. We also present a scheme that allows us to compute the coefficients of the central difference quotients immediately with some restrictions with respect to the order of the scheme. The coefficient vector $c = (c_1, \dots, c_N)$ fulfils a linear equation system

$$A \cdot c = b,$$

where A is a $N \times N$ -matrix. In case one wants to involve a large number of function values for the computation of central difference quotients the condition number $\text{cond}(A)$ of A tends to infinity. A short note on the central difference quotients for multivariate functions finishes that section.

Some notes on boundary value problems (BVPs) and homotopy methods conclude the chapter. Homotopy methods become for example important when geodesic joins of two points p and q on a Riemannian manifold are required. The general form of such two point boundary value problems can be stated as follows:

$$\begin{aligned} y''(t) &= f(t, y(t), y'(t)), \\ y(0) &= A, \\ y(1) &= B. \end{aligned}$$

Only in few cases it is possible to find an analytical solution of such problems. If for example $f \equiv 0$ then

$$y(t) = A + t(B - A)$$

constitutes a solution of the aforementioned system. Convex homotopy methods treat the class of BVPs of the form

$$y''(t, \lambda) = \lambda f(t, y(t, \lambda), y'(t, \lambda)),$$

assuming that λ is a real number. The major goal is now to numerically approximate a differentiable function $G(\lambda)$ such that $y'(0, \lambda) = G(\lambda)$ and $y(1, \lambda) = B$ holds. We will explain this approach by the classical Sturm-Liouville problem.

In the section **Elements Of Differential Geometry** some classical and non classical aspects of modern differential geometry will be explained and we shall discuss the question why these aspects need to be referred to in the context of medial sets in Riemannian manifolds. Not only the general ideas behind Riemannian geometry but also the foundations of variations of vector fields will be presented in the course of this section. The geodesic equations and the Jacobi equations will be two important results. Further, it seems to be convenient to introduce the ideas of tubes and related concepts, which will be a natural generalisation of the geodesic normal coordinates. The normal coordinates give a natural reparametrisation of a given manifold M as they use the exponential function for its representation. According to the aforementioned reparametrisation the Fermi coordinates introduce an alternative reparametrisation from the point of view of a given submanifold $\bar{M} \subset M$. This reparametrisation heavily involves the normal space of this submanifold with respect to M . A tube can be seen as an adequate generalisation of parallel vector spaces in that way, that if \bar{M} is a submanifold of M , then the tube $S = T(\bar{M}, s)$, $s \in \mathbb{R}$, is the submanifold of M only consisting of points with distance s to the set \bar{M} . We will derive an equation of Riccati type that allows us to find the principal curvature values of tubes, which may be important for the medial axis inverse transform.

The offset function as stated in the section **Offsets And Offset Functions** describes the relation between the original parametrisation f of a manifold M and its reparametrisation employing Fermi coordinates. It turns out that this relation can be expressed in terms of a differential equation system, the geodesic differential equations. However this concept has the important disadvantage that the flux of Fermi coordinates can not be obtained numerically without reasonable endeavours. We will give examples for the computation of the Fermi coordinates and offset functions for dimensions two and three for points, curves and surfaces. They will be required for the reconstruction of solids for a given medial axis transform.

One application of the reconstruction theorem is the **Geodesic Medial Modeller** (GMM), a project that arose during the Master Thesis of Cem Doğan, a graduate student of the Welfenlab. We believe that this modelling system enables the user to overcome some frequent deficiencies in standard modelling tools. An alternative field

of applications is that the GMM can be seen as an interface between haptical input devices and a personal computer. All this is discussed in section 5.

The emphasis of this thesis lies in the determination of medial sets in Riemannian manifolds and in particular the medial axis transform of a solid and the geodesic Voronoi diagram in Riemannian 3-Space. Crucial for the implementation of the so called medial differential equations is that their initial values are a priori unknown. We will explain a homotopy method that makes it possible to find such initial values without employing standard Newton methods or related methods since they have the essential disadvantage that they lack a good initial approximation of the solution. The computation of the Voronoi diagram can be heavily simplified, if the topology of the Voronoi diagrams (which are also called Dirichlet fundamental polygons in the literature) complies with only few requirements. It can be shown that the construction of the geodesic Voronoi diagram can be achieved in expected time complexity $O(n^2)$, where n denotes the number of sites. The foundations of the shortest joins represent the central result within this section, since it is required for the construction of the generalised circumspheres that are strongly related to the Euclidean circumspheres.

Some global remarks on the shape of Voronoi diagram and medial sets will be stated as well. The classification of the topology of the 3D medial axis that has been investigated by Giblin and Kimia for the Euclidean case is generalised. They laid the most stress on the consideration of lines where the inscribed spheres are tritangent to the boundary of the solid. But also the classification of the boundary curves of the outer medial axis patches appears to be important. The corresponding results are presented in the section **Medial Axis Transform** and **Medial Axis Inverse Transform**.

The **Outlook** finishes this thesis and proposes some ideas that have not been implemented during this work. In particular the systematic meshing of the faces of the Voronoi cells and the patches of the medial axis have to be mentioned using the concepts of the 2D medial axis that have been subject of earlier works at the Welfenlab (see [TR99] for more details).

2 Preliminaries

Accurate medial axis computations require some advanced and powerful tools. We will therefore deal with some important results that can be derived from

1. Differential Geometry
2. Ordinary Differential Equations
3. Numerical Analysis

Some essential concepts of ordinary differential equations will be discussed in this section. A homotopy method for solving boundary value problems will be introduced in the context of Sturm-Liouville problems.

Scientific computing not only deals with the question of how problems can be modelled but how they can be solved efficiently. The **Finite Element Method** that was introduced first in 1915 by Galerkin is one of the most universal techniques in that discipline. It can be used to solve hyperbolic, parabolic and elliptic partial differential equations and is very often applied in situations where an exact solution is a priori unknown. A famous substitute of these classes of problems is for example the computation of viscous flow over an air vehicle for subsonic, transonic or supersonic flow. Often some very unnatural constraints are introduced to simplify these problems. For real world problems there rarely exist analytical solutions that can be expressed directly by elementary functions. This holds even in case the problems are simplified and it holds not only for PDEs and for ODEs but also for algebraic equations.

Another approach is often used in the field of **Finite Difference Methods** or **Finite Volume Methods** as a time and space discretisation scheme, the latter involving unstructured grids. It is known as the Method of Central Difference Quotients and can only be applied to functions whose derivatives exist to the specified order k .

2.1 A First Example

Consider again example 1.0.1 from the introduction. From various aspects it is not advisable to compute the Euclidean medial axis as a limit set of a sequence of sets since the latter are even harder to obtain. This was not the intention of the introductory example. It was rather the aim of the author to show that many of the problems that arise in the context of Computational Geometry can be viewed from different

perspectives. The limits of modern numerical methods are often characterised by the fact that they have weak requirements. Yet, certain approaches often lead to static formulations that neglect additional information about the problem. The following example shows that sophisticated approaches often have the disadvantage that the formulation of the underlying equations is difficult to obtain. It is one of the central aspects of this thesis to become acquainted with such formulations in the context of the medial axis transform.

Let $r : \mathbb{R} \rightarrow \mathbb{R}$ be a smooth, positive and periodic function with period 2π and $r(0) = r(2\pi)$. Consider the curves

$$c_1 : \begin{cases} \mathbb{R} & \rightarrow & \mathbb{R}^2 \\ \phi & \mapsto & r(\phi) \begin{pmatrix} \cos(\phi) \\ \sin(\phi) \end{pmatrix} \end{cases}$$

and

$$c_2 : \begin{cases} \mathbb{R} & \rightarrow & \mathbb{R}^2 \\ s & \mapsto & sv \end{cases},$$

$v = (v_1, v_2) \in \mathbb{R}^2$ being a unit vector. c_2 parametrises a straight line containing the origin and c_1 borders a star shaped domain with star center 0. It can be shown that the curves c_1 and c_2 only intersect in two points. There exists an exhaustive list of iteration methods like the Newton-Raphson method with quadratic convergence rate that treat such intersection problems. However, these methods have the disadvantage that they need a good initial approximation for the intersection points. Therefore, it is more convenient to discuss a variation of the curve c_1 in terms of

$$c_1(\phi, t) = ((1 - t) + r(\phi)t) \begin{pmatrix} \cos(\phi) \\ \sin(\phi) \end{pmatrix}.$$

For every fixed parameter t the curve $\phi \mapsto c_1(\phi, t)$ borders a star shaped domain Ω_t with star centre 0. This variation is sketched in figure 2.1. Let $S_1(t)$ and $S_2(t)$ be the intersection points of the curves $\phi \mapsto c_1(\phi, t)$ and $s \mapsto c_2(s)$. In case $t = 0$ the intersection problem is easily understood and we have two solutions $S_1(0)$ and $S_2(0)$ given by the intersection of a line and a circle ($s_i^0 = 1, v_1 = \cos(\phi_i^0)$ and $v_2 = \sin(\phi_i^0)$, $i = 1, 2$). Unfortunately, it is not clear how to get a good approximation of $S_1(t)$ and $S_2(t)$ for $t \neq 0$.

Define the function

$$F(s, \phi, t) = c_1(\phi, t) - c_2(s).$$

We will call this function **natural system function** with regard to the intersection problem. The zeros of F correspond to the intersection points $S_1(t)$ and $S_2(t)$. The tangent vector $\frac{\partial}{\partial \phi} c_1 = F_\phi$ of $\partial \Omega_t$ at the intersection point $S_i(t)$ and the vector $v = F_s$ are always linear independent. Thus, the matrix $A = [F_\phi F_s]$ is always regular at this point. Since $F(s_i^0, \phi_i^0, 0) = 0$ we can apply the implicit function theorem which yields functions $s_i : [0, 1] \rightarrow \mathbb{R}, t \mapsto s_i(t)$ and $\phi_i : [0, 1] \rightarrow \mathbb{R}, t \mapsto \phi_i(t)$ such that

$$F(s(t), \phi(t), t) = 0 \tag{2.1.1}$$

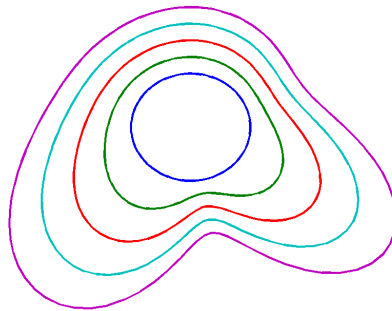


Figure 2.1: Homotopic deformation of a circle

for every $t \in [0, 1]$ and $s_i(0) = s_i^0$ and $\phi_i(0) = \phi_i^0$. For the derivatives of the functions s_i and ϕ_i we get (by implicit differentiation of (2.1.1))

$$\begin{pmatrix} s'_i \\ \phi'_i \end{pmatrix} = -A^{-1}F_t.$$

This method uses the fact that the subdeterminant of a so called natural system function never vanishes on the relevant solution spaces. This can not be assured in arbitrary cases since the method can not detect situations where the curve c_2 is tangential to the curve $c_1(\cdot, t)$ for a fixed parameter t .

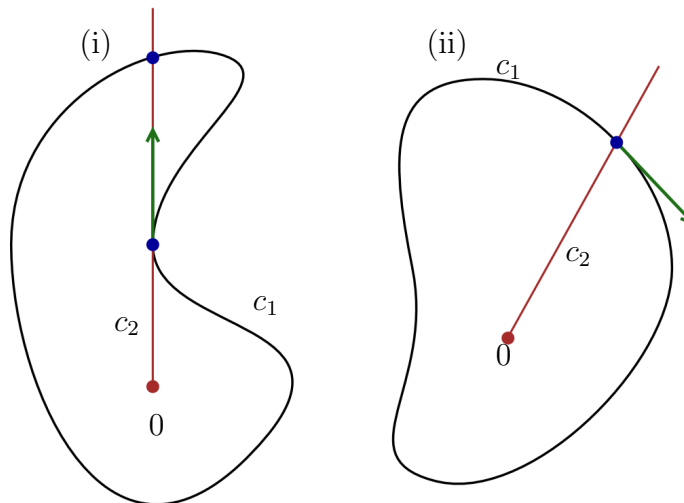


Figure 2.2: (i) c_1 is tangential to c_2 and (ii) c_1 is not tangential to c_2

The prescribed concept is related to the concepts that come up with the definition of the **mapping degree** of functions $f : \bar{\Omega} \subset \mathbb{R}^n \rightarrow \mathbb{R}^n$. There exist a large variety of

definitions of the mapping degree. The following theorem was first stated by Brouwer (1912) and later by Nagumo (1951).

Theorem 2.1.1

If f is continuous and $p \in \mathbb{R}^n \setminus f(\partial\Omega)$ then there exists a number $d(f, \Omega, p) \in \mathbb{N}$ with the properties:

- (i) If $d(f, \Omega, p) \neq 0$, then there exists $x_0 \in \Omega$ with $f(x_0) = p$.
- (ii) If $f(x, t) : \bar{\Omega} \times [0, 1] \rightarrow \mathbb{R}^n$ is continuous and if for $p \in \mathbb{R}^n$ the inequality $p \neq f(x, t)$ holds for all $x \in \partial\Omega$ and $t \in [0, 1]$, we have

$$d(f(\cdot, 0), \Omega, p) = d(f(\cdot, 1), \Omega, p).$$

- Let $\Omega = \bigcup_{i=1}^m \Omega_i$, where every Ω_i is open, $\Omega_i \cap \Omega_j = \emptyset$ for $i \neq j$, $\text{diam}(\Omega_i) < \infty$ for $i = 1, \dots, m$ and $\partial\Omega_i \subset \Omega$. Then

$$d(f, \Omega, p) = \sum_{i=1}^m d(f, \Omega_i, p)$$

holds for all $p \notin f(\partial\Omega)$.

Notice that the second part (ii) shows that the mapping degree is invariant under homotopies. The Brouwer theorem is heavily applied in the context of partial differential equations, like for example quasilinear elliptical equations. In this scope of applications it was helpful to get some ideas of how large classes of boundary value problems that are geometrically motivated can be solved using the mapping degree and related concepts. The Hopf-Poincaré index formula that was first proved by Poincaré for dimension 2 and later by Hopf for any dimension n can be stated in the following form:

”The index of a vector field with finitely many zeros on a compact, oriented manifold coincides with the Euler characteristic of the manifold.”

For more details concerning the proof of this theorem we refer the reader to [HH24].

2.2 Central Difference Quotients

We want to compute partial derivatives of a function employing function values only. Therefore, it makes sense to discuss the Taylor expansion of such functions. [BF98] gives an overview of the results presented in this section. We will start with univariate functions $f : D = [a, b] \rightarrow \mathbb{R}$. The main goal of this section is to approximate $f^{(k)}(x_c), x_c \in D$, only by the values

$$f(x_{-N}), f(x_{1-N}), \dots, f(x_{-1}), f(x_c), f(x_1), \dots, f(x_{N-1}), f(x_N).$$

The x_j shall be arranged uniformly around x_c , i.e.

$$|x_j - x_c| = |j| \cdot h$$

for a fixed number $h > 0$.

Example 2.2.1

Consider a function $f \in C^4([0, 1])$ and numbers $0 \leq x_{-1} < x_c < x_1 \leq 1$ like in the notation above. Then there exists a $\xi \in (x_{-1}, x_c)$ with the property that

$$f(x_{-1}) = f(x_c) - f'(x_c)h + \frac{1}{2}f''(x_c)h^2 - \frac{1}{6}f'''(x_c)h^3 + \frac{1}{24}f^{(4)}(\xi)h^4$$

This is an immediate consequence from the mean value theorem. Likewise, $\eta \in (x_c, x_1)$ exists such that

$$f(x_1) = f(x_c) + f'(x_c)h + \frac{1}{2}f''(x_c)h^2 + \frac{1}{6}f'''(x_c)h^3 + \frac{1}{24}f^{(4)}(\eta)h^4.$$

Combining these two equations and using the fact that $f^{(4)}$ is uniformly continuous on $[0, 1]$ we get

$$\frac{f(x_{-1}) - 2f(x_c) + f(x_1)}{h^2} = f''(x_c) + \frac{1}{24} \underbrace{(f^{(4)}(\xi) + f^{(4)}(\eta))}_{\leq K} h^2.$$

The left side of the last equation already denotes the **central difference quotient** of order $O(h^2)$ for the second order derivative of f . The general form of such quotients shall be derived systematically in the following.

Definition 2.2.1

Let $D = [a, b]$, $N \in \mathbb{N}$, $x \in D$ such that $x + jh \in D$ for $j = -N, \dots, N$. The quotient

$$\frac{\sum_{j=-N}^N \alpha_j f(\cdot + jh)}{h^k}$$

is called **central difference quotient of order** (M, k) if and only if for every function $f \in C^{M+k}([a, b])$

$$\frac{\sum_{j=-N}^N \alpha_j f(x + jh)}{h^k} = f^{(k)}(x) + O(h^M) \tag{2.2.1}$$

is satisfied for sufficiently small h .

Central difference quotients of order $O(h)$ cause numerical instabilities and are therefore not capable of producing reliable numerical results. The next example is slightly harder than that from 2.2.1 and includes five function evaluations.

Example 2.2.2

We will show the subsequent identity

$$\frac{-f(x_{-2}) + 16f(x_{-1}) - 30f(x_c) + 16f(x_1) - f(x_2)}{12h^2} = f''(x_c) + O(h^4)$$

assuming that f is of class $C^6([a, b])$. The coefficients c_i showed up as weighting factors of some proper Taylor expansions around x_c in the last example. This is true in every case. It turns out that they can be determined by an adequate linear system of equations.

Assume that the standard polynomial functions

$$e_i(x) = x^i, i = 1, \dots, 4$$

satisfy

$$h^2 f''(x_c) = \alpha_{-2}f(x_{-2}) + \alpha_{-1}f(x_{-1}) + \alpha_c f(x_c) + \alpha_1 f(x_1) + \alpha_2 f(x_2).$$

By comparison of the coefficients of the terms $x^i h^j$ we get:

$$\begin{pmatrix} 1 & 1 & 1 & 1 & 1 \\ -2 & -1 & 0 & 1 & 2 \\ 4 & 1 & 0 & 1 & 4 \\ -8 & -1 & 0 & 1 & 8 \\ 16 & 1 & 0 & 1 & 16 \end{pmatrix} \begin{pmatrix} \alpha_{-2} \\ \alpha_{-1} \\ \alpha_c \\ \alpha_1 \\ \alpha_2 \end{pmatrix} = \begin{pmatrix} 0 \\ 0 \\ 2 \\ 0 \\ 0 \end{pmatrix}.$$

The corresponding matrix on the left side of the last equation is invertible. Therefore, the solution is uniquely determined by the vector of coefficients

$$\vec{\alpha} = (-1/12, 4/3, -5/2, 4/3, -1/12).$$

Surprisingly e_5 also fulfils the above condition, whereas e_6 does not. For e_6 we have

$$\alpha_{-2}e_6(x_{-2}) + \alpha_{-1}e_6(x_{-1}) + \alpha_c e_6(x_c) + \alpha_1 e_6(x_1) + \alpha_2 e_6(x_2) = e_6''(x_c)h^2 - 8h^6.$$

Division by h^2 then provides the desired result. This means that the corresponding central difference coefficient is of order $(4, 2)$.

The following theorem summarises the most important features of the central difference quotient.

Lemma 2.2.1

Let $k, N > 0$ be natural numbers such that $2N \geq k$.

a) $\vec{\alpha} = (\alpha_{-N}, \dots, \alpha_N)$ satisfies

$$h^k e_i^{(k)}(x) = \sum_{j=-N}^N \alpha_j e_i(x + jh) \tag{2.2.2}$$

for $i = 0, \dots, 2N$ if and only if $\vec{\alpha}$ meets the linear system

$$A\vec{\alpha} = k! \vec{e}_{k+1}$$

where $A = (a_{ij})$, $a_{ij} = (j - N - 1)^{i-1}$ for $i, j = 1, \dots, 2N + 1$.

b) Suppose

$$\sum_{m=-N}^N \alpha_m m^j = 0$$

for $j = 2N, \dots, j_{\max} - 1$ but

$$\sum_{m=-N}^N \alpha_m m^{j_{\max}} \neq 0$$

Then the corresponding central difference quotient is of order $(j_{\max} - k, k)$.

Proof: The main goal of this proof is to show that starting with $i = 0$ and ending with $i = 2N$ system (2.2.2) only yields one new equation for $\vec{\alpha}$ at every step.

a) Let $0 \leq i \leq 2N$. Putting

$$\beta_j^i := \binom{i}{j} \sum_{m=-N}^N \alpha_m m^{i-j}$$

and applying the binomial theorem we have

$$\begin{aligned} \sum_{j=-N}^N \alpha_j e_i(x + jh) &= \sum_{j=-N}^N \alpha_j (x + jh)^i \\ &= \sum_{j=0}^i x^j h^{i-j} \beta_j^i. \end{aligned}$$

Since

$$h^k e_i^{(k)}(x) = \begin{cases} 0 & i < k \\ h^k \binom{i}{k} k! x^{i-k} & i \geq k \end{cases},$$

$\beta_j^i \neq 0$ if and only if $j = i - k$, which means that

$$\sum_{m=-N}^N \alpha_m m^k = k!.$$

This already proves a).

b) For sufficiently small $h \geq 0$ there exists for every j a number $\xi_j \in (x - Nh, x + Nh)$ such that

$$f(x + jh) = \sum_{m=0}^{j_{\max}-1} \frac{f^{(m)}(x)}{m!} j^m h^m + \frac{f^{(j_{\max})}(\xi_j)}{(j_{\max})!} j^{j_{\max}} h^{j_{\max}}.$$

By simply setting

$$C = \sum_{j=-N}^N \alpha_j \frac{f^{(j_{\max})}(\xi_j)}{(j_{\max})!} j^{j_{\max}}$$

it follows that

$$\begin{aligned}
 \sum_{j=-N}^N \alpha_j f(x + jh) &= \sum_{j=-N}^N \alpha_j \left(\sum_{m=0}^{j_{\max}-1} \frac{f^{(m)}(x)}{m!} h^m j^m + \frac{f^{(j_{\max})}(\xi_j)}{(j_{\max})!} j^{j_{\max}} h^{j_{\max}} \right) \\
 &= \sum_{m=0}^{j_{\max}-1} \frac{h^m}{m!} f^{(m)}(x) \sum_{j=-N}^N \alpha_j j^m + Ch^{j_{\max}} \\
 &= \frac{h^k}{k!} f^{(k)}(x) k! + Ch^{j_{\max}} \\
 &= h^k (f^{(k)}(x) + Ch^{j_{\max}-k}).
 \end{aligned}$$

This constitutes the proof of b) since (2.2.1) holds.

□

Note that for large N the coefficient matrix A is ill conditioned. The next examples shows that accurate numerical results can be expected even if the number of function values is moderate.

Example 2.2.3

Let $f(x) = \sin(x)$. We want to compute the second derivative of f at $x = 2.1$ using 7 function values only ($N = 3$) and the increment $h = 0.01$. The absolute error is less than $\frac{1}{2} \cdot 10^{-11}$. The same test for $f(x) = x^5$ provides an approximation with more than 9 correct digits.

The central difference quotients for multivariate functions typically involve the **tensor product** scheme. Consider for example a bivariate function

$$f : D \subset \mathbb{R}^2 \rightarrow \mathbb{R}^2.$$

If α constitutes the coefficient vector of the central difference quotient of order (M_1, k_1) and β the coefficient vector of the central difference quotient of order (M_2, k_2) , the definition of tensor product schemes yields for sufficiently small h

$$h^k \frac{\partial^k f}{\partial x^{k_1} \partial y^{k_2}} = \sum_{i,j} \alpha_i \beta_j f(x + ih, y + hj) + O(h^M)$$

provided that $M = \min(M_1, M_2)$ and $k = k_1 + k_2$.

This simple scheme is easy to implement on a personal computer. We have another

Example 2.2.4

Using the notation from above let $f(x, y, z) = x \sin(y) \exp(z)$, $h = 0.01$, $N = 7$, $(k_1, k_2, k_3) = (0, 1, 2)$ and $(x, y, z) = (1, 0.2, -4)$. Here the result for $\frac{\partial^3}{\partial y \partial z^2} f$ proves to have 11 correct digits.

We will use this central difference quotient scheme as an approximation scheme for offset functions in section 4.5. The central difference quotient allows us to solve the medial equations with less effort, since it reduces the time complexity.

2.3 Boundary Value Problems

The solution of boundary value problems (short BVPs) plays an important role in differential geometry. The computation of shortest geodesic paths joining any two points on a given Riemannian manifold is a basic geometric problem (BVP), which is described in almost every textbook on differential geometry. This BVP may be viewed at from different perspectives. It turns out that the given BVP can also be identified as an implicit initial value problem (IVP) for which we shall deduce its initial condition. More precisely we shall use solutions of a family of IVPs to solve the given BVP. Unfortunately, this increases the time complexity of this method. The key idea of our approach shall be described by an example given by the Sturm-Liouville problem.

Definition 2.3.1

Let $r, p, q \in C([a, b], \mathbb{R})$ and

$$Lu = (pu')' + qu$$

be a self-adjoint differential operator of order 2. Define the boundary operator

$$R_u(a) = \alpha_0 u(a) + \alpha_1 p(a)u'(a), \quad (2.3.1)$$

$$R_u(b) = \beta_0 u(b) + \beta_1 p(b)u'(b), \quad (2.3.2)$$

assuming that $\alpha_0^2 + \alpha_1^2 > 0$, $\beta_0^2 + \beta_1^2 > 0$. Then the related Sturm-Liouville BVP is given by

$$\begin{cases} (Lu)(x) = r(x) \\ R_u(a) = \eta_a, R_u(b) = \eta_b \end{cases} \quad (2.3.3)$$

For didactical reasons we will focus on the special case where $p \equiv 1$ and q is strictly negative. The solution function u shall meet the simplified boundary conditions, where only the function values of u appear. This yields

$$u''(x) + q(x)u(x) = r(x), \quad (2.3.4)$$

$$u(a) = \eta_a, \quad (2.3.5)$$

$$u(b) = \eta_b. \quad (2.3.6)$$

An additional time parameter $t \in [0, 1]$ leads to a family of IVPs of the form

$$\frac{\partial^2 w(x)}{\partial x^2} + tq(x)w(x) = r(x), \quad (2.3.7)$$

$$w(a) = \eta_a, \quad (2.3.8)$$

$$\frac{\partial w(a)}{\partial x} = \psi. \quad (2.3.9)$$

For every parameter t system (2.3.7)-(2.3.9) has a unique solution denoted by $w(x, \psi, t)$. This simply follows from the Lipschitz continuity of the first order ODE from (2.3.7).

It is not hard to see by the fundamental theorem of calculus that for $t = 0$ the solution of (2.3.7)-(2.3.9) can be written in the form

$$w(x, \psi, 0) = \int_a^x \int_a^y r(t) dt dy + \eta_a + \psi(x - a).$$

ψ has to be specified such that the boundary condition $w(b, \psi, 0) = \eta_b$ holds, namely

$$\psi_0 = \psi(t = 0) = \frac{\eta_b - \eta_a - \int_a^b \int_a^y r(t) dt dy}{b - a}.$$

ψ_0 can be reinterpreted as an initial value of another IVP as we will see.

The **implicit function theorem** is one of the most fascinating mathematical theorems. It will be required several times throughout this thesis. It can be found in almost every textbook on standard analysis.

Theorem 2.3.1

Let $f : \mathbb{R}^{n+m} \rightarrow \mathbb{R}^m$ be a continuously differentiable function and assume

$$f(a_1, \dots, a_n, b_1, \dots, b_m) = 0.$$

We think of \mathbb{R}^{n+m} as the Cartesian product $\mathbb{R}^n \times \mathbb{R}^m$ and denote this by

$$(x, y) = (x_1, \dots, x_n, y_1, \dots, y_m) \in \mathbb{R}^n \times \mathbb{R}^m.$$

If the matrix

$$\begin{pmatrix} \frac{\partial f_1}{\partial y_1}(a, b) & \dots & \frac{\partial f_1}{\partial y_m}(a, b) \\ \vdots & \ddots & \vdots \\ \frac{\partial f_m}{\partial y_1}(a, b) & \dots & \frac{\partial f_m}{\partial y_m}(a, b) \end{pmatrix}$$

is invertible, then there exists an open set $U \subset \mathbb{R}^n$ containing (a_1, \dots, a_n) , an open set $V \subset \mathbb{R}^m$ containing (b_1, \dots, b_m) and a differentiable function $g : U \rightarrow V$ such that $f(x, y) = 0$ is equivalent to $y = g(x)$ for every $x \in U$ and $y \in V$.

We want to apply the implicit function theorem to the Sturm-Liouville problem (2.3.7)-(2.3.9). Therefore, define a new system function

$$F(\psi, t) := w(b, \psi, t) - \eta_b.$$

We already know that

$$F(\psi_0, 0) = 0.$$

Furthermore,

$$F_\psi(\psi_0, 0) = \frac{\partial w}{\partial \psi}(b, \psi_0, 0) = b - a \neq 0.$$

By the implicit function theorem there exists an $\epsilon > 0$ and a function $\psi : [0, \epsilon] \rightarrow \mathbb{R}$ such that

$$F(\psi(t), t) = 0.$$

This means that the function ψ is differentiable with respect to t . Differentiating with respect to the time parameter t yields the final version of our IVP:

$$\psi'(t) = -\frac{\frac{\partial}{\partial t}w(b, \psi(t), t)}{\frac{\partial}{\partial \psi}w(b, \psi(t), t)}, \quad (2.3.10)$$

$$\psi(0) = \psi_0. \quad (2.3.11)$$

The implicit function theorem is valid for a small $\epsilon > 0$ and in general $\epsilon = 1$ can not be assumed without further considerations. It can be deduced from the fact that q is strictly negative. In addition the partial derivatives of w with respect to t and ψ are required. They can only be obtained by solving additional IVPs. Taking into account that w not only depends on x but on ψ and t , differentiating of (2.3.7) with respect to t yields

$$\frac{\partial^2}{\partial x^2} \frac{\partial}{\partial t} w(x, \psi, t) + q(x)w(x, \psi, t) + tq(x) \frac{\partial}{\partial t} w(x, \psi, t) = 0, \quad (2.3.12)$$

$$\frac{\partial}{\partial t} w(a, \psi, t) = 0, \quad (2.3.13)$$

$$\frac{\partial}{\partial x} \frac{\partial}{\partial t} w(a, \psi, t) = 0. \quad (2.3.14)$$

The same approach for ψ provides the key idea why the assumption $\epsilon = 1$ is correct:

$$\frac{\partial^2}{\partial x^2} \frac{\partial}{\partial \psi} w(x, \psi, t) + tq(x) \frac{\partial}{\partial \psi} w(x, \psi, t) = 0, \quad (2.3.15)$$

$$\frac{\partial}{\partial \psi} w(a, \psi, t) = 0, \quad (2.3.16)$$

$$\frac{\partial}{\partial x} \frac{\partial}{\partial \psi} w(a, \psi, t) = 1. \quad (2.3.17)$$

It remains to prove the strict monotony of the function $\frac{\partial}{\partial \psi} w(x, \psi, t)$ for fixed parameters ψ and t . For $t = 0$ the solution of (2.3.15)-(2.3.17) is just

$$\frac{\partial}{\partial \psi} w(x, \psi, 0) = x - a,$$

which is a strict monotone C^∞ -function.

Proof: Set $f(x) := \frac{\partial}{\partial \psi} w(x, \psi, t)$. Since $f'(a) = 1$, there exist an $\epsilon > 0$, such that f strictly increases on $[a, a + \epsilon]$. Let $\epsilon = \epsilon_{\max}$ be maximal with the above property. Make sure that such an ϵ_{\max} exists. Clearly, $f(a + \epsilon_{\max}) > 0$ and hence f is positive in a neighbourhood U of the point $a + \epsilon_{\max}$. Because of (2.3.15), f'' then must also be positive on U . It follows that f' is monotonically increasing on U . Finally, this yields $f'(a + \epsilon_{\max}) > 0$, which is a contradiction to the maximality of ϵ_{\max} .

□

Remark 2.3.1

In the context of Riemannian geometry we will see that (2.3.15) corresponds to the Jacobi equations for surfaces having negative Gaussian curvature. In the latter case it is known that the solutions are monotonically increasing functions.

Example 2.3.1

Using the notion from above let $r(x) = 1$, $q(x) = -\exp(-x^2)$, $(a, b) = (-5, 5)$ and $(\eta_a, \eta_b) = (-1, 1)$. Figure 2.3 sketches the solution for the cases $t = 0$ and $t = 1$. For

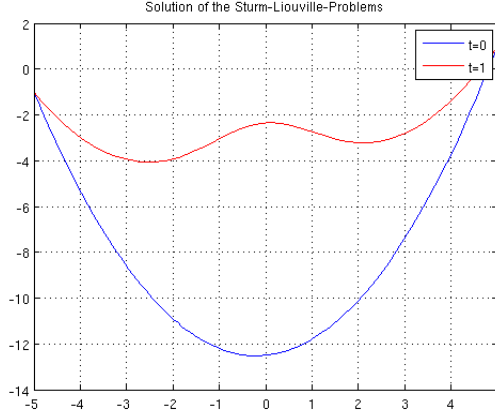


Figure 2.3: Plot of two solution functions defined by example 2.3.1

the absolute error we get

$$|w(b, \psi(1), 1) - \eta_b| \leq 0.5 \cdot 10^{-5}.$$

and it can be reduced in case the step size of the solver is reduced.

To make use of equation (2.3.10) we must evolve the right side. It is therefore convenient to state (2.3.12) - (2.3.14) and (2.3.15) - (2.3.17) as a first order ordinary differential equation:

| | |
|-------------------------|--|
| $y'_1 = y_2$ | $y_1(x) = w(x, \psi, t)$ |
| $y'_2 = r - tqy_1$ | $y_2(x) = \frac{\partial}{\partial x} w(x, \psi, t)$ |
| $y'_3 = y_4$ | $y_3(x) = \frac{\partial}{\partial t} w(x, \psi, t)$ |
| $y'_4 = -q(y_1 + ty_3)$ | $y_4(x) = \frac{\partial^2}{\partial t \partial x} w(x, \psi, t)$ |
| $y'_5 = y_6$ | $y_5(x) = \frac{\partial}{\partial \psi} w(x, \psi, t)$ |
| $y'_6 = -tqy_5$ | $y_6(x) = \frac{\partial}{\partial x \partial \psi} w(x, \psi, t)$ |

2.4 Homotopy Methods

From the last section we have seen that the Sturm-Liouville problem is equivalent to the problem of finding the zeros of a function $f : \mathbb{R} \rightarrow \mathbb{R}$, $f(\psi) = w(b, \psi, 1) - \eta_b$. In

the course of these considerations we constructed a function

$$F : \mathbb{R} \times [0, 1] \rightarrow \mathbb{R}$$

with the following properties:

- F is a smooth function,
- $F(\cdot, 0)$ is a very simple function, i.e. the zeros of this function can be obtained very easily,
- $F(\cdot, 1) = f$.

We call the function F **homotopy** of the function f . To summarise the above it will be of great use to employ techniques that trace the zero set of a function $F : \mathbb{R}^{N+1} \rightarrow \mathbb{R}^N$. It can be shown that $F^{-1}(0)$ only consists of components that are topologically equivalent to \mathbb{R} and S^1 respectively in case zero is a regular value of F , i.e. the Jacobi matrix of $F'(\bar{p})$ has full rank whenever $F(\bar{p}) = 0$. If \tilde{p} is an approximation of \bar{p} one can employ the Newton-Raphson method to improve \tilde{p} .

Definition 2.4.1

Let A be an $N \times (N + 1)$ -matrix with maximal rank. $A^+ := A^T(AA^T)^{-1}$ is called **Moore Penrose inverse** of A . The map

$$\mathcal{N}(p) = p - F'(p)^+ F(p)$$

is called **Newton map** and $\mathcal{N}(p)$ **Newton point**.

Theorem 2.4.1

Assume \tilde{p} is sufficiently close to \bar{p} . Then the sequence $(\mathcal{N}^i(\tilde{p}))_i$ converges quadratically towards a point $\mathcal{N}^\infty(\tilde{p}) \in F^{-1}(0)$.

For a proof of theorem 2.4.1 we refer to [AG03].

In fact, one critical point of the last discussion is the Moore Penrose matrix which employs the matrix $F'(p)$. We can use chord methods instead to avoid this drawback, but then only **superlinear convergence** can be expected.

Definition 2.4.2

Let A be an $N \times (N + 1)$ -matrix with rank N . The normalised vector $t(A) \in \mathbb{R}^{N+1}$ from $\ker(A)$ with

$$\det \begin{pmatrix} A \\ t^T \end{pmatrix} > 0$$

is called **tangent vector induced by A**.

We can now employ a **Euler-Newton method** to trace the zero set of the function F in a neighbourhood of a point $u_0 \in \mathbb{R}^{N+1}$

Algorithm 1 Euler-Newton method

Require: $u_0 \in \mathbb{R}^{N+1}$ such that $F(u_0) = 0$;

Require: $h > 0$;

repeat

$v := u + ht(F'(u))$

repeat

$w := v - F'(v)^+ F(v)$;

$v := w$;

until convergence

$u := w$;

choose a new steplength $h > 0$;

until traversing is stopped

Details concerning the above method can be found in [AG03]. It required that zero is a regular value of the function F . We will see later on, how to overcome this drawback. Note also that the method is called a **Predictor-Corrector-Method** (PC-Method).

Indeed, this is only one way to trace the zero set of the function F . It is also possible to define the initial value problem:

- $\dot{u} = t(F'(u))$
- $u(0) = u_0$

Both methods are used in practise but we will prefer Predictor-Corrector-Methods since they have been proven to be more stable.

2.4.1 Bifurcation Theory

So far we have assumed that 0 is a regular value of the given function F . This is indeed very restrictive. Often bifurcation points have to be taken into account. The following discussion about bifurcation points is also hold by Allgower and Georg (see [AG03]).

Definition 2.4.3

Let $F : \mathbb{R}^{N+1} \rightarrow \mathbb{R}^N$ be a smooth function and $c : I \rightarrow \mathbb{R}^{N+1}$ be an arc length parametrised curve such that $F(c(s)) = 0$ for all $s \in I$. Assume $0 \in I$ and I to be an open interval. $c(0)$ is called **bifurcation point** if there exists an $\epsilon > 0$ such that every neighbourhood of $c(0)$ contains a point from

$$F^{-1}(0) \cap (\mathbb{R}^{N+1} \setminus c(-\epsilon, \epsilon)).$$

It is obvious that $\bar{u} = c(0)$ is a singular value of the function F . Here and in the following it will be assumed that

$$\dim \ker F'(\bar{u}) = 2.$$

Let $X_1 := \ker F'(\bar{u})$, $X_2 := X_1^\perp$ and $Y_2 := \text{range } F'(\bar{u})$, $Y_1 = Y_2^\perp$. Deduce that

$$\begin{aligned}\dim X_1 &= 2 \\ \dim X_2 &= N - 1 \\ \dim Y_1 &= 1 \\ \dim Y_2 &= N - 1.\end{aligned}$$

Let e be a vector that spans Y_1 and $\{e_1, \dots, e_{N-1}\}$ be linear independent vectors that span Y_2 . Then there exist a function $F_1 : X_1 \rightarrow \mathbb{R}$ and functions $F_2^i : X_2 \rightarrow \mathbb{R}$ such that

$$F(u_1, u_2) = F(u) = eF_1(u_1, u_2) + \sum_{i=1}^{N-1} F_2^i(u_1, u_2)e_i.$$

If F_2 denotes the component vector $(F_2^1, \dots, F_2^{N-1})$ we can deduce that

$$F'(\bar{u}) = \begin{pmatrix} 0 & 0 \\ 0 & \partial_2 F_2(\bar{u}_1, \bar{u}_2) \end{pmatrix}.$$

Since $\partial_2 F_2(\bar{u})$ is a regular matrix we can apply the implicit function theorem to conclude that there exists a function $g : U_1 \rightarrow U_2$ such that $F_2(u) = 0$ corresponds to

$$u_2 = g(u_1)$$

in a neighbourhood (U_1, U_2) of (\bar{u}_1, \bar{u}_2) where U_1 and U_2 are defined as usual. Set

$$h(u_1) := F_1(u_1, g(u_1)) = 0.$$

The function h meets the conditions:

$$\begin{aligned}h(\bar{u}_1) &= 0, \\ h'(\bar{u}_1) &= 0, \\ h''(\bar{u}_1) &= \partial_1^2 F_1(\bar{u}).\end{aligned}$$

If the Hessian $h''(\bar{u}_1)$ has two non vanishing eigenvalues λ_1, λ_2 of different sign, we call \bar{u} **simple bifurcation point** of F . Notice that \bar{u} would be an isolated point in case $\lambda_1 \cdot \lambda_2 > 0$. It follows immediately that near a simple bifurcation point \bar{u} the zero set $F^{-1}(0)$ coincides with the union of two intersecting regular curves c_1 and c_2 that intersect transversely at \bar{u} . For every i the determinant of the matrix

$$\begin{pmatrix} F'(c_i(s)) \\ c_i'(s)^T \end{pmatrix}$$

changes sign at $s = 0$.

Without going to much into detail it is possible to show that the above criterion is a powerful tool in the context of numerical integration of the solution set $F^{-1}(0)$ near bifurcation points. It is even possible to jump from one solution branch to another. For details we again refer the reader to [AG03].

3 Elements Of Differential Geometry

3.1 Manifolds

Differentiable geometry is a classical field of mathematics with many applications like the theory of relativity and the theory of Lie groups. The subsequent explanations can be found in similar form in standard textbooks like [dC92] or in [KN63].

Differentiable manifolds will build the fundament of all considerations in this thesis. They differ from topological manifolds in so far that they own a differentiable structure which will be discussed in the following.

Definition 3.1.1

Let M be a topological space with topology \mathcal{T} . M is called a **topological manifold of dimension n** , if and only if

- 1) M is Hausdorffian, which means that distinct points in M always own disjoint neighbourhoods.
- 2) \mathcal{T} has a countable basis.
- 3) M is locally homeomorphic to \mathbb{R}^n .

We call the homeomorphisms from 3) **coordinate charts**. In general topological manifolds own infinitely many of these coordinate charts that cover M .

No calculus can be realised on such general spaces unless M has a differentiable structure. Let for example $f : M \rightarrow \mathbb{R}$ be a function on M and $x_i : U_i \subset M \rightarrow V_i \subset \mathbb{R}^n$ a chart of M . We want to call f differentiable at $p \in U_i$ if $f \circ x_i^{-1} : V_i \rightarrow \mathbb{R}$ is differentiable at $x_i(p) \in V_i$. Maybe that there is another chart $x_j : U_j \subset M \rightarrow V_j \subset \mathbb{R}^n$ with $p \in U_j$. If the transition map

$$x_i \circ x_j^{-1} : V_i \cap V_j \rightarrow V_i \cap V_j$$

is only a homeomorphism, then $f \circ x_j^{-1} = (f \circ x_i^{-1}) \circ (x_i \circ x_j^{-1})$ is only continuous at $x_j(p)$. Hence, differentiability can only be defined for an atlas with C^∞ compatible charts.

Definition 3.1.2

Let M be a topological manifold with coordinate charts $x_i : U_i \rightarrow V_i$, $i \in I$, and

$$\bigcup_{i \in I} U_i = M,$$

i.e. the charts totally cover M . We call this atlas $A = \{x_i, i \in I\}$ a C^∞ -**atlas**, if for every two charts the corresponding transition map is a C^∞ - diffeomorphism. If there is no other chart of M that is C^∞ compatible with every chart in A , we call A a **differentiable structure** and the pair (M, A) a n -dimensional **differentiable manifold**.

Not surprisingly, the tangent space $T_p M$ of a point $p \in M$ and the directional derivative of a function $f : M \rightarrow \mathbb{R}$ can be defined using the differentiable structure as well. A tangent vector at $p \in M$ is the equivalence class of differentiable curves $c : (-\epsilon, \epsilon) \rightarrow M$ with $c(0) = p$ fulfilling an additional condition. Two curves that pass through p are called equivalent, if their image curves have the same tangent vectors with respect to a fixed chart $x : U \rightarrow V$, $p \in U$. This definition however does not depend on the special choice of the chart x .

3.2 Riemannian Geometry

Definition 3.2.1

Let M be a differentiable manifold and

$$g_p : T_p M \times T_p M \rightarrow \mathbb{R}$$

a symmetric non degenerate positive definite bilinear form for every $p \in M$. Define for a fixed chart $x : U \rightarrow V$ of M the function $g_{ij} : V \rightarrow \mathbb{R}$ by

$$g_{ij}(v) := g|_{x^{-1}(v)} \left(\left. \frac{\partial}{\partial x^i} \right|_{x^{-1}(v)}, \left. \frac{\partial}{\partial x^j} \right|_{x^{-1}(v)} \right).$$

Then g is called a **Riemannian metric** and (M, g) a **Riemannian manifold** whereas the matrix (g_{ij}) is called **first fundamental tensor**.

It is clear that g is fixed by the values g_{ij} since g is a bilinear form. Namely, if $p \in M$ and $x : U \rightarrow V$ is a chart of M with $p \in V$ then we have for $\xi = \sum_{i=1}^n \xi^i \left. \frac{\partial}{\partial x^i} \right|_p$ and $\eta = \sum_{i=1}^n \eta^i \left. \frac{\partial}{\partial x^i} \right|_p$

$$g_p(\xi, \eta) = \sum_{i,j=1}^n \xi^i \eta^j g_{ij}(x(p)).$$

An important tool for introducing geodesics on a Riemannian manifold is the definition of the **covariant derivative** or the **Levi-Civita connection** respectively. If $p \in M$ and $\eta : U \rightarrow TM$ is a smooth vector field in the neighbourhood U of the point $p \in M$ and $\xi \in T_pM$, then we get a local representation of the Levi-Civita connection ∇ by

$$\nabla_{\xi^i \frac{\partial}{\partial x_i}} \eta^j \frac{\partial}{\partial x_j} = \xi^i \left(\frac{\partial \eta^k}{\partial x_i} \Big|_{x(p)} + \eta^j \Big|_{x(p)} \Gamma_{ij}^k(x(p)) \right) \frac{\partial}{\partial x_k} \Big|_p. \quad (3.2.1)$$

It follows that ∇ is a mapping $\nabla : T_pM \times \Theta_p \rightarrow T_pM$, where Θ_p is the space of smooth vector fields in a neighbourhood of the point p . In the aforementioned definition the **Christoffel symbols** Γ_{ij}^k were used which are specified by the expression:

$$\Gamma_{ij}^k = \frac{1}{2} \sum_{m=1}^n g^{mk} \left(\frac{\partial g_{im}}{\partial x_j} + \frac{\partial g_{jm}}{\partial x_i} + \frac{\partial g_{ij}}{\partial x_m} \right). \quad (3.2.2)$$

Remark 3.2.1

- The above expression generalises the concepts of directional derivatives from classical analysis employing a projection onto the tangent space T_pM afterwards. It has similar properties like the directional derivative. From equation (3.2.1) for example we can easily deduce the linearity of ∇ in the first argument. A detailed description of other properties can be found for example in [TS96], [BN83] and [dC92] or in many standard textbooks on differential geometry.
- The Levi-Civita connection is **torsion free**, which means that

$$\nabla_{\frac{\partial}{\partial x_i}} \frac{\partial}{\partial x_j} = \nabla_{\frac{\partial}{\partial x_j}} \frac{\partial}{\partial x_i}.$$

Definition 3.2.2

Let M be a differentiable manifold and $x : U \rightarrow V$ be a local chart of M . We call the inverse map $f = x^{-1}$ local **parametrisation** of M .

Definition 3.2.3

Let M be a submanifold of \overline{M} . If $\dim(M) = n$ and $\dim(\overline{M}) = n + k$, then M is said to have **codimension** k .

Definition 3.2.4

Let M, \overline{M} be two given Riemannian manifolds where M is a submanifold of \overline{M} . M is called Riemannian **hypersurface** if it has codimension 1.

Here and in the following we will use the subsequent notation. Let $h : D \subset \mathbb{R}^n \rightarrow \mathbb{R}$ be a smooth function. Then

$$\begin{aligned} h_i &= \frac{\partial}{\partial x_i} h, \\ h_{ij} &= \frac{\partial^2}{\partial x_i \partial x_j} h. \\ &\dots \end{aligned}$$

In the next example we give an idea of how the calculation of the Christoffel symbols for a hypersurface M can be achieved in case the parametrisation f has a special form.

Example 3.2.1

Consider a n -dimensional hypersurface $M \subset \mathbb{R}^{n+1}$ and a local parametrisation of M given by

$$f(x_1, \dots, x_n) = (x_1, \dots, x_n, h(x_1, \dots, x_n)).$$

We will show that the Christoffel symbols fulfil the equation

$$\Gamma_{ij}^k = \frac{h_{ij}h_k}{1 + \|\nabla h\|^2}. \quad (3.2.3)$$

Since M has codimension 1, the normal space of M has dimension 1 which means that for every pair (i, j) we have

$$f_{ij} = \Gamma_{ij}^k f_k + L_{ij}N, \quad (3.2.4)$$

where N denotes a normal vector of M . N can be written in the form

$$N = \frac{1}{\sqrt{1 + \|h\|^2}} \begin{pmatrix} -h_1 \\ \vdots \\ -h_n \\ 1 \end{pmatrix}.$$

Multiplication of (3.2.4) with N provides that

$$L_{ij} = \langle f_{ij}, N \rangle = -\frac{h_{ij}}{\sqrt{1 + \|h\|^2}}.$$

For $k = 1, \dots, n$ we then get

$$\Gamma_{ij}^k = \frac{h_{ij}h_k}{1 + \|\nabla h\|^2}.$$

This already proves the claim.

There are other interesting classes of hypersurfaces, especially those which are invariant with respect to rotations around a straight line l . We have the following

Definition 3.2.5

A hypersurface $M \subset \mathbb{R}^{n+1}$ is said to be of **revolution**, if M is invariant with respect to the group G_l of rotations around a line l .

The next example gives an idea of how such hypersurfaces of revolution can be parametrised.

Example 3.2.2

Let $\alpha : I \rightarrow \mathbb{R}^2$, $\alpha(t) = (g_1(t), g_2(t))$ an arc length parametrised curve with no double points and $g_1(t) > 0$ for all $t \in I$. Let $\phi, \psi \in (-\frac{\pi}{2}, \frac{\pi}{2})$ and $\rho \in (-\pi, \pi)$. Consider the following parametrisation of a hypersurface of revolution

$$f(t, \phi, \psi, \rho) = \begin{pmatrix} g_1(t) \cos(\phi) \cos(\psi) \cos(\rho) \\ g_1(t) \cos(\phi) \cos(\psi) \sin(\rho) \\ g_1(t) \cos(\phi) \sin(\psi) \\ g_1(t) \sin(\phi) \\ g_2(t) \end{pmatrix}.$$

It has to be verified that the parametrisation f maps its parameter space

$$U = I \times \left(-\frac{\pi}{2}, \frac{\pi}{2}\right)^2 \times (-\pi, \pi)$$

diffeomorphically onto the image $f(U)$. We first show the injectivity. Let

$$g_1(t_1) \cos(\phi_1) \cos(\psi_1) \cos(\rho_1) = g_1(t_2) \cos(\phi_2) \cos(\psi_2) \cos(\rho_2) \quad (3.2.5)$$

$$g_1(t_1) \cos(\phi_1) \cos(\psi_1) \sin(\rho_1) = g_1(t_2) \cos(\phi_2) \cos(\psi_2) \sin(\rho_2) \quad (3.2.6)$$

$$g_1(t_1) \cos(\phi_1) \sin(\psi_1) = g_1(t_2) \cos(\phi_2) \sin(\psi_2) \quad (3.2.7)$$

$$g_1(t_1) \sin(\phi_1) = g_1(t_2) \sin(\phi_2) \quad (3.2.8)$$

$$g_2(t_1) = g_2(t_2) \quad (3.2.9)$$

The sum of the squares of the left sides of equations (3.2.5) and (3.2.6) agree with the corresponding sum of the squares of the right sides, i.e.

$$g_1(t_1) \cos(\phi_1) \cos(\psi_1) = g_1(t_2) \cos(\phi_2) \cos(\psi_2) \quad (3.2.10)$$

The same trick can be applied to (3.2.7) and (3.2.10) which leads to the equation

$$g_1(t_1) \cos(\phi_1) = g_1(t_2) \cos(\phi_2). \quad (3.2.11)$$

Together with (3.2.8) we have that

$$g_1(t_1) = g_1(t_2),$$

$$g_2(t_1) = g_2(t_2).$$

Deduce that f is a bijection and that the first fundamental tensor $G = (g_{ij})$ is given by

$$g_{11} = 1,$$

$$g_{22} = g_1^2,$$

$$g_{33} = g_1^2 \cos^2(\phi),$$

$$g_{44} = g_1^2 \cos^2(\phi) \cos^2(\psi)$$

and

$$g_{ij} = 0 \quad \forall i \neq j.$$

Hence, G and G^{-1} are both diagonal matrices and f is a global diffeomorphism. (3.2.2) can therefore be simplified due to

$$\Gamma_{ij}^k = \frac{1}{2} g^{kk} \left(\frac{\partial g_{ik}}{\partial x^j} + \frac{\partial g_{jk}}{\partial x^i} - \frac{\partial g_{ij}}{\partial x^k} \right). \quad (3.2.12)$$

The next figure illustrates how a 2-dimensional surface of revolution may look like. Observe that the isoparameter lines are always perpendicular.

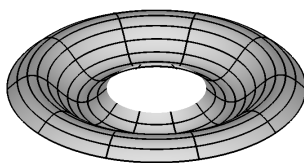


Figure 3.1: Surface of revolution

Let $\alpha : \mathbb{R} \rightarrow M$ be a curve on M and $v(t)$ be a vector field along α . We define the **covariant derivative** by

$$\frac{D}{dt} v(t) := \nabla_{\dot{\alpha}(t)} v(t). \quad (3.2.13)$$

Furthermore, suppose that (M, d) is **metric complete**, i.e. that every Cauchy sequence in M converges in M . This allows us to use the theorem of Hopf and Rinow. Now and in the sequel let M be a complete and orientable Riemannian manifold unless otherwise stated.

Definition 3.2.6

Let I be an interval and $\gamma : [a, b] \rightarrow M$ be a differentiable curve. γ is called a **geodesic**, if the covariant derivative of the tangent vector $\dot{\gamma}$ vanishes everywhere, i.e.

$$\frac{D}{ds} \dot{\gamma}(s) = 0. \quad (3.2.14)$$

Geodesics are local minimiser of the energy functional

$$E(\alpha) = \frac{1}{2} \int_a^b g(\dot{\alpha}(t), \dot{\alpha}(t)) dt, \quad (3.2.15)$$

where $\alpha : [a, b] \rightarrow M$ is a C^1 -curve. Let $I_\epsilon = (-\epsilon, \epsilon)$, $\epsilon > 0$, be an interval and $\gamma : [a, b] \rightarrow M$ be a geodesic. For every **variation** $c : I_\epsilon \times [a, b] \rightarrow M$ with $c(0, \cdot) = \gamma$, $c(\xi, a) = \gamma(a)$, $c(\xi, b) = \gamma(b) \forall \xi \in (-\epsilon, \epsilon)$, we must have that

$$\frac{d}{d\xi} E(c(\xi, \cdot))|_{\xi=0} = 0. \quad (3.2.16)$$

The theorem of Hopf and Rinow states that two arbitrary points in a complete Riemannian manifold can be joined by a global minimiser of the energy functional. This minimiser is a geodesic. The uniqueness can not be guaranteed in all cases. In local coordinates, employing a local parametrisation f of M , we have

$$f((x_1(s), \dots, x_n(s))) = \gamma(s), \quad (3.2.17)$$

which leads to the geodesic differential equations,

$$\ddot{x}_k(s) + \Gamma_{ij}^k \dot{x}_i(s) \dot{x}_j(s) = 0. \quad (3.2.18)$$

The theory of geodesics can be applied to measure distances on manifolds. The **exponential map** can now be defined as follow. Let $v \in T_p M$ and $\gamma : [0, 1] \rightarrow M$ be a geodesic with $\gamma(0) = p$ and $\dot{\gamma}(0) = v$ then $\exp_p(v) := \gamma(1)$. \exp_p operates on the tangent space $T_p M$ without further restrictions in case M is complete.

It is known that differentiable manifolds and submanifolds can be represented in different ways. Nash proved a fundamental theorem that says:

Theorem 3.2.1

Every Riemannian manifold can be isometrically embedded into \mathbb{R}^n where n must be sufficiently large.

Nash states in his theorem that a Riemannian manifold M corresponds to a manifold $\widetilde{M} \subset \mathbb{R}^n$, where \widetilde{M} is the image of a bijective map $\phi : M \rightarrow \mathbb{R}^n$ such that for all $p, q \in M$

$$d_M(p, q) = d_{\widetilde{M}}(\phi(p), \phi(q))$$

holds.

Example 3.2.3

Assume there exists a function $h : U \subset \mathbb{R}^3 \rightarrow \mathbb{R}$ with **regular value** 0, which means that for ever $x^* \in h^{-1}(0)$, $\nabla h|_{x^*} \neq 0$. Then

$$M = \{x \in \mathbb{R}^3 \mid h(x) = 0\}$$

is a Riemannian manifold. Locally M is the graph of a height function. That seems crucial in the context of the geodesic equations in the sense of example 3.2.1. Let for example $h_3(x^*) \neq 0$. In a neighbourhood of the point $x^* = (x_1^*, x_2^*, x_3^*)$ the function h

has a gradient with non vanishing third component, since h is continuously differentiable. Then by the implicit function theorem there exists a neighbourhood U of the point (x_1^*, x_2^*) and a smooth function $g : U \rightarrow \mathbb{R}$ that meets

$$h(x_1, x_2, g(x_1, x_2)) = 0.$$

Implicit differentiation yields

$$\begin{aligned} g_1 &= -\frac{h_1}{h_3}, \\ g_2 &= -\frac{h_2}{h_3}. \end{aligned}$$

Note that higher order derivatives of g can be obtained in a similar fashion. This result can be generalised to hypersurfaces of arbitrary dimension in implicit representation. With the partial derivatives of g we can compute the Christoffel symbols like in example 3.2.1.

In some cases it is advantageous to use the **implicit geodesic differential equations** instead of calculating the Christoffel symbols like in example 3.2.3. We will explain this for the case $n = 2$. Since the curve c is wanted to be arc length parametrised with vanishing geodesic curvature, the following conditions must be met:

$$\langle \nabla h, c'' \rangle = -c'^T \cdot \text{Hess}(h) \cdot c', \quad (3.2.19)$$

$$\langle c', c'' \rangle = 0, \quad (3.2.20)$$

$$\langle \nabla h \times c', c'' \rangle = 0. \quad (3.2.21)$$

(3.2.19) can be obtained by implicit differentiation of $h(c(t)) = 0$ with respect to t , whereas (3.2.20) means that c is parametrised by arc length. (3.2.21) indicates that the geodesic curvature of c is zero.

In the higher dimensional cases a little variation of the idea just presented leads to equivalent results. Since the codimension of the manifold M is 1, this yields the following decomposition

$$\mathbb{R}^n = T_p M + N_p M,$$

where $N_p M$ denotes the **normal space** of $p \in M$ with the dimension 1. We must now assure that the curvature vector c'' lies in the normal space $N_p M$, which means that

$$c''(t) = k(t)N(c(t)). \quad (3.2.22)$$

k is the normal curvature of the curve c that is a priori unknown. If $N = \frac{\nabla h}{\|\nabla h\|}$ denotes the normal vector of M , then from

$$\langle c', N \rangle = 0 \quad (3.2.23)$$

the equation

$$k' + \langle c', N'' \rangle = 0 \quad (3.2.24)$$

can be deduced by implicit differentiation of (3.2.23). Equation (3.2.22) and (3.2.24) define an explicit ordinary differential system of equations for the geodesic c on an implicit given manifold M .

3.2.1 The Curvature Tensor

Definition 3.2.7

Let $\xi \in T_p M$ and η, ρ be two vector fields on M . We will call

$$\nabla_{\xi\eta}^2 \rho := \nabla_{\xi} \nabla_{\eta} \rho - \nabla_{\nabla_{\xi} \eta} \rho$$

the **second covariant derivative** of ρ with respect to ξ and η .

Definition 3.2.8

Let $\xi, \eta \in T_p M$ and ρ be a vector field on M in a neighbourhood of p .

$$R : \begin{cases} T_p \times T_p M \times T_p M & \rightarrow T_p M \\ (\xi, \eta, \rho) & \mapsto \nabla_{\xi\eta}^2 \rho - \nabla_{\eta\xi}^2 \rho \end{cases}$$

is called **Riemannian curvature tensor** at p .

It follows immediately that there exist numbers R_{ijk}^l such that

$$R \left(\frac{\partial}{\partial x_i}, \frac{\partial}{\partial x_j} \right) \frac{\partial}{\partial x_k} = R_{ijk}^l \frac{\partial}{\partial x_l}.$$

The next proposition outlines the most important properties of the curvature tensor.

Theorem 3.2.2

Let $p \in M$ and $\xi, \eta, \rho, \mu \in T_p M$. This yields

- R is trilinear,
- $g|_p(R(\xi, \eta)\rho, \mu) = g|_p(R(\rho, \mu)\xi, \eta)$,
- $g|_p(R(\xi, \eta)\rho, \mu) = -g|_p(R(\xi, \eta)\mu, \rho)$,
- $R(\xi, \eta)\rho + R(\eta, \rho)\xi + R(\rho, \xi)\eta = 0$ and
- $R(\xi, \eta)\mu = -R(\eta, \xi)\mu$.

3.2.2 Jacobi Fields

An essential tool that describes the tangent space of tubes (a matter discussed later) is the concept of **Jacobi fields** (cf. [Gra04]). It is based on the characterisation of geodesic variations.

Definition 3.2.9

Let M be a Riemannian manifold, $I_{\epsilon} = (-\epsilon, \epsilon)$ for $\epsilon > 0$ and $\gamma : I \rightarrow M$ a geodesic. $c : I_{\epsilon} \times I \rightarrow M$ is called **geodesic variation** of γ if $c(0, s) = \gamma(s)$ and $c(t, \cdot)$ is a geodesic for all $t \in I_{\epsilon}$.

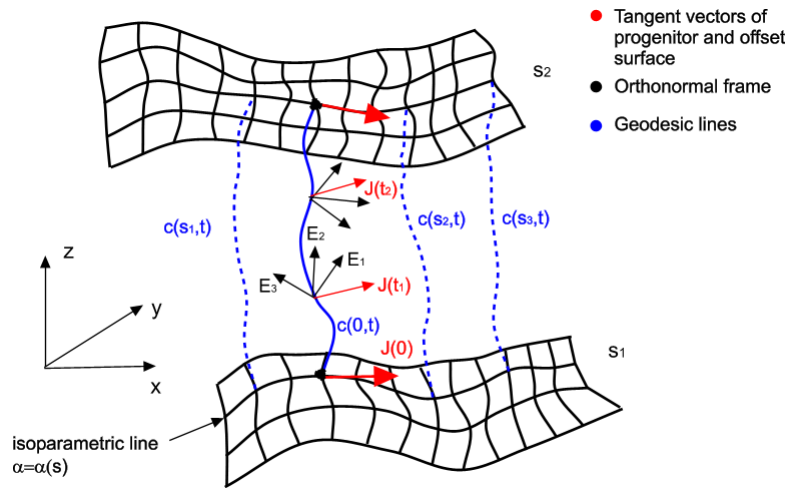


Figure 3.2: Jacobi Fields

Note that figure 3.2 uses a different notion than we use here (the roles of s and t are interchanged). If $\xi(s) = \frac{\partial}{\partial t} c(0, s)$ denotes the corresponding variation field, we have the Jacobi equations,

$$\frac{D^2}{ds^2} \xi(s) = R(\dot{c}_0, \xi) \dot{c}_0, \quad (3.2.25)$$

presuming that R denotes the curvature tensor of the manifold M . Now fix $s_0 \in I$ and let $\{e_1(s_0), \dots, e_n(s_0)\}$ be an orthonormal basis of $T_{\gamma(s_0)}$, where $e_1(s_0) = \dot{c}(s_0)$. A parallel transport of this basis yields a system $\{e_1(s), \dots, e_n(s)\}$ that is an orthonormal basis for all $s \in I$ such that $\frac{D}{ds} e_i(s) = 0$ for $i = 1, \dots, n$. Again assume $e_1(s) = \dot{c}(s)$. If

$$R(\dot{c}(s), e_j(s)) \dot{c}(s) = \sum_{k=1}^n a_j^k(s) e_k(s) \quad (3.2.26)$$

holds, the Jacobi equations can locally be rewritten as

$$\ddot{v}^k(s) = \sum_{j=1}^n a_j^k(s) v^j(s) \quad (3.2.27)$$

assuming that $\xi(s) = \sum_{j=1}^n v^j(s) e_j(s)$. This yields the known formula

$$a_j^k = \langle R(\dot{c}, e_j) \dot{c}, e_k \rangle \quad (3.2.28)$$

which for $j = k$ is just the negative of the **sectional curvature** $K(\dot{c}, e_k)$.

3.3 The Notion Of Tubes And Fermi Coordinates

As we have seen in the last subsection Riemannian manifolds have an induced distance function that measures the distance of two points by the length of the shortest curve

joining these two points. Employing the Gram-Schmidt orthonormalisation scheme an orthonormal basis $E = \{e_1, \dots, e_n\}$ of the tangent space $T_p M$ can be found for every $p \in M$. Hence, for $1 \leq j \leq n$ define functions x_j such that

$$x_j \left(\exp_p \left(\sum_{i=1}^n t_i e_i \right) \right) = t_j. \quad (3.3.1)$$

The functions x_j are often called **normal coordinates** with respect to the orthonormal basis E .

The **Fermi coordinates** are in some respect a generalisation to the normal coordinates of points. Consider a differentiable submanifold $S \subset M$ of dimension $m < n$, n being the dimension of M , and a point $p \in S$. In a neighbourhood U of the point p the submanifold S has a coordinate chart $x = (x^1, \dots, x^m)$:

$$x : U \rightarrow V \subset \mathbb{R}^m. \quad (3.3.2)$$

Moreover, $n - m$ orthonormal and differentiable vector fields E_{m+1}, \dots, E_n exist on U such that

$$\langle E_i(q), v \rangle = 0 \quad (3.3.3)$$

for every $q \in U$ and $v \in T_q S$. We will write $E_i(q) \in T_q S^\perp$ for this condition. Then the Fermi coordinates x_i are defined by the identities

$$x_i \left(\exp_q \left(\sum_{k=m+1}^n t_k E_k(q) \right) \right) = x^i(q), \quad (3.3.4)$$

$$x_j \left(\exp_q \left(\sum_{k=m+1}^n t_k E_k(q) \right) \right) = t_j, \quad (3.3.5)$$

$$(3.3.6)$$

for $i = 1, \dots, m$ and $j = m+1, \dots, n$. The Fermi coordinates yield a reparametrisation of M in a neighbourhood of S . They can be employed for the construction of **tubular hypersurfaces**.

Definition 3.3.1

If we define

$$T(S, r) = \bigcup_{p \in S} \{ \exp_p(v); v \in T_p S^\perp \text{ and } \|v\| \leq r \}, \quad (3.3.7)$$

then for $t \leq r$ the set

$$S_t = \{ m \in T(S, r); d_S(m) = t \} \quad (3.3.8)$$

is called tubular hypersurface at distance t from S . If the Fermi coordinates yield an injective parametrisation of $T(S, r)$ we can state that $S_t = \partial T(S, t)$.

3.4 Applications

In the following we will briefly describe how the shortest distance problem on surfaces can be solved using homotopy methods. Let M_0 be the graph of a function h_0 , i.e. $z = h_0(x, y)$, $p_0, q_0 \in M$ be two given surface points and $\gamma : [0, 1] \rightarrow M$ be a geodesic that joins p_0 and q_0 . Let $\{v_0, w_0\} \subset T_{p_0}M_0$ be an orthonormal system. According to the definition of normal coordinates define the function

$$g_0(s, \phi) = \exp_{p_0}(s(\cos(\phi)v_0 + \sin(\phi)w_0)).$$

Assume we have been given a family $M_\epsilon, \epsilon \in \mathbb{R}$, of surfaces such that the following identities hold:

- M_ϵ is the graph of a smooth function $h(x, y, \epsilon)$.
- $h(x, y, 0) = h_0(x, y)$ for all $(x, y) \in \mathbb{R}^2$.
- There exist smooth functions $p(\epsilon)$ and $q(\epsilon)$ such that $p(0) = p_0$ and $q(0) = q_0$.
- There exist smooth functions $v(\epsilon)$ and $w(\epsilon)$ such that $v(0) = v_0, w(0) = w_0$.
- $\{v(\epsilon), w(\epsilon)\}$ is an orthonormal basis of $T_{p(\epsilon)}M_\epsilon$ for all $\epsilon \in \mathbb{R}$.

Let

$$g(s, \phi, \epsilon) = \exp_{p(\epsilon)}(s(\cos(\phi)v(\epsilon) + \sin(\phi)w(\epsilon)))$$

denote the exponential function at $p(\epsilon)$ with respect to M_ϵ . Clearly,

$$g(s, \phi, 0) = g_0(s, \phi)$$

for all (s, ϕ) and g is a smooth function. Let (s_0, ϕ_0) be given such that

$$g(s_0, \phi_0, 0) = q_0$$

holds.

Suppose that p_0 is not conjugate to q_0 in M_0 . i.e.

$$g_\phi(s_0, \phi_0, 0) \neq 0.$$

In the following we will show that it is possible to find an $\epsilon_0 > 0$ and smooth functions

$$s, \phi : I = (-\epsilon_0, \epsilon_0) \rightarrow \mathbb{R}$$

that meet the conditions

$$\begin{aligned} g(s(\epsilon), \phi(\epsilon), \epsilon) &= q(\epsilon), \\ s(0) &= s_0, \\ \phi(0) &= \phi_0. \end{aligned}$$

Define the function

$$F(\epsilon) = g(s(\epsilon), \phi(\epsilon), \epsilon) - q(\epsilon).$$

Differentiation of the equation $F = 0$ with respect to ϵ yields

$$g_s s' + g_\phi \phi' = q_\epsilon - g_\epsilon. \quad (3.4.1)$$

Multiplication of (3.4.1) with g_s and g_ϕ respectively yields the following identities:

$$\begin{aligned} s' &= \langle g_s, q_\epsilon - g_\epsilon \rangle, \\ \phi' &= \frac{\langle g_\phi, q_\epsilon - g_\epsilon \rangle}{\|g_\phi\|^2}. \end{aligned}$$

This is a system of ordinary differential equations with smooth right hand side and initial conditions $s(0) = s_0$ and $\phi(0) = \phi_0$. For this type of equations there exist a unique solution

$$s, \phi : I = (-\epsilon_0, \epsilon_0) \rightarrow \mathbb{R}$$

for some $\epsilon_0 > 0$.

Let $M \subset \mathbb{R}^{n+1}$ be a complete smooth hypersurface and

$$\{x_i, i \in I\}$$

be a maximal C^∞ -atlas of M . Let

$$H : \begin{cases} \mathbb{R}^{n+1} \times [0, 1] & \rightarrow \mathbb{R}^{n+1} \\ (x, t) & \mapsto H(x, t) \end{cases}$$

be a smooth function for which $H(x, 1) = x$ holds for all $x \in \mathbb{R}^{n+1}$.

Definition 3.4.1

H is called **compatible with the differentiable structure** of the given manifold M , if and only if $H(M, t)$ is a smooth hypersurface and

$$\{(H(x_i^{-1}, t))^{-1}; i \in I\}$$

is a C^∞ -atlas of $H(M, t)$ for all $t \in [0, 1]$.

Example 3.4.1

$$H(x, t) = \begin{pmatrix} x_1 \\ \vdots \\ x_n \\ tx_{n+1} \end{pmatrix}$$

is compatible with the differentiable structure of a graph M and $M_t = H(M, t)$ constitutes a family of graphs.

4 Offsets And Offset Functions

The construction of medial sets being the main subject of this thesis will be based on the theory of offset functions. Gray gives some advanced remarks concerning this subject (cf. [Gra04]) in the Riemannian case. An Euclidean specialisation of offsets can be found in [PM02]. The following section presents an overview of some definitions and theorems being useful for the treatment of computational medial sets.

4.1 Difference Between Offsets And Offset Functions

Definition 4.1.1

Consider a metric space (M, d) and a closed subset $A \subset M$.

$$\text{Offset}(A, r) := \{x \in M; d(x, A) = r\}$$

is called the **offset** of A with respect to the distance r .

The definition of $\text{Offset}(A, r)$ employs the continuous distance function

$$d(x, A) := \min\{d(x, a); a \in A\}.$$

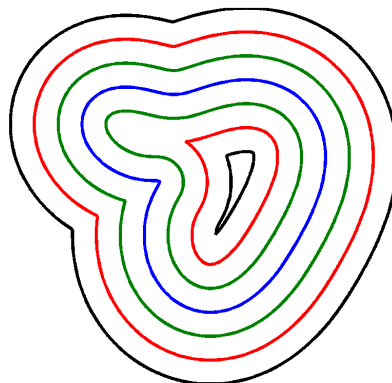


Figure 4.1: Euclidean offset of an arbitrary closed curve

Definition 4.1.1 only yields weak requirements on the construction of offsets. In this context we will not deal with such abstract metric spaces and even the set A will not be arbitrary. Figure 4.1 sketches the offset A_r of a closed curve (here indicated in blue) for different values $r = 1, 2, 3$. Note that the offset of the reference curve consists of two components, both being piecewise differentiable curves.

The construction of offsets has some very interesting but surprising phenomena. This can for example be demonstrated again by picture 4.1. Offset curves are no longer smooth curves, their tangent vector fields have discontinuities. This basically can be derived from the fact that the distance function d_A is only a continuous function. The calculation of medial sets therefore must account for this behaviour.

B possesses points p_i where a tangent vector of B is not defined. The question that arises is how these points can be characterised. In fact, all the points p_i have in common that the so called progenitor curve (blue curve) contains at least two points being globally distance minimal to p_i . We will call these points cut locus points.

Another fact is not evident at first glance. Consider again the situation of planar progenitor curves like the curve A in figure 4.1. The distance function that is responsible for the construction of the offset $\text{Offset}(A, r_1)$ employs the Euclidean metric. What happens, when the **progenitor curve** (blue curve) is embedded into \mathbb{R}^3 ? It is clear that the offset of a circle becomes a torus while it is an annulus in the plane. It is therefore indispensable to talk about triples (M, A, r) in the context of offsets with M being the metric space, A the reference (progenitor set) and r the distance. No component of this triple can be left out.

In the following we will analyse offsets for points, curves and surface in different situations. The definition of offset functions that is necessary for the computation of offsets is given as well as the justification why these functions are essential for the computation of medial sets. Only offsets in 2-dimensional and 3-dimensional manifolds are presented.

4.2 Offsets On 2-dimensional Manifolds

There are only two basic types of offsets in case the metric space M containing the progenitor set A is a surface.

4.2.1 Point Offsets

The offsets of a simple point are strongly related to the distance circles or the geodesic circles of a point. Consider a point $p \in M$ and an orthonormal basis $\{e_1, e_2\}$ of T_pM ,

i.e. the tangential space of $p \in M$. The offset function \mathcal{O}_p of p with respect to a local parametrisation f of M in a neighbourhood of p is defined as

$$f(\mathcal{O}_p(s, \phi)) := \exp_p(s \cdot (\cos(\phi)e_1 + \sin(\phi)e_2)). \quad (4.2.1)$$

$\phi \in [0, 2\pi)$ corresponds to a rotation of the vector e_1 in the tangential space. Indeed, the definition of the offset function depends on the choice of the orthonormal basis, however all such offset functions should strive for the same goal. The corresponding system $\{x_1, x_2\}$ of normal coordinates is given through

$$\begin{aligned} x_1(f(\mathcal{O}_p(s, \phi))) &= s \cos(\phi), \\ x_2(f(\mathcal{O}_p(s, \phi))) &= s \sin(\phi). \end{aligned}$$

Figure 4.2 shows an example of some offset circles.

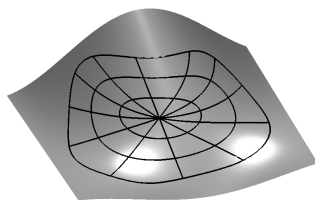


Figure 4.2: Geodesic offset of a point

Theorem 4.2.1

Let A be a singleton only consisting of the element p and let f be a parametrisation of M in a neighbourhood of p . If $x \in \text{Offset}(A, r)$, where r is sufficiently small, then there exists a $\phi_0 \in [0, 2\pi)$ such that

$$f(\mathcal{O}_p(r, \phi_0)) = x \quad (4.2.2)$$

holds.

Proof: This can be deduced from the completeness of the surface M .

□

4.2.2 Offsets of Curves

The construction of curve offsets yields a proper coordinate system on the surface and a smooth normal vector field $N : M \rightarrow NM$. Let $\alpha : I \rightarrow M$ be an arc length

parametrised surface curve and f a local parametrisation of M in a neighbourhood of $\alpha(t_0)$. Then for sufficient small s the offset function \mathcal{O}_α meets the condition

$$f(\mathcal{O}_\alpha(s, t)) = \exp_{\alpha(t)}(s(N(\alpha(t)) \times \alpha'(t))). \quad (4.2.3)$$

There is a slight difference in the treatment of offsets of closed and non-closed curves.

Theorem 4.2.2

Let $A = \{\alpha(t); t \in I = [0, 1]\}$, $p \in \text{Offset}(A, r)$ and f a parametrisation of M in a neighbourhood of p . Then for sufficiently small r we have

- If α is closed, smooth and $\alpha'(0) = \alpha'(1)$ then there exists $t_0 \in I$ such that

$$p = f(\mathcal{O}_\alpha(r, t_0)) \quad \text{or} \quad p = f(\mathcal{O}_\alpha(-r, t_0)). \quad (4.2.4)$$

- If α is smooth but not closed and none of the conditions in (4.2.4) are satisfied, then one of the subsequent requirements must hold for $\phi_0 \in [0, 2\pi)$:

$$p = f(\mathcal{O}_{\alpha(a)}(r, \phi_0)) \quad \text{or} \quad p = f(\mathcal{O}_{\alpha(b)}(r, \phi_0)). \quad (4.2.5)$$

Proof: These results can be derived by closer inspection of the function

$$f(t) = d(p, \alpha(t)).$$

f has a local minimum at t_{min} if $f'(t_{min}) = 0$. This immediately leads to one of the conditions under (4.2.4). It is however possible, that f takes its minimum value at the boundary of the interval I . Then the conditions under (4.2.5) must hold.

□

Figure 4.3 sketches the geodesic offsets of a curve on a graph M

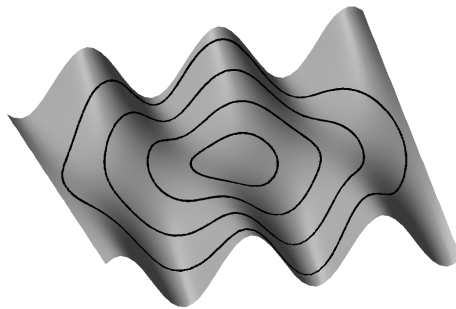


Figure 4.3: Geodesic offset of a curve

4.3 Offsets On 3-dimensional Manifolds

In the case of 3-dimensional manifolds three important types of offsets arise, the offsets of points, curves and surfaces.

4.3.1 Offsets of Points

The situation is similar to the offsets of points on 2-dimensional manifolds described in the last subsection. Given a point $p \in M$ and an orthonormal basis $\{e_1, e_2, e_3\}$ of the tangential space $T_p M$ the definition of the offset function is simply

$$f(\mathcal{O}_p(s, \phi, \psi)) = \exp_p(s(\cos(\phi) \cos(\psi)e_1 + \cos(\phi) \sin(\psi)e_2 + \sin(\phi)e_3)).$$

Again the definition depends on the basis vectors. \mathcal{O}_p is defined on the parameter domain $\mathbb{R}_{\geq 0} \times [-\frac{\pi}{2}, \frac{\pi}{2}] \times [0, 2\pi]$. The next theorem is almost equal to theorem 4.2.1.

Theorem 4.3.1

Let A be a singleton only consisting of the element $p \in M$ and let f be a parametrisation of M in a neighbourhood of p . If $x \in \text{Offset}(A, r)$, where r is sufficiently small, then there exists a $\psi_0 \in [0, 2\pi]$ and $\phi_0 \in [-\frac{\pi}{2}, \frac{\pi}{2}]$ such that

$$f(\mathcal{O}_p(r, \phi_0, \psi_0)) = x \tag{4.3.1}$$

holds.

Proof: This can be deduced from the completeness of the surface M . □

An example of an offset sphere is illustrated on page 98.

4.3.2 Offsets of Curves

Consider a 3-dimensional hypersurface M and an arc length parametrised space curve $\alpha : I \rightarrow M$. The vector $E_1(t) := \frac{d}{dt}\alpha(t)$ is the unit tangent vector of the space curve α . We call α **regular** of order $k \leq n$, if and only if the vectors

$$\frac{d}{dt}\alpha(t), \frac{D}{dt} \frac{d}{dt}\alpha(t), \dots, \frac{D^{k-1}}{dt^{k-1}} \frac{d}{dt}\alpha(t) \tag{4.3.2}$$

are linear independent. For $2 \leq i \leq k$ define

$$\tilde{E}_i(t) := \frac{D^{i-1}}{dt^{i-1}} \frac{d}{dt}\alpha(t) + \sum_{j=1}^{i-1} \left\langle E_j(t), \frac{D^{i-1}}{dt^{i-1}} \frac{d}{dt}\alpha(t) \right\rangle E_j(t), \tag{4.3.3}$$

$$E_i(t) := \frac{\tilde{E}_i(t)}{\|\tilde{E}_i(t)\|}. \tag{4.3.4}$$

The above scheme yields an Gram-Schmidt orthonormalisation of the aforementioned frame under (4.3.2). The vectors E_i , $i = 1, 2, 3$, will be used for the construction of the offset function. They have similar properties like the Frenet frame. The functions $t \mapsto E_i(t)$ are differentiable functions. The offset function \mathcal{O}_α can now be defined in a neighbourhood of $\alpha(t_0)$ by

$$f(\mathcal{O}_\alpha(s, t, \phi)) = \exp_{\alpha(t)}(s(\cos(\phi)E_2(t) + \sin(\phi)E_3(t))), \quad (4.3.5)$$

using a local parametrisation $f : V \subset \mathbb{R}^3 \rightarrow U$ of M . Thus, the last identity only holds for small parameters s and $t \in (t_0 - \epsilon, t_0 + \epsilon)$. For the Fermi coordinates one can simply deduce

$$x_1 = t, \quad x_2 = s \cos(\phi), \quad x_3 = s \sin(\phi). \quad (4.3.6)$$

Figure 4.4 shows the tubular hypersurface S_r of a curve α with respect to the distance value r .

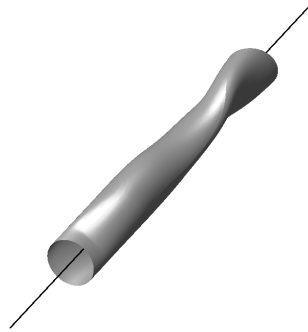


Figure 4.4: Tubular hypersurface

Without going into detail note that similar results like in the case Case 1, 2 and 3 can be deduced for $p \in \text{Offset}(A, r)$, for A being a curve.

4.3.3 Offsets of Surfaces

Let M be a 3-dimensional complete hypersurface and $S \subset M$ a 2-dimensional submanifold of M . Let $p \in S$ be an arbitrary point on S and

$$x : U \subset S \rightarrow V \subset \mathbb{R}^2$$

a coordinate chart of S in a neighbourhood U of p . Since S is a hypersurface, a normal vector field $N : U \rightarrow NS$ along S can be defined in a neighbourhood of p . If f denotes a local parametrisation of M in a neighbourhood of p then

$$f(\mathcal{O}_S(s, x(p))) = \exp_p(sN(p))$$

holds for sufficiently small values s .

Remark 4.3.1

- Typically N can be computed using a generalisation of the cross product in \mathbb{R}^3 .
- Again for $A \subset M$ being a surface and $p \in \text{Offset}(A, r)$ an analogous result like in Case 1, 2 and 3 can be obtained.
- The family of offset spheres of a point $p \in M$ already represents a family of offset surfaces of one of these spheres.

4.4 Focal Sets

An imprecise definition of focal sets would make use of the offset function itself. A definition however should not exhibit such deficiencies.

Definition 4.4.1

Let $S \subset M$ be a Riemannian submanifold with $\dim(S) < \dim(M)$. Let $p \in S$ and $\gamma : I = [0, 1] \rightarrow M$ be a geodesic with $\gamma(0) = p$ and $\gamma'(0) \in T_p S^\perp$. $q = \gamma(1)$ is called **focal point** along γ , if a non-trivial Jacobi field $J : I \rightarrow TM$ along γ exists such that $J(0) \in T_p(S)$ and $J(1) = 0$ holds.

A more classical approach is the concept of conjugate points.

Definition 4.4.2

Let $\gamma : I \rightarrow M$ be a geodesic. $\gamma(t_1)$ and $\gamma(t_2)$, $t_1 \neq t_2$, $t_i \in I$, are called **conjugate points** along γ , if a non-trivial Jacobi-field $J : I \rightarrow TM$ along γ exists such that $J(t_1) = 0$ and $J(t_2) = 0$ holds.

The subsequent lemma originates is a classical result from differential geometry and can be found in almost every textbook.

Lemma 4.4.1

Let M be a Riemannian manifold and $\gamma : [a, b] \rightarrow M$ be a geodesic. If there exists a $t_0 \in (a, b)$ such that $\gamma(t_0)$ is conjugate to $\gamma(a)$, then γ can not be the shortest geodesic join between $\gamma(a)$ and $\gamma(b)$.

In fact, there is another possibility for a geodesic γ to lose the property of being a shortest join to a reference set. This is the case when there exist at least two different joins to the reference set. However, only these two cases can occur.

In addition to the concepts of medial sets we will explain the difference of the cut locus and the symmetry set of a reference set. Therefore, we give a first definition of symmetry points.

Definition 4.4.3

Let M be a Riemannian manifold and $S \subset M$ be a submanifold. Let p be a point in M that is not contained in S . p is called a **symmetry point**, if there exist two points $w_1, w_2 \in S$ such that the function

$$\rho : \begin{cases} S & \rightarrow \mathbb{R}_{>0} \\ x & \mapsto d(x, p) \end{cases} \quad (4.4.1)$$

has a local minimum in w_1 and w_2 with $\rho(w_1) = \rho(w_2)$. The set of all symmetry points is called **symmetry set**.

We can compare the symmetry set with the so called **cut locus**.

Definition 4.4.4

The cut locus is the subset of the symmetry set where the corresponding function ρ from (4.4.1) has a global minimum.

The symmetry set and the cut locus need to be distinguished for a reliable medial axis computation. Consider for example the parabola $S = \{(x, y) \in \mathbb{R}^2 \mid y = x^2\}$. It can be shown that the cut locus of S consists of the points

$$C_S = \left\{ (0, t) \mid t \geq \frac{1}{2} \right\}.$$

Figure 4.5 sketches the parabola together with the cut locus (red) and the focal set (green). The cut locus and the focal set intersect at $p = (0, \frac{1}{2})$. This is a point where the cut locus ends and the radius of the circle of curvature of the parabola has a global minimum. Every circle in p with radius greater than $\frac{1}{2}$ intersects with the parabola in more than one point. This is only one reason why focal points play a key role for reliable computations.

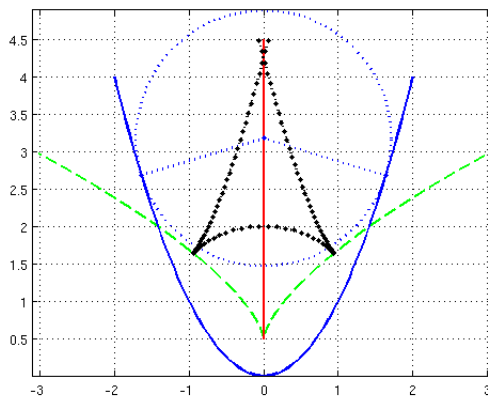


Figure 4.5: Parabola and its cut locus

The following theorem was proved by Rausch in his PhD thesis (cf. [TR99]). It uses the focal radius of a point on a submanifold being defined later in this thesis.

Theorem 4.4.1

Let $M \subset \mathbb{R}^3$ be a Riemannian hypersurface of dimension 2 and α a regular parametrised surface curve. Let $p \in M$ be a point and $r > 0$ be given such that the geodesic circle $K(p, r)$ around p is tangent to α in a point q . If r coincides with the focal radius of the point q and p is a nearest conjugate point of q , then K and α have the same geodesic curvature in q except for their signs.

The local parametrisation of medial sets can be achieved by implicit parametrisation employing the medial equations. They can be defined for arbitrary progenitor objects.

Definition 4.4.5

Let A and B be two compact progenitor objects, $A, B \subset M$. Put

$$F : \begin{cases} M & \rightarrow & \mathbb{R} \\ x & \mapsto & d_A(x) - d_B(x) \end{cases} .$$

Then the zeros of F are called **symmetry points** and the equation $F = 0$ is called **medial equation**.

The focal sets of submanifolds of the Euclidean spaces are well understood. The discussion of the focal set automatically leads to the principal curvature values of the corresponding tubes.

4.4.1 Curvature Computations Of Euclidean Tubes

We begin with the study of planar curves.

Focal sets of planar curves

Let $\alpha : I \rightarrow \mathbb{R}^2$ be an arc length parametrised curve representing the progenitor set $A = \alpha(I)$. Consider a fixed distance value $r > 0$ and a point $p \in \text{Offset}(A, r)$. Assume p is a point of the tubular hypersurface A_r being defined under 3.3.1. Then A_r can locally be parametrised by

$$\alpha_r(t) = \alpha(t) + rN(t),$$

where N is a normal vector of α . The tangent direction of α_r fulfils the condition

$$\alpha'_r(t) = \alpha'(t)(1 - rk(t)). \tag{4.4.2}$$

k is the curvature of α in $\alpha(t)$. This is mainly the Frenet formula for the planar case.

The Weingarten map is substantial for the computation of the the principal curvature values.

Definition 4.4.6

Let $M \subset \mathbb{R}^{n+1}$ be a hypersurface of dimension n and $p \in M$. Let f be a local parametrisation of M in a neighbourhood of p and N a local parametrisation of a normal vector field of M in a neighbourhood of p with Jacobi matrix DN . Then the map

$$S : \begin{cases} T_p M & \rightarrow & T_p M \\ Df \cdot v & \mapsto & DN \cdot v \end{cases} \quad (4.4.3)$$

is called **Weingarten map**.

For the definition of the Weingarten map we used that every tangent vector w in $T_p M$ is a linear combination of the vectors $f_i = \frac{\partial}{\partial x_i} f$. Hence, w can be rewritten in the form $w = Df \cdot v$ for some $v \in \mathbb{R}^n$. The linear operator S is symmetric and has therefore only real eigenvalues. The eigenvalues of S correspond to the principal curvature values of M .

Again using the Frenet formulae, application of the Weingarten map S to the local offset curve α_r shows

$$S\alpha'_r = N' = -k\alpha' = -\frac{k}{1-rk}\alpha'_r.$$

This implies that

$$k_r(t) = \frac{k(t)}{1-rk(t)}$$

is the curvature of α_r . Let $k(t) \neq 0$. Then $\alpha(t)$ has a focal point in $\alpha_{\frac{1}{k(t)}}(t)$.

Focal sets of hypersurfaces

Similarly, the principal curvature values of offset surfaces can be obtained. Let $M \subset \mathbb{R}^3$ be a hypersurface, $p \in M$ and f a local parametrisation of M in a neighbourhood of p . Let $q \in M_r$ for sufficient small $r > 0$. Then a local parametrisation of M_r in a neighbourhood of q can be expressed in the form

$$f_r(x_1, x_2) = f(x_1, x_2) + rN(x_1, x_2),$$

where N denotes a local parametrisation of a normal vector field of M in a neighbourhood of p . Without loss of generality assume that f is parametrised in such a way that the partial derivatives of f correspond to the principal curvature directions of M in p . This can be achieved by linear transformation of the parameter space of f . Using the aforementioned assumption we get

$$S \frac{\partial}{\partial x_1} f = -k_1 \frac{\partial}{\partial x_1} f = \frac{\partial}{\partial x_1} N$$

where S denotes the Weingarten map of M in p . k_1 and k_2 are the principal curvature values of S in p . This yields

$$\frac{\partial}{\partial x_1} f_r = \frac{\partial}{\partial x_1} f + r \frac{\partial}{\partial x_1} N = \frac{\partial}{\partial x_1} f \cdot (1 - rk_1).$$

If \tilde{S} denotes the Weingarten map of M_r in q , we obtain

$$\tilde{S} \frac{\partial}{\partial x_1} f_r = \frac{\partial}{\partial x_1} N = -k_1 \frac{\partial}{\partial x_1} f = -\frac{k_1}{1 - rk_1} \frac{\partial}{\partial x_1} f_r.$$

The principal curvature values of M at p are the negative eigenvalues of the Weingarten map, hence

$$\lambda_i = \frac{k_i}{1 - rk_i}.$$

Note that the focal points can be identified similarly to case 1.

Focal sets of space curves

Let $\alpha : I \rightarrow \mathbb{R}^3$ be an arc length parametrised space curve and $A = \alpha(I)$. The Frenet frame T, N and B ¹ of the curve α yields a natural representation of the offset function. Let $p = \alpha(t)$ and $q \in A_r$ for $r > 0$ sufficiently small. The tube A_r can be locally parametrised by a map f^r in a neighbourhood of q by

$$f^r(x_1, x_2) = \alpha(x_1) + r \cos(x_2)N(x_1) + r \sin(x_2)B(x_1).$$

The following steps are necessary for the computation of the principal curvature values of A_r :

- Determine the first fundamental tensor $G = (g_{ij})$, where $g_{ij} = \langle f_i, f_j \rangle$.
- Determine the second fundamental tensor $L_{ij} = \langle f_{ij}, n \rangle$, where n is a normal vector of A_r in q .

The Weingarten matrix $S = G^{-1}L$ is then a lower triangular matrix and the principal curvature values are given through:

$$\begin{aligned} \lambda_1 &= \frac{k \cos(\phi)}{1 - rk \cos(\phi)}, \\ \lambda_2 &= -\frac{1}{r}. \end{aligned}$$

Observe that the normal vector n can be defined by

$$n = -\cos(\phi)N - \sin(\phi)B.$$

4.4.2 Equations Of Riccati Type

The principal curvature values of tubes, which is also a result from classical differential geometry, can be obtained using the curvature tensor and the concept of Jacobi fields. It can be used in the context of the medial axis inverse transform.

¹ T is the tangent vector of α , N the normal vector and B the binormal

Definition 4.4.7

A smooth function $f : M \rightarrow \mathbb{R}$ is called **generalised distance function**, if the length of the gradient is 1 everywhere.

The definition of the generalised distance function implies that the level sets

$$N_s := \{x \in M; f(x) = s\}, \tag{4.4.4}$$

are hypersurfaces of dimension n , if M has dimension $n + 1$. The main principal curvature values of N_s are the negative eigenvalues of the Weingarten map. Moreover, the vector $\nu_x := \text{grad}_x f$ is a normal vector on $N_{f(x)}$. We get the Weingarten map

$$S_x : T_x N_s \rightarrow T_x N_s, \quad S_x(\xi) = -\nabla_\xi \nu = -\nabla_\xi \text{grad} f. \tag{4.4.5}$$

Equivalently, the eigenvalues of the Hessian matrix of f represent the principal curvature values of N_s as well. The behaviour of the Weingarten matrix can be described by an ordinary differential equation of Riccati type.

Theorem 4.4.2

Using the notation

$$R_\nu : \begin{cases} T N_s & \rightarrow & T N_s \\ \xi & \mapsto & R(\xi, \nu)\nu \end{cases} \tag{4.4.6}$$

the identity

$$\nabla_\nu S = R_\nu + S^2 \tag{4.4.7}$$

holds.

One can apply this theorem on the Medial Axis Inverse Transform to obtain the principal curvature values of the so called envelope which simply represents the boundary of a reconstructed solid that is described by its medial axis and its radius function.

Remark 4.4.1

The Riccati equation builds up a non-autonomous differential equation of a matrix, since the curvature tensor depends differentiable on the coordinates of the geodesic point $\gamma(s)$.

4.4.3 Computation Of Focal Sets

In this section we focus on the determination of focal points of point offsets. In Euclidean spaces the corresponding focal sets are empty. This must not hold for point offsets on Riemannian manifolds. The most famous example on this subject is reflected by the sphere S^2 , where every point is counjugate to the corresponding diametral point. Let M be a Riemannian manifold and $p \in M$ be a point of this manifold. We need the following

Definition 4.4.8

The **focal radius** s_f of a point p is meant to be the geodesic distance of the nearest conjugate point:

$$s_f := \min_{q \in M} \{d(p, q); q \text{ is conjugate to } p\}.$$

Let $E^1 = \{e_1^1, \dots, e_N^1\}$ be an orthonormal basis of the tangent space $T_p M$ and

$$S_{N-1} = \{x \in \mathbb{R}^n; \|x\|_2 = 1\}$$

be the unit sphere in \mathbb{R}^n . Every $x \in S_{N-1}$ identifies an arc length parametrised geodesic γ with the properties

- $\gamma(0, x) = p$,
- $\gamma'(0, x) = \sum_{i=1}^N x_i e_i$.

For $v \in T_p M$ let ξ_x^v denote the Jacobi vector field along the geodesic γ such that

$$\begin{aligned} \xi^v(0, x) &= 0, \\ \frac{D}{ds} \xi^v(0, x) &= v, \\ \frac{D^2}{ds^2} \xi^v(s, x) &= R(\dot{\gamma}(s), \xi^v(s, x)) \xi^v(s, x) \end{aligned}$$

holds. For fixed values $x \in S_{N-1}$ and $s \in \mathbb{R}$ the map $v \mapsto \xi^v(s, x)$ is a linear map which can simply be deduced from the Jacobi equations. The vector $v \in T_p M$ corresponds to a component vector (v_1, \dots, v_N) with respect to the basis E^1 and the aforementioned linear map corresponds to a $N \times N$ -matrix $T(s, x)$ with respect to this basis. Let $E^2 = \{e_1^2, \dots, e_N^2\}$ be an orthonormal basis of $T_{\gamma(s, x)}$. If $\xi^v(s, x)$ has the components $(\xi^{v,1}(s, x), \dots, \xi^{v,N}(s, x))$ with respect to E^2 then $T(s, x)$ can completely be described by the equation

$$T(s, x) \begin{pmatrix} v_1 \\ \vdots \\ v_N \end{pmatrix} = \begin{pmatrix} \xi^{v,1}(s, x) \\ \vdots \\ \xi^{v,N}(s, x) \end{pmatrix}. \quad (4.4.8)$$

With the above notations we can define the function

$$F(s, x) = \left(\frac{\det T(s, x)}{\|x\|^2 - 1} \right).$$

F plays the key role for the computation of the focal set of p . The point $q \in M$ is a focal point if and only if there exists a geodesic γ with the following properties

$$\begin{aligned} \gamma(0, x) &= p, \\ \gamma(s, x) &= q, \\ \gamma'(0, x) &= \sum_{i=1}^N x_i e_i, \\ F(s, x) &= 0. \end{aligned}$$

This definition of focal points does not depend on the special choice of the basis E^1 and E^2 . For an explicit parametrisation of the zero set of F our main goal lies in the determination of the gradient of $\det T(s, x)$. Since \det is a multilinear map it suffices to compute only the derivatives $\frac{\partial}{\partial s}T(s, x)$ and $\frac{\partial}{\partial x_i}T(s, x)$. This is however the crucial factor of our computations. To avoid this it is e.g. possible to apply **PL Continuation Methods** being described in [AG03] (chapter 15).

4.5 Approximation Of Offset Functions

For accurate and reliable computations of medial sets it is of the utmost significance to use adaptive integration methods of the medial equations that heavily involve the (implicit) geodesic equations. A parametrisation of the face of a Voronoi region for example will not only employ the geodesic equations but also the Jacobian equations and related for the detection of so called focal points. The evaluation of the geodesic equations is time consuming in case of highly curved hypersurfaces, when adaptive integration methods are used. For real time applications it is not advisable to integrate the geodesic equations in every time step. It is more convenient to precompute a discrete version of the offset function on a **regular grid**

$$G = \left\{ (x_1, \dots, x_n) \mid x_i = a_i + \frac{j_i}{n_i}(b_i - a_i), j_i = 0, \dots, n_i \right\}.$$

Then all partial derivatives of the offset function can be approximated when we employ the central difference quotient from chapter 2.2. Subsequent usage of the Newton method will improve the numerical results when it is required. For the Newton method however the exact offset function has to be employed again.

5 Medial Axis Inverse Transformation

Let M be a Riemannian manifold of dimension n . Given a compact subset $K \subset M$ the medial axis of K is of special interest in lots of applications. We give the following definition of the medial axis.

Definition 5.0.1

The **medial axis** $MA(K)$ of K consists of all the points $p \in K$ such that there exists a maximal ball $B(p, r(p)) \subset K, r(p) > 0$. $B(p, r)$ is called **maximal** if and only if no $q \in K$ and $\tilde{r} > 0$ exist such that

$$B(p, r(p)) \subsetneq B(q, \tilde{r}) \subset K.$$

The definition of a ball employs the **Riemannian distance** function

$$d(p, q) = \inf \{L[c] ; c \in C^1([a, b], M), c(a) = p, c(b) = q\}$$

of the Riemannian manifold. Note that L specifies the length of differentiable curves due to:

$$L[c] = \int_a^b \|\dot{c}(t)\| dt.$$

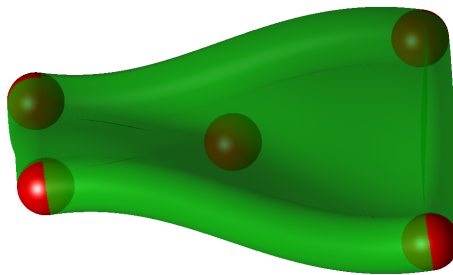


Figure 5.1: Medial axis inverse transform of a surface

Figure 5.1 points up a typical configuration of maximal balls inside a compact set K . The pair $(MA(K), r)$ with the associate radius function

$$r : MA(K) \rightarrow \mathbb{R}_{\geq 0}$$

is called **medial axis transformation** whereas the reconstruction of the set K according to

$$K = \bigcup_{p \in MA(K)} B(p, r(p)) \quad (5.0.1)$$

is called **medial axis inverse transformation**. Note that this reconstruction is possible under some very weak conditions. We will focus on the special case where $MA(K)$ is a C^k -submanifold of dimension $n - 1$ and where

$$r : MA(K) \rightarrow \mathbb{R}_{\geq 0}$$

is a k -times continuously differentiable function. Since we must employ the geodesic equations only for the reconstruction it will be of great use to apply adaptive integration methods that account for dedicated curvature criterions. If this is assured highly accurate results can be expected.

Remark 5.0.1

If K has C^2 -boundary, then $MA(K)$ is a **deformation retract** of K , which means that there exists a retract function

$$R : K \setminus \partial K \rightarrow MA(K) \setminus \partial K$$

and a **homotopy** $f : K \setminus \partial K \times [0, 1] \rightarrow K \setminus \partial K$ such that

- $f(p, 0) = p$ for all $p \in K \setminus \partial K$,
- $f(p, 1) = R(p)$ for all $p \in K \setminus \partial K$,
- $f(p, t) = p$ for all $p \in MA(K), t \in [0, 1]$

A detailed discussion of this issue can be found in [Wol92].

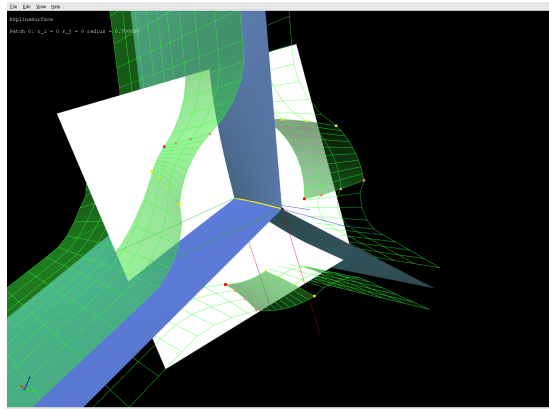


Figure 5.2: Medial axis of an object

In almost every application the medial axis $MA(K)$ consists of a union of sets S_i , i.e.

$$MA(K) = \bigcup_{i=1}^m S_i,$$

where every S_i denotes a bordered and bounded submanifold of dimension $n - 1$, when n denotes the dimension of M . The case $m > 1$ was studied by Guido Böttcher in this diploma thesis [Boe04] in Euclidean geometry. Figure 5.2 sketches a result of the inverse transform. A sharper look at the reconstruction scheme will show that this scheme does not depend on the number m of bordered submanifolds S_i . We will therefore focus on the case $m = 1$.

First of all we recall some important facts concerning the generalised distance function which is defined as follows:

Theorem 5.0.1

Let M be a Riemannian manifold and $K \subset M$ be a compact subset. The function

$$d_K(x) = d(K, x) = \min_{p \in K} d(p, x)$$

is a generalised distance function.

We claim that the gradient of d_K has length 1. Since K is compact, we can find a point $p_0 \in K$ such that $d_K(x) = d(x, p_0)$. If d_K is differentiable at x p_0 is unique and there exists an arc length parametrised geodesic $\gamma : [0, d] \rightarrow M$ with $\gamma(0) = p_0$ joining x and p_0 starting from p_0 . Because $d_K(\gamma(t)) = t$ we get

$$\partial_{\dot{\gamma}(d_K(x))} d_K = \frac{d}{dt} d_K(\gamma(t))|_{t=d_K(x)} = \frac{d}{dt} t|_{t=d_K(x)} = 1. \quad (5.0.2)$$

It immediately follows that $\|\text{grad}_x d_K\| \geq 1$. For another $\eta \in T_x M$ with $\|\eta\| = 1$ it exists an arc length parametrised curve $\alpha : (-\epsilon, \epsilon) \rightarrow M$ satisfying $\alpha(0) = x$ and $\dot{\alpha}(0) = \eta$. In order to estimate an upper limit for $\text{grad}_x d_K$ an upper limit for the difference quotient has to be found:

$$\begin{aligned} d_K(\alpha(s)) &= d(K, \alpha(s)) \\ &\leq d(K, x) + d(x, \alpha(s)) \\ &\leq d_K(x) + s \end{aligned}$$

The last equation indicates that $\frac{d_K(\alpha(s)) - d_K(x)}{s}$ is bounded by 1, but since this term converges to $\langle \text{grad}_x d_K, \eta \rangle$ for $s \rightarrow 0$ the postulated property of the generalised distance function holds.

Remark 5.0.2

(5.0.2) says that the gradient of the generalised distance function at a point x points in the direction of the unique geodesic joining the nearest point in K with x . This fundamental concept will be of great use within the next chapters.

Remark 5.0.3

The above result was proven by Wolter in a more generalised context in [Wol85].

5.1 2D Medial Axis Inverse Transform

Assume a complete 2-dimensional Riemannian manifold is given as well as local parametrisation functions $m_j : I_j \rightarrow M$ of all related subarcs of the medial axis of a compact domain $\Omega \subset M$. Let $r_j : I_j \rightarrow \mathbb{R}_{\geq 0}$ denote the corresponding radius functions. One important question naturally appears in the context of the medial axis inverse transform. For arbitrary parametrisation functions m_i and positive radius functions r_i does there exist a domain Ω having exactly this medial axis transform? One striking criterion for proper functions m_i would be that they cannot have double points. Several considerations have to be involved to answer the main question from above appropriately. A major difficulty for example arises from the fact that it is not allowed that a certain disc $B(m_i(t), r_i(t))$ intersects with the boundary curve at a point $p \in \partial\Omega$. So a naive implementation of the subsequent reconstruction scheme would then probably lead to topological inconsistencies like self intersections of boundary curve segments.

Let $m : I = [a, b] \rightarrow M$ be a regular parametrisation of $MA(\Omega)$ near $x \in MA(\Omega)$. Suppose $B(m(t), r(t))$ touches the **envelope** of $MA(\Omega)$ at points $p_1, p_2 \in \partial\Omega$ such that

- $d(p_1, m(t)) = d(p_2, m(t)) = r(t)$,
- $d(p, m(t)) \geq r(t) \forall p \in \partial\Omega$.

Accordingly, there exist two arc length parametrised geodesics $\gamma_i : [0, r(t)] \rightarrow M$ with the following properties:

1. $\gamma_i(0) = p_i$.
2. $\gamma_i(r(t)) = m(t)$,
3. γ_i is distance minimal.

Let α denote the parametrisation of the segment of the envelope in the neighbourhood of p_1 . The next goal is to find the direction $\gamma_1'(r(t))$ to obtain the boundary point p_1 . Let $f : U \rightarrow M$ be a parametrisation of M in a neighbourhood of $m(t)$ and \mathcal{O}_α be the offset function of α with respect to f . Differentiation of

$$f(\mathcal{O}_\alpha(r(t), t)) = m(t)$$

with respect to t provides the equation

$$Df \left(\frac{\partial}{\partial s} \mathcal{O}_\alpha r'(t) + \frac{\partial}{\partial t} \mathcal{O}_\alpha \right) = m'(t). \quad (5.1.1)$$

Knowing that

$$\begin{aligned} \|\gamma_1'\| &= 1, \\ \gamma_1'(r(t)) &= Df \frac{\partial}{\partial s} \mathcal{O}_\alpha \quad \text{and} \\ 0 &= \left\langle Df \frac{\partial}{\partial s} \mathcal{O}_\alpha, Df \frac{\partial}{\partial t} \mathcal{O}_\alpha \right\rangle \end{aligned}$$

we obtain

$$\langle \gamma_1'(r(t)), m'(t) \rangle = r'(t) \quad (5.1.2)$$

by multiplication of equation (5.1.1) with $\gamma_1'(r(t))$. Let $\{e_1, e_2\}$ be an orthonormal basis of $T_{m(t)}M$. Then there exist real numbers a_1, a_2 such that

$$\gamma_1'(r(t)) = a_1 e_1 + a_2 e_2.$$

This yields the conditions

$$a_1 \langle e_1, m'(t) \rangle + a_2 \langle e_2, m'(t) \rangle = r'(t) \quad (5.1.3)$$

$$a_1^2 + a_2^2 = 1 \quad (5.1.4)$$

It can be shown that (5.1.2) together with (5.1.3) and (5.1.4) has two solutions in case

$$r'(t)^2 < \|m'(t)\|^2.$$

This is subject of the next lemma.

Lemma 5.1.1

Let $v_1, \dots, v_{n-1} \in \mathbb{R}^n$ be an orthonormal frame and $r_i \in \mathbb{R} \forall i = 1, \dots, n-1$. The minimum of the function

$$f(x) = \|x\|^2$$

under the constrains

$$g_i(x) = \langle v_i, x \rangle - r_i = 0 \quad i = 1, \dots, n-1 \quad (5.1.5)$$

is given by $f(x_{\min}) = \sum_{i=1}^{n-1} r_i^2$ with the solution vector

$$x_{\min} = \sum_{i=1}^{n-1} r_i v_i.$$

Proof: Define the Lagrange function

$$H(x, \lambda) = f(x) - \sum_{i=1}^n \lambda_i g_i(x).$$

The gradient of H is critical for the calculation of the relative minimum of f under the given constraints. Looking carefully at the first n components of $\text{grad } H$, we can conclude

$$x = \sum_{i=1}^{n-1} \frac{1}{2} \lambda_i v_i.$$

In addition x has to met the equations (5.1.5). Since $\{v_i\}$ is an orthonormal frame, we get

$$\lambda_i = 2r_i.$$

This completes the proof of the lemma. □

Example 5.1.1 is intended to illuminate the foregoing results.

We have presented a reconstruction scheme that allows us to parametrise two segments α_1 and α_2 of the envelope $\partial\Omega$. For a proper but arbitrary parametrisation m of the medial axis with corresponding radius function r there is only little chance that $\alpha_1 \cup \alpha_2$ is a closed curve. However, if these segments can be joined with the corresponding segments c_a and c_b of the distance circles $K_{m(a)}(r(a))$ and $K_{m(b)}(r(b))$ respectively such that the resulting curve is differentiable, then we have found a full parametrisation of the envelope. The union of these segments will be denoted by α . At $m(a)$ there exists an orthonormal basis $\{e_1, e_2\}$ of $T_{m(a)}M$ and angles ϕ_1, ϕ_2 such that

$$c_a(\phi) = \exp_{m(a)}(r(a)(\cos(\phi)e_1 + \sin(\phi)e_2))$$

for $\phi \in [\phi_1, \phi_2]$. Similar results can be obtained for the segment c_b .

Advanced applications often involve tangent directions of the envelope and curvature values. The following subsection is addresses to this problem.

5.1.1 Geodesic Curvature Computation Of Envelope Points

Since the geodesic curvature coincides with the curvature for planar curves α , the curvature κ of an envelope α can simply be deduced by

$$\kappa = \frac{\|\alpha'(t) \times \alpha''(t)\|}{\|\alpha'(t)\|^3}.$$

The last equation employs the tangent vector α' and the second derivative α'' of the envelope parametrisation α . Without going into detail these vectors can be implicitly or explicitly derived from the **reconstruction formula**

$$\alpha(t) = m(t) - r(t)N(t).$$

We will focus on a more general case. Let M be a 2-dimensional Riemannian manifold, $p \in M$ be a progenitor point and $\alpha : I \rightarrow M$ be a progenitor curve respectively. For these progenitor objects we have introduced offset functions $\mathcal{O}(s, t)$, assuming that the parameters s and t correspond to the parameters being used in equation (4.2.1) and (4.2.3) respectively. Let f be a local parametrisation of M in a neighbourhood of p and $\alpha(t_0)$ respectively. Define the function $\tilde{f} = f \circ \mathcal{O}$. Rausch showed in his thesis that the length $y(s, t)$ of the Jacobi vector $\frac{\partial}{\partial t}\tilde{f}(s, t)$ meets the condition

$$\frac{\partial^2}{\partial s^2}y(s, t) = K(s, t)y(s, t), \tag{5.1.6}$$

K being the Gaussian curvature of M at $\tilde{f}(s, t)$. This is a special version of a classical result from differential geometry being stated for example in [doC92] or any other textbook. Since the vectors $\frac{\partial}{\partial s}\tilde{f}(s, t)$ and $\frac{\partial}{\partial t}\tilde{f}(s, t)$ represent orthogonal vectors, the length $y(s, t)$ of the latter vector entirely describes the Jacobi vector $\frac{\partial}{\partial t}\tilde{f}(s, t)$. Moreover, Rausch could show that the quotient $\frac{\frac{\partial}{\partial s}y(s, t)}{y(s, t)}$ is incident to the geodesic curvature of the tubular curve of the corresponding progenitor object, unless $\tilde{f}(s, t)$ is not a focal point. The proof is similar to the proof stated in [BL73], where the progenitor objects are points. Thus, it is sufficient to derive the initial conditions of the ordinary differential equation (5.1.6).

For points the initial conditions can be stated as follows:

$$y(0, t) = 0 \quad \text{and} \quad \frac{\partial}{\partial s}y(0, t) = 1. \quad (5.1.7)$$

These conditions will be useful for the determination of the geodesic curvature of geodesic circle segments. The initial conditions for progenitor curves require some more work. From $y(s, t) = \langle \tilde{f}_t, \tilde{f}_t \rangle^{\frac{1}{2}}$ and $\langle \tilde{f}_s, \tilde{f}_t \rangle = 0$ we can easily derive the equation

$$\frac{\partial}{\partial s}y(s, t) = \frac{\langle \frac{D}{ds}\tilde{f}_t, \tilde{f}_t \rangle}{y(s, t)} = -\frac{\langle \tilde{f}_s, \frac{D}{dt}\tilde{f}_t \rangle}{y(s, t)}. \quad (5.1.8)$$

We already deduced the equation

$$\tilde{f}_s r' + \tilde{f}_t = m'$$

for the detection of envelope points. $-\tilde{f}_s$ represents the initial direction of the geodesic joining the medial point with one of the two nearest envelope points being defined by the maximal inscribed disc that is tangent to the envelope in these two points. Application of $\frac{D}{dt}$ to the last equation and multiplication with \tilde{f}_s yields

$$-\left\langle \tilde{f}_s, \frac{D}{dt}\tilde{f}_t \right\rangle = r'' - \left\langle \frac{D}{dt}m', \tilde{f}_s \right\rangle.$$

Finally, we get

$$\frac{\partial}{\partial s}y(s, t) = \frac{r'' - \left\langle \frac{D}{dt}m', \tilde{f}_s \right\rangle}{y(s, t)}.$$

Example 5.1.1

Consider a 2-dimensional manifold

$$M = \{(x, y, z); z = h(x, y)\},$$

where $h(x, y) = x \sin(y) - \frac{1}{2}e^x$. Let $\mu(t) = (\cos(t), \sin(t))$ and $m(t) = f(\mu(t))$, where $t \in [0, \pi]$ and f is the parametrisation of M corresponding to the height function h . Let $r(t) = \frac{1}{2} + 0.3 \sin(t) \cos(t)$. We get a proper reconstruction of the envelope sketched in figure 5.3. The geodesic curvature of the envelope is shown as well and lies within the range $[-0.85, 9.47]$.

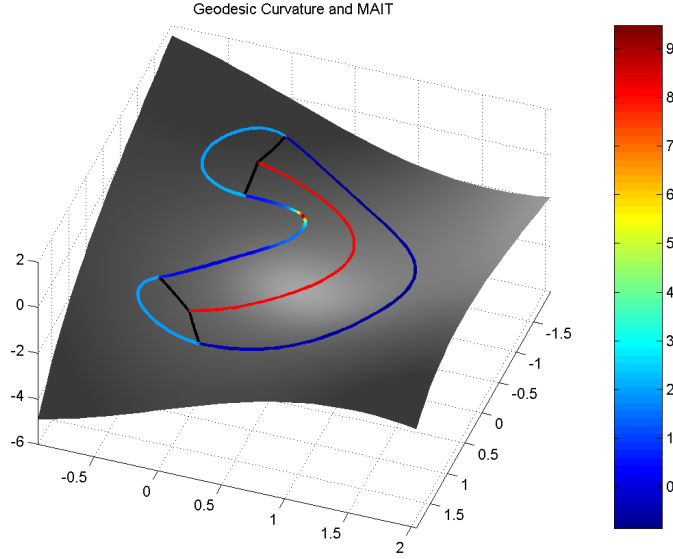


Figure 5.3: Geodesic curvature of the envelope

5.2 3D Medial Axis Inverse Transform

Let M be a complete 3-dimensional manifold and $\Omega \subset M$ be a solid with medial axis $MA(\Omega)$ and corresponding radius function r . Assume $MA(\Omega) \subset M$ is a 2-dimensional bordered surface that can be parametrised by

$$m : D_m = [u_1, u_2] \times [v_1, v_2] \rightarrow MA(\Omega).$$

Let $r : D_m \rightarrow \mathbb{R}_{>0}$ be a positive radius function. Ω can be reconstructed using the functions m and r . We sketch a method that reconstructs the boundary representation of Ω . Let $S = \partial\Omega$ be the envelope of $MA(\Omega)$. Under the conditions of a proper reconstruction scheme that is explained below the envelope can be divided into 3 subsets, called A_1 , A_2 and A_3 . The definition of these sets is subject of the following considerations.

Definition 5.2.1

Set

$$\begin{aligned} D_m^1 &:= \dot{D}_m \quad (\text{interior of } D_m), \\ D_m^2 &:= \{u_1\} \times (v_1, v_2) \cup \{u_2\} \times (v_1, v_2) \cup (u_1, u_2) \times \{v_1\} \cup (u_1, u_2) \times \{v_2\}, \\ D_m^3 &:= \{(u_1, v_1), (u_1, v_2), (u_2, v_1), (u_2, v_2)\}, \end{aligned}$$

where D_m^1 represents the interior of the rectangular domain D_m , D_m^2 the boundary of D_m without the vertices and D_m^3 the vertices of D_m . Then the sets A_i can simply be defined by

$$A_i := \{x \in M; \exists p \in m(D_m^i) : r(p) = d(p, \partial\Omega) = d(p, x)\}. \quad (5.2.1)$$

Figure 5.4 sketches the three different sets A_i . A_1 is colored in blue, whereas A_2 and A_3 are colored in green and red respectively. In the sequel it will be briefly described how these sets can be obtained.

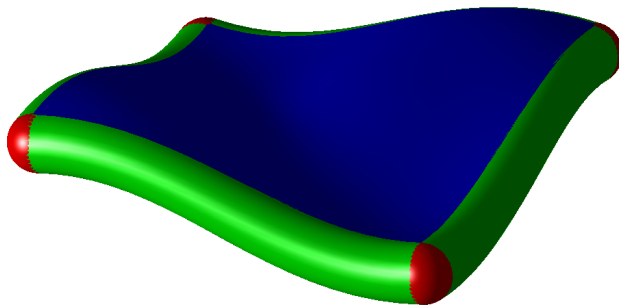


Figure 5.4: The sets A_i

5.2.1 The Set A_1

The essential idea of how a parametrisation of A_1 can be obtained is to make use of theorem 5.0.1

It will turn out that each component of A_1 can be parametrised over the parameter domain D_m . Let $(u, v) \in D_m$ and $f : U \rightarrow M$ be a parametrisation of M in a neighbourhood of $m(u, v)$. If \mathcal{O}_1 denotes the offset function of a component of A_1 with respect to f , we obtain

$$f(\mathcal{O}_1(r(u, v), u, v)) = m(u, v). \quad (5.2.2)$$

Differentiation with respect to u and v respectively and multiplication with $w = Df \cdot \frac{\partial}{\partial s} \mathcal{O}_1$ yields

$$r_u = \langle m_u, w \rangle, \quad (5.2.3)$$

$$r_v = \langle m_v, w \rangle, \quad (5.2.4)$$

where w is a vector from the normal space of the tubular surface $(A_r)_{r(u,v)}$ at $m(u, v)$.

Since $w \in TM$, the following conditions must hold:

$$\|w\| = 1, \quad (5.2.5)$$

$$w = \sum_{i=1}^3 a_i e_i, \quad (5.2.6)$$

where $\{e_1, e_2, e_3\}$ represents an orthonormal basis of $T_{m(u,v)}M$. (5.2.3)-(5.2.6) yield a system of equations with at most two solutions $w_{1,2}$. Each of the inverted directions $-w_i$ is the initial direction of a geodesic $\gamma_i : [0, r(u, v)] \rightarrow M$ with $\gamma_i(0) \in MA(\Omega)$ and $\gamma_i(r(u, v)) \in S$. The point $\gamma_i(r(u, v))$ is then the sought progenitor point. Equations (5.2.3) and (5.2.4) indicate the bi-tangency of the maximal inscribed sphere of the solid Ω . (5.2.3) and (5.2.4) build up a system of two linear equation with three unknowns:

$$\begin{pmatrix} \langle m_u, e_1 \rangle & \langle m_u, e_2 \rangle & \langle m_u, e_3 \rangle \\ \langle m_v, e_1 \rangle & \langle m_v, e_2 \rangle & \langle m_v, e_3 \rangle \end{pmatrix} \begin{pmatrix} a_1 \\ a_2 \\ a_3 \end{pmatrix} = \begin{pmatrix} r_u \\ r_v \end{pmatrix}. \quad (5.2.7)$$

The affine set L that contains all solutions of the above equation can now be stated as

$$L = \{a \in \mathbb{R}^3; a = v_1 + v_2 t; t \in \mathbb{R}\}, \quad (5.2.8)$$

for which the vectors v_i must be chosen appropriately. A real normalised solution vector has to fulfil the quadratic equation

$$t^2 \|v_2\|^2 + 2t \langle v_1, v_2 \rangle + \|v_1\|^2 - 1 = 0. \quad (5.2.9)$$

We will denote this by $w \in L^1$.

5.2.2 The Set A_2

For the computation of the set A_2 we again require a parametrisation of the envelope. The edge curve $\alpha(t) = m(u_1, t)$, $t \in (v_1, v_2)$, is assumed to be an arc length parametrised curve that meets some regularity requirements. It must be ensured that the frame

$$\left\{ \frac{d}{dt}\alpha, \frac{D}{dt} \frac{d}{dt}\alpha, \frac{D^2}{dt^2} \frac{d}{dt}\alpha \right\}$$

is a linear independent frame along α . Since $\dim T_{\alpha(t)}M = 3$ for all t the aforementioned system yields a basis of $T_{\alpha(t)}M$ for all possible parameters t .

The frame E_1, E_2, E_3 from (4.3.4) can be used to obtain the parametrisation of the set A_2 . Note that the construction of this frame only depends on α and the Riemannian structure of the given manifold since it basically involves the covariant derivative and the inner product.

Define the function

$$f(t, \phi) = \exp_{\alpha(t)}(-s \cdot w(t, \phi)) \quad (5.2.10)$$

with the direction

$$\begin{aligned} w(t, \phi) &= r'(t)E_1(t) \\ &+ \sqrt{1 - r'(t)^2} (\cos(\phi)E_2(t) + \sin(\phi)E_3(t)), \end{aligned} \quad (5.2.11)$$

using $r(t) = r(\alpha(t))$. f parametrises the piece of A_2 that corresponds to α . For the vector $w(t, \phi) \in T_{\alpha(t)}M$ the identities

$$\|w(t, \phi)\| = 1 \quad (5.2.12)$$

$$\langle w(t, \phi), \alpha'(t) \rangle = r'(t) \quad (5.2.13)$$

hold. Notice that for fixed t the map $\phi \mapsto w(t, \phi)$ describes the rotation of the vector $w(t) = Df \cdot \frac{\partial}{\partial s} \mathcal{O}_1(r(t), u_1, t)$ around $\alpha'(t)$. The angle parameter ϕ lies within the range $[\phi_{\min}(t), \phi_{\max}(t)]$. The orientation of the system E_2 and E_3 has to be involved in order to specify this range as well as the limit vectors

$$\lim_{u \rightarrow u_1} w_i(u, t)$$

from the construction of A_1 (see 5.2.6).

5.2.3 The Set A_3

The vertices of the medial surface contribute to the set A_3 . Every component of A_3 is a segment of a distance sphere around the aforementioned vertices. These segments are colored in red (see figure 5.4).

It is certainly possible to describe the remaining points that are needed for a complete Medial Axis Inverse Transform by sophisticated coordinate transformations. An alternative approach would be to describe the initial directions w of the joining geodesics by inequalities. For a vertex p we obtain such directions using the system

$$\begin{aligned} \langle m_u, w \rangle &< r_u, \\ \langle m_v, w \rangle &< r_v, \\ \|w\| &= 1. \end{aligned}$$

It is clear that a similar formulation can be made in case of the 2D Medial Axis Inverse Transformation. The inequality

$$\langle m'(0), w \rangle < r'(0)$$

then would automatically lead to envelope points located on the outer circle segment with radius $r(0)$ of the point $m(0) = p_1$ (see figure 5.3).

5.2.4 A Proper Reconstruction Scheme

The following two conditions are sufficient for a reconstruction scheme that will not lead to inconsistencies of the envelope of $MA(\Omega)$.

- For all $(u, v) \in D_m$ we must ensure that $r_u < \|m_u\|$ and $r_v < \|m_v\|$. This mainly results from equations (5.2.3) and (5.2.4). We can not admit $r_u = \|m_u\|$ for example, since then the direction of the gradient of the distance function would be contained in the tangent plane of $MA(\Omega)$.
- r is bounded by the minimum focal radius of the envelope (see the definition of the focal radius).

Example 5.2.1

The latter constraint for the proper reconstruction scheme shall be analysed in a special situation where Ω is a planar domain. Let m denote an arc length parametrisation of the medial curve with radius function r both being defined on the parameter space I and α a local parametrisation of a piece of the boundary of Ω that does not belong to the outer circle segments mentioned above. Let N_m be the normal vector of m . Then α can be locally parametrised by

$$\alpha(t) = m(t) - r(t) \left(r'(t)m'(t) + \sqrt{1 - r'(t)^2}N_m(t) \right). \quad (5.2.14)$$

We must avoid situations where the tangent vector α' vanishes. Differentiation of (5.2.14) with respect to t leads to

$$\begin{aligned} \alpha'(t) &= a_1(t)m'(t) + a_2(t)N_m(t), \\ a_1(t) &= 1 - r'(t)^2 - r(t)r''(t) + k_m(t)r(t)\sqrt{1 - r'(t)^2}, \\ a_2(t) &= r'(t)\sqrt{1 - r'(t)^2} - r(t)r'(t)k_m(t) + \frac{r(t)r'(t)r''(t)}{\sqrt{1 - r'(t)^2}}. \end{aligned}$$

In case

$$k_m(t) = -\frac{1 - r'(t)^2 - r(t)r''(t)}{r(t)\sqrt{1 - r'(t)^2}},$$

the coefficients a_1 and a_2 vanish. This means that the parametrisation α of the specific boundary segment is not regular at this point. The Medial Axis Inverse Transformation is then unsuitable for a description of a planar domain Ω with smooth boundary. Unfortunately, with the aforementioned condition it is not possible to exclude the more sophisticated cases of the Medial Axis Inverse Transformation. One would have to apply topological methods to assure that the respective geodesic joins are distance minimal.

5.3 The Geodesic Medial Modeller

The Geodesic Medial Modeller is a modelling environment designed at the institute of Men-Machine-Interaction at the Leibniz Universität Hannover. It is a result of

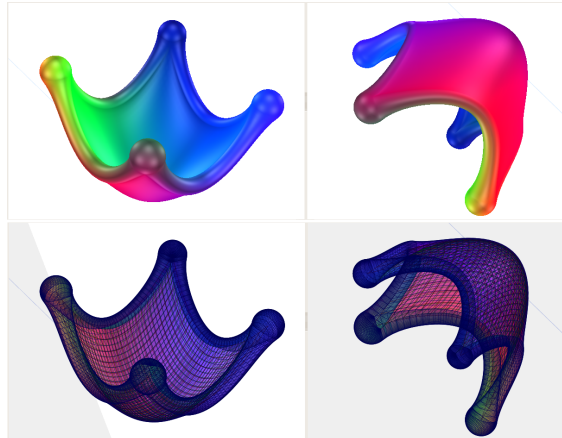


Figure 5.5: Medial Axis Inverse Transform of a paraboloid

the master thesis of Cem Doğan. In contrast to the original Medial Modeller, that has been developed at the same institute as well, the user is now in the position to generate solids with more flexibility. The shape design tools used so far have been restricted by the fact, that special kinds of deformations could only be modelled with considerable expenditure. This was because the geometry of the embedding space was lacking obstacles that were able to extremely deform the distance vector field given by the radius function. Locally the metric can be changed by simply changing the curvature tensor. This can be achieved only by superposing the parametrisation of the manifold M , which is the graph of a function h at hand. h is superposed with functions of the kind

$$x \mapsto a \cdot \exp(-c\|x - \mu\|^2). \quad (5.3.1)$$

Recall that such functions only have little influence on the behaviour of h outside a compact ball around μ , whose radius has to be specified. The functions $\exp(-c\|x - \mu\|^2)$ correspond to spheres, where the centre of these spheres represent the vector μ and the radius is given by c . Figure 5.5 gives an example of a solid that was obtained by the Medial Axis Inverse Transform using the Geodesic Medial Modeller.

6 Medial Axis Transformation

The computation of the medial axis transform is indeed a difficult scenario in cases one needs reliable and accurate solutions. Roughly speaking there has been developed a variety of algorithms that barely operate on the solution spaces of the medial equations using Predictor Corrector methods. A comprehensive overview of such algorithms can be found in [GR04]. See [Lee82] and [LL92] and references therein for other approaches. The presented methods do not treat the general case of arbitrary length spaces with induced metric d_1 and are therefore not applicable in our present case. Nevertheless, there are some approaches in non Euclidean geometry. Especially Level Set Methods and Fast Marching Methods [Set99] appear to be suitable methods for the non Euclidean medial axis transform.

Nearly every method that treats the medial axis transform has the property that it does not reflect the exact topological behaviour. We will return to this issue later on in this section.

A brief note on the length spaces from above should be given next. Consider a metric space (M, d) and a curve

$$\alpha : I = [0, 1] \rightarrow M.$$

Choose arbitrary points

$$0 = t_0 < t_1 < \dots < t_N = 1.$$

If the number

$$\delta := \max\{t_{i+1} - t_i, i = 0, \dots, N\}$$

is small, we consider the sum

$$\sum_{i=0}^{N-1} d(\alpha(t_{i+1}), \alpha(t_i))$$

as a good (polygonal) approximation of the length of the curve α . Let $L(\alpha)$ be the smallest number such that every polygonal approximation is smaller than $L(\alpha)$ or equal to it. If $L(\alpha) < \infty$ then α is called **rectifiable**. The intrinsic metric d_1 finally measures the length of the shortest join of two points and (M, d_1) is called **length space**.

The computation of medial sets relies here on the application of offset functions being described in chapter 4. The choice of the right offset function depends on the geometry of the boundary of the solid. The focus of our computations lies in the determination of pairs of points $p, q \in \partial\Omega$ and spheres S that are tangent to $\partial\Omega$ in p and q respectively.

However, the center points of these spheres often only refer to the symmetry set of $\partial\Omega$ and not to the cut locus. We say that the sphere S is **bitangent** to the boundary $\partial\Omega$. In general the cut locus of a compact set A is the set of points $x \notin A$ where the distance function $d(\cdot, A)$ is not differentiable.

6.1 Basics

Some basics concerning the medial axis transform will be introduced.

- Figure 6.1 sketches the medial axis of a planar domain. It is a geometrical graph (V, E) with vertices $V_i \in V$ and edges $e_j \in E$. This simple example already has 8 vertices that correspond to the n-prongs (see the following definition of n-prongs). Three of these vertices correspond to the 3-prongs whereas the others are centers of curvature. For our purposes it will be assumed that the medial axis of the domain Ω is a geometrical graph in the length space (\mathbb{R}^2, d_1) .

Let $t \rightarrow \alpha(t)$ denote the parametrisation of the boundary of a simply connected domain. We briefly describe how the medial axis transform can be obtained in such cases.

1. Find the local extrema of the curvature function $t \rightarrow k(t)$.
 2. Compute the 3-prongs using the Predictor Corrector method and the system (6.2.4)-(6.2.9) starting with the points with negative extrema of the curvature function.
 3. Determine the structure of the geometrical graph (V, E) .
 4. Compute the focal bisectors (where a focal point is involved) and bisectors where no focal point is involved.
- Let $M = \mathbb{R}^3$ and $G(x) = (g_{ij}(x))$ be a positiv definite matrix for all $x \in M$. g_{ij} is called the **metric tensor** and

$$(y, z) \mapsto y^T G(x) z$$

denotes the **first fundamental tensor**. Let $\alpha : [0, 1] \rightarrow M$ be a differentiable curve in M . Define the length of α using

$$L(\alpha) = \int_0^1 \sqrt{\alpha'(t)^T G(\alpha(t)) \alpha'(t)} dt.$$

The distance d_1 of two points p and q again is defined by the length of the shortest join of these points. Without proof it can be shown that (M, d_1) is a length space. In the following we will only refer to those length spaces with metric induced by a metric tensor.

- Let $\Omega \subset M$ be a domain and $p \in MA(\Omega)$. p is called **n-prong**, if

$$B(p, r(p)) \cap \partial\Omega$$

has n connected components.

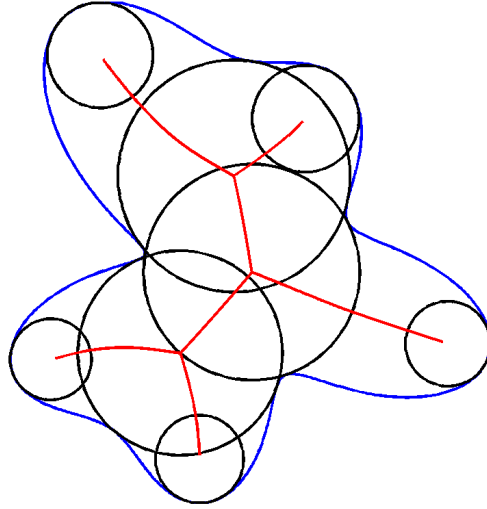


Figure 6.1: Medial axis of a simple domain

- Let $\Omega \subset M$ be a domain with smooth boundary. Define

$$\text{Skel}(\text{MA}(\Omega)) := \{p \in \text{MA}(\Omega) : p \text{ is } n\text{-prong and } p \neq 2\}.$$

Typically, the skeleton of $\text{MA}(\Omega)$ is a topological graph. The determination of this topological graph is one of our major issues.

- We define $\text{SS}(\Omega)$ as the closure of the set of symmetry points of $\partial\Omega$ being contained in Ω . $\text{MA}(\Omega)$ can be obtained from $\text{SS}(\Omega)$ by trimming. Figure 6.2 gives an example for this.



Figure 6.2: The symmetry set and the medial axis of a rectangle

- For two given compact reference sets K_1 and K_2 and the corresponding generalised distance functions d_i the **medial equation** of the bisector $B(K_1, K_2)$ is given by

$$F(x, y, z) = d_1(x, y, z) - d_2(x, y, z) = 0. \quad (6.1.1)$$

We will see later on that the gradient of the distance functions can be obtained using the offset functions from section 4.

- Typically, there is only little chance that the medial equation can be solved analytically. One famous example is for example given in [RF94], where the

bisector of a point and a parametric curve is deduced. If $\alpha : [0, 1] \rightarrow \mathbb{R}^2$ is a differentiable curve with normal vector field $N : [0, 1] \rightarrow \mathbb{R}^2$ and $p \in \mathbb{R}^2$ is a point then 6.1.1 yields the identity

$$\|\alpha(t) + s(t)N(t) - p\|^2 = s(t)^2$$

which leads to

$$s(t) = \frac{\|\alpha(t) - p\|^2}{2\langle p - \alpha(t), N(t) \rangle}.$$

6.2 Medial Differential Equations

One important fact will be useful in the context of the Medial Axis Transformation. Consider a 3D-solid Ω with smooth boundary $S = \partial\Omega$ and a point $p \in \Omega$ inside this solid. It can be easily shown that p has a nearest boundary point q and the shortest (geodesic) join $\gamma_{p,q}$ of p and q intersects with S orthogonally with respect to the first fundamental tensor of the length space (M, d) .

In the sequel let $S_1, S_2 \subset \mathbb{R}^3$ be two bordered reference surfaces with generalised distance function

$$d_i(p) = \inf_{q \in S_i} \{d(p, q)\}.$$

Let \mathcal{O}_i denote the offset function of S_i with respect to some parametrisation functions $f_i : U_i \subset \mathbb{R}^2 \rightarrow S_i$. Consider a point $(x_0, y_0, z_0) \in \mathbb{R}^3$ such that

$$F(x_0, y_0, z_0) = d_1(x_0, y_0, z_0) - d_2(x_0, y_0, z_0) = 0. \quad (6.2.1)$$

We will briefly describe in the next subsection how such a point can be obtained. From the implicit function theorem deduce that for

$$(F_y, F_z)|_{(x_0, y_0, z_0)} \neq (0, 0)$$

there exist smooth functions $y(t), z(t) : I \rightarrow \mathbb{R}$ such that

$$F(x_0, y(t), z(t)) = 0 \quad (6.2.2)$$

holds for all $t \in I$, where I must be chosen appropriately. Note that the above approach must be treated with caution since the functions d_i are only C^0 at cut locus points. So we will assume that (x_0, y_0, z_0) is not a cut locus point of both S_1 or S_2 and that this is even true in a neighbourhood of this point. Differentiation of 6.2.2 with respect to t yields the tangent vector

$$\begin{pmatrix} y'(t) \\ z'(t) \end{pmatrix} = \frac{1}{F_y^2 + F_z^2} \begin{pmatrix} -F_z \\ F_y \end{pmatrix} \quad (6.2.3)$$

of the arc length parametrised curve $t \mapsto (y(t), z(t))$.

The first question that arises is how can we obtain the gradient ∇F ? The solution to it is rather short. Since

$$d_i(\mathcal{O}_i(s, u_i, v_i)) = s$$

it simply follows that

$$\nabla d_i \circ D\mathcal{O}_i = (1 \ 0 \ 0).$$

This yields the following

Lemma 6.2.1

The gradient of the distance function d coincides with the first row vector of the inverse Jacobian matrix of the offset function \mathcal{O} .

From 6.2.1 we obtain

$$\nabla F = \nabla d_1 - \nabla d_2.$$

By differentiation of

$$\mathcal{O}_i(s(t), u_i(t), v_i(t)) = \begin{pmatrix} x_0 \\ y(t) \\ z(t) \end{pmatrix}$$

with respect to t we get

$$\begin{pmatrix} s'(t) \\ u_i'(t) \\ v_i'(t) \end{pmatrix} = D\mathcal{O}_i^{-1} \cdot \begin{pmatrix} 0 \\ y'(t) \\ z'(t) \end{pmatrix}.$$

Note that both u_i and v_i correspond to the parameters of the function f_i as described above.

To summarise the results a system of ordinary differential equation have been evolved in order to parametrise an isoline on the medial patch of two progenitor surface patches S_1 and S_2 that fulfil some regularity requirements concerning the offset functions \mathcal{O}_i . This isoline is a curve with the specific isoparameter $x = x_0$. Equivalently, every point $(x_0, y(t), z(t))$ serves as an initial point of a family of isolines with isoparameter y and z respectively. The derivation of the corresponding equations will be left out. Yet, this is analogue to the prescribed approach. Observe that the aforementioned method completely fails in only few situations that must be detected before. Consider for example the solid

$$\Omega = \{(x, y, z), x^2 + y^2 \leq r^2, |z| \leq K\}.$$

For $K > r$ it can be shown that $MA(\Omega)$ contains the medial arc

$$m(t) = \begin{pmatrix} 0 \\ 0 \\ t \end{pmatrix},$$

where $|t| < K - r$. Observe that every $m(t)$ is a 1-prong whereas $[0, 0, K - r]^T$ and $[0, 0, r - K]^T$ are not.

In Euclidean space the classification of such n-prongs has been proven to be a powerful tool in the context of the medial axis transform. This has been done for example by Giblin and Kimia (see [GK04]). It is based on the discussion of distance functions and contact functions. To explain this carefully let (\mathbb{R}^3, d) be a length space, $\Omega \subset \mathbb{R}^3$ be a solid and $S = \partial\Omega$ be a complete and compact hypersurface. Let $p \in \Omega$ and $B(p, r)$ be tangent to S at q . Suppose that S can be parametrised by a function f in a neighbourhood of $q = f(u^q, v^q)$. One major issue with regard to the last remark is the Taylor expansion of the function

$$r(u, v) = d_1(f(u, v), p)$$

in a neighbourhood of (u^q, v^q) , where d_1 again denotes the intrinsic distance function with respect to d . The Taylor expansion of r can be approximated using the concepts of finite differences since the Taylor series will not directly contribute to the computation of medial axis points.

Example 6.2.1

Let

$$\alpha(t) = \begin{pmatrix} a \cos(t) \\ b \sin(t) \end{pmatrix}$$

be a parametrisation of an ellipsis and $p = ((a^2 - b^2)/a, 0)$ be a point. Then

$$r(t) = d_1(\alpha(t), p) = \left[a^2 \cos^2(t) - 2 \cos(t)(a^2 - b^2) + b^2 \sin^2(t) + \frac{a^2 - b^2}{a^2} \right]^{\frac{1}{2}}.$$

Deduce that

$$\begin{aligned} r(0) &= \frac{b^2}{|a|}, \\ r'(0) &= 0, \end{aligned}$$

which means that p is a curvature centre.

See [GK04] for the discussion of the next issue.

Definition 6.2.1

The bivariate function r from above is said to have a A_k -singularity if locally r can be rewritten in the form

$$r(u, v) = \pm u^2 \pm v^{k+1}$$

for some $k \geq 0$ and it is said to have a D_k -singularity, if r can locally be represented by

$$r(u, v) = \pm v u^2 \pm v^{k-1}$$

for some $k \geq 4$. This property is invariant under diffeomorphisms.

As we have seen before the skeleton of the medial axis $\text{MA}(\Omega)$ is a topological graph that contains all relevant information concerning the distribution of the n -prongs. One major issue towards the computation of $\text{Skel}(\text{MA}(\Omega))$ will be the determination of the 1-prongs and the 3-prongs.

Let us consider one special case to illustrate how 3-prongs can be obtained. Given $\Omega \subset \mathbb{R}^2$, where $S = \partial\Omega$ is a smooth closed curve being parametrised by $\gamma : [0, 1] \rightarrow S$, a 3-prong $x \in \mathbb{R}^2$ must meet the conditions

$$\|\gamma(t_1) - x\| - \|\gamma(t_2) - x\| = 0, \quad (6.2.4)$$

$$\|\gamma(t_2) - x\| - \|\gamma(t_3) - x\| = 0, \quad (6.2.5)$$

$$\left\langle \gamma'(t_1), \frac{\gamma(t_1) - x}{\|\gamma(t_1) - x\|} \right\rangle = 0, \quad (6.2.6)$$

$$\left\langle \gamma'(t_2), \frac{\gamma(t_2) - x}{\|\gamma(t_2) - x\|} \right\rangle = 0, \quad (6.2.7)$$

$$\left\langle \gamma'(t_3), \frac{\gamma(t_3) - x}{\|\gamma(t_3) - x\|} \right\rangle = 0, \quad (6.2.8)$$

$$k\|\gamma(t_1) - \gamma(t_2)\|\|\gamma(t_1) - \gamma(t_3)\|\|\gamma(t_2) - \gamma(t_3)\| - 1 = 0. \quad (6.2.9)$$

The last equation ensures that the numbers t_1 , t_2 and t_3 are pairwise different.

Finally, we give some notes on the computation of isolines of medial surface patches. Assume we have

$$F_z(x_0, y_0, z_0) \neq 0.$$

Then by the implicit function theorem it is possible to find a function

$$\phi : U \subset \mathbb{R} \rightarrow \mathbb{R}$$

such that

$$F(x_0, y, \phi(y)) = 0$$

for all $y \in U$, where U is considered to be maximal with the above property. For the derivation of 6.2.3 it was not important whether $F_y \neq 0$ or $F_z \neq 0$. It was only required that $(F_y, F_z) \neq (0, 0)$. This is the reason why we used this approach here. We give an example:

Example 6.2.2

Consider a function

$$F(x, y) = x^2 + y^3 - 1.$$

The gradient of this function is zero only for $(x, y) = (0, 0)$, where (x, y) lies outside the zero level set of F . The classical implicit function theorem states that if $F(x_0, y_0) = 0$ and $F_y(x_0, y_0) \neq 0$ there exists an $\epsilon > 0$ and a function

$$g : I_\epsilon^{x_0} = (x_0 - \epsilon, x_0 + \epsilon) \rightarrow \mathbb{R}$$

with $F(x, g(x)) = 0$ for all $x \in I_\epsilon$. However, ϵ is a function of x_0 and y_0 , i.e. $\epsilon = \epsilon(x_0, y_0)$. Take for example the point $(x_0, y_0) = (0, 1)$. Since $F_y(0, 1) = 3$ the implicit function theorem can be applied. ϵ must be chosen smaller than 1 because $(-1, 0)$ is another point of the zero level with $F_y(-1, 0) = 0$ and $F_x(-1, 0) = -2$, i.e. x is locally a function of y but not vice versa.

The non classical approach however yields functions $x : I_\epsilon \rightarrow \mathbb{R}$ and $y : I_\epsilon \rightarrow \mathbb{R}$ with

$$\begin{aligned} 2x(t)x'(t) + 3y(t)^2y'(t) &= 0 \\ x'(t)^2 + y'(t)^2 &= 1 \\ (x(0), y(0)) &= (0, 1) \\ (x'(0), y'(0)) &= (-1, 0) \end{aligned}$$

Conclude that

$$(x'(t), y'(t)) = \frac{1}{\sqrt{4x(t)^2 + 9y(t)^4}} (-3y(t)^2, 2x(t)).$$

Figure 6.3 sketches the trajectory of the above system for $\epsilon = -1.5$. Observe that the definition of $(x(t), y(t))$ only requires that the solution curve does not contain the origin. The classical approach is more restrictive in that sense.

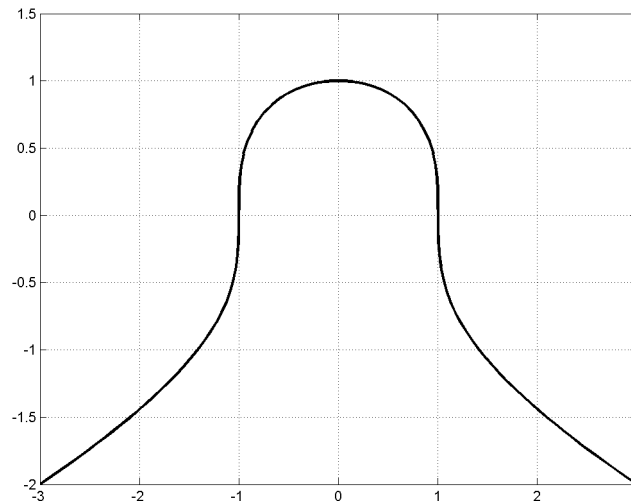


Figure 6.3: Solution curve of an implicit equation of type $F(x, y) = 0$

The next section deals with the question of how an initial point of the medial differential equations can be found.

6.3 Initial Values Of The Medial Differential Equations

For the discussion of initial values we will begin with the standard (convex) homotopy methods.

6.3.1 Convex Homotopy Method

Given two bordered surfaces S_1 and S_2 there are several possibilities to find an initial point of the medial equation

$$F(x, y, z) = d_1(x, y, z) - d_2(x, y, z) = 0.$$

For the first approach we will therefore employ the offset functions of S_1 and S_2 respectively. If we choose arbitrary parameter values $(s^0, u_1^0, v_1^0, u_2^0, v_2^0)$ it follows easily that the function

$$H(s, u_2, v_2, \lambda) = \mathcal{O}_1(s, u_1^0, v_1^0) - \mathcal{O}_2(s, u_2, v_2) + (\lambda - 1) (\mathcal{O}_1(s^0, u_1^0, v_1^0) - \mathcal{O}_2(s^0, u_2^0, v_2^0))$$

vanishes at $(s^0, u_2^0, v_2^0, 0)$. Using the results from 2.4 one can find (s^*, u_2^*, v_2^*) such that

$$H(s^*, u_2^*, v_2^*, 1) = 0$$

under some regularity assumptions. This yields

$$\mathcal{O}_1(s^*, u_1^0, v_1^0) - \mathcal{O}_2(s^*, u_2^*, v_2^*) = 0$$

and finally

$$F(\mathcal{O}_1(s^*, u_1^0, v_1^0)) = 0$$

in case $d_1(\mathcal{O}_i(s^*, u_1^0, v_1^0)) = s^*$ and $d_2(\mathcal{O}_i(s^*, u_2^*, v_2^*)) = s^*$. Note that it is not apriori clear that after the integration is finished the above condition holds. Note that for the definition of the functions \mathcal{O}_i the orientation of S_i plays a key role.

The discussion of initial points of the medial equations for the computations of symmetry sets can be simplified in case we have two reference surfaces

$$S_i := \{(x, y, z); z = h_i(x, y)\}$$

for $i = 1, 2$. It is reasonable to define

$$\begin{aligned} \tilde{S}_1 &:= \{(x, y, z); z = h_1(x, y)(1 - \rho(x))\}, \\ \tilde{S}_2 &:= \{(x, y, z); z = h_2(x, y)(1 - \rho(x))\}, \end{aligned}$$

assuming that ρ is a smooth function with $\rho(x) = 0$ for all $x \leq r$ and $\rho(x) = 1$ for $x \geq R$. This function will be constructed in the next subsection. Figure 6.4 sketches how ρ effects the behaviour of a given surface $z = \sin(x) \sin(y)$.

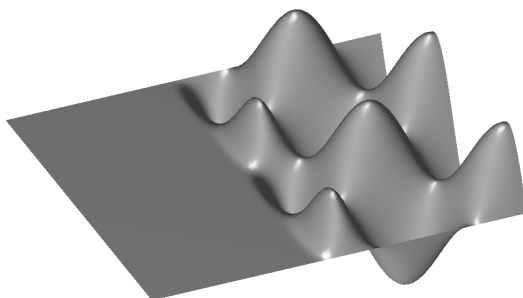


Figure 6.4: Plot of a perturbed surface $z = \sin(x) \sin(y)$

Define

$$\tilde{F}(x, y, z) = \tilde{d}_1(x, y, z) - \tilde{d}_2(x, y, z),$$

where \tilde{d}_i denotes the generalised distance function with respect to \tilde{S}_i . Evidently

$$\tilde{F}(R, y, 0) = 0$$

for all $y \in \mathbb{R}$. Every such point serves as initial value of an arc length parametrised curve

$$c: \begin{cases} I_\epsilon = [0, \epsilon] & \rightarrow & \mathbb{R}^3 \\ t & \mapsto & c(t) = (x(t), y, z(t)) \end{cases}$$

such that $c(0) = (R, y, 0)$ and $\tilde{F}(c(t)) = 0$ for all $s \in I_\epsilon$. The Predictor Corrector method introduced in 2.4 can be employed to trace this curve α . Note that the Jacobi equations and the geodesic equations are involved in the Predictor step as well as in the Corrector step. This increases the time complexity of this approach. It suffices to trace α until the condition $x(t) \leq r$ holds.

Perturbation Functions

For the construction of initial values of the medial differential equations in the context of the Medial Axis Transform we made use of a sufficiently differentiable function ρ that vanishes for $x \leq r$ and that is 1 for $x \geq R$. Such a function can be defined in different ways. Two approaches will be discussed here.

Without loss of generality we will begin with a piecewise polynomial function $p_{0,1} \in C^4([0, 1])$. The following conditions on $p_{0,1}$ are posed:

- $p_{0,1}^{(n)}(0) = 0$,

- $p_{0,1}^{(n)}(1) = \delta_n^0$,

for all $n = 0, \dots, 4$. Then

$$p_{0,1}|_{[0,1)}(t) = a_5t^5 + a_6t^6 + a_7t^7 + a_8t^8 + a_9t^9.$$

The definition of the coefficients a_i requires that

$$\begin{pmatrix} 1 & 1 & 1 & 1 & 1 \\ 5 & 6 & 7 & 8 & 9 \\ 20 & 30 & 42 & 56 & 72 \\ 60 & 120 & 210 & 336 & 504 \\ 120 & 360 & 840 & 1680 & 3024 \end{pmatrix} \begin{pmatrix} a_5 \\ a_6 \\ a_7 \\ a_8 \\ a_9 \end{pmatrix} = \begin{pmatrix} 1 \\ 0 \\ 0 \\ 0 \\ 0 \end{pmatrix}$$

and hence

$$p_{0,1}|_{[0,1)}(t) = 126t^5 - 420t^6 + 540t^7 - 315t^8 + 70t^9.$$

For $(r, R) \neq (0, 1)$ a simple affine transformation yields the new perturbation function

$$p_{r,R}(t) = p_{0,1}\left(\frac{t-r}{R-r}\right).$$

Figure 6.5 sketches a plot of the perturbation function $\tilde{p}_{1,3}$.

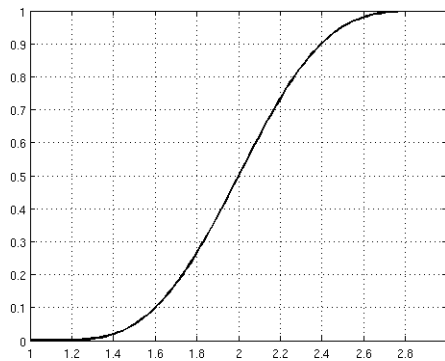


Figure 6.5: Plot of a perturbation function

Since piecewise differentiable functions cannot be infinitely often differentiable (except for the trivial cases), another trick has to be employed for the construction of a smooth function ρ with the aforementioned properties. Put

$$\psi(t) = \begin{cases} 0 & x \leq 0 \\ e^{-1/x} & x > 0 \end{cases}.$$

It is easy to show that ψ is smooth. Define

$$\phi_{r,R}(t) = \psi(t-r)\psi(R-t)$$

and finally put

$$p_{r,R}(t) = \frac{\int_r^t \phi_{r,R}(y) dy}{\int_r^R \phi_{r,R}(y) dy}.$$

Clearly, $p_{r,R}$ is a smooth function that meets the above conditions. See figure 6.6 for the plots of the related functions.

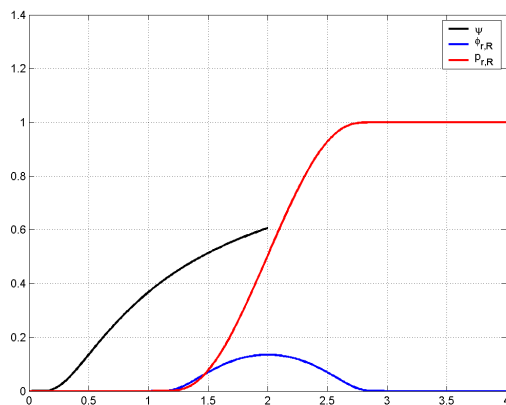


Figure 6.6: Plot of the functions ψ , $p_{r,R}$ and $\phi_{r,R}$

Remark 6.3.1

The second definition of the smooth function $p_{r,R}$ has the disadvantage that it involves an integral representation, yet it yields better numerical results. In contrast the first definition can be implemented more easily. The evaluation of the polynomial function however produces some numerical errors.

$\rho(x) := p_{r,R}(x)$ has the desired properties that were required for the homotopy method from section 6.3.

6.3.2 Nelder-Mead Method

Another possibility to find an initial point of the medial equations is to apply the **Nelder-Mead method**. A nice description of this also called **downhill-simplex method** can e.g. be found in [Mil99]. Though it is called a simplex method it has nothing to do with the simplex method known from linear programming. The method can be applied to (non-smooth) multivariate functions without using derivatives. Typically, many evaluations of the function are needed for the determination of the zeros of such a function. Starting from a simplex S_k with vertices x^0, \dots, x^n a smaller simplex needs to be found based on the function values $f(x^0), \dots, f(x^n)$. Let

$$f(x^m) = \max\{f(x^0), \dots, f(x^n)\}.$$

x^m is then replaced by a new point with function value smaller than $f(x^m)$ in order to construct a new simplex with this vertex. The vector

$$b^m = \frac{1}{n} \sum_{\substack{i=0 \\ i \neq m}}^n x^i$$

is called the **barycenter** of the points $x^i, i \neq m$. Three different geometric operations outline how the point x^m is replaced in the next step.

- **Reflection:** x^m is reflected at the barycenter b^j with reflection constant $0 \leq \alpha_r < 1$:

$$x^r = b^i + \alpha_r(b^i - x^m).$$

- **Expansion:** x^m is translated in the direction $x^r - x^m$ with expansion constant $\alpha_e > 1$:

$$x^e = b^i + \alpha_e(x^r - b^i).$$

- **Contraction**

- **Partial inner contraction:** x^m is translated in the direction $b^i - x^m$ with contraction constant $0 < \alpha_c < 1$. The new point lies inside the simplex S_k :

$$x^c = b^i + \alpha_c(x^m - b^i).$$

- **Partial outer contraction:** x^i is translated in the direction $b^i - x^r$ with contraction constant $0 < \alpha_c < 1$. The new point lies outside the simplex S_k :

$$x^c = b^i + \alpha_c(x^r - b^i).$$

- **Total contraction:** Every point $x^i, i \neq m$ is replaced by the point

$$\hat{x}^i = \frac{1}{2}(x^i + x^m).$$

6.4 Example

The next example shows some results of a Medial Axis Transform of two surface patches S_1 and S_2 .

Consider a 3-dimensional length space with metric tensor

$$g_{ij} = \begin{pmatrix} 1 + \cos(y)^2 & -x \sin(y) \cos(y) & -0.3 \cos(y) \\ -x \sin(y) \cos(y) & 1 + x^2 \cos(y)^2 & 0.3x \sin(y) \\ -0.3 \cos(y) & 0.3x \sin(y) & 1.09 \end{pmatrix}$$

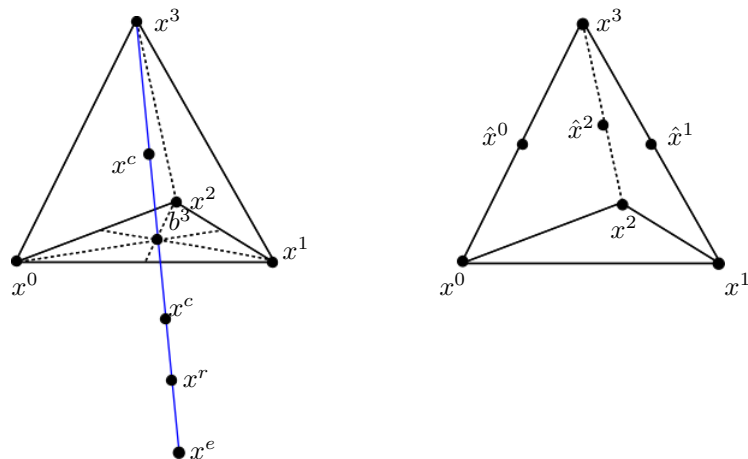


Figure 6.7: Reflection, expansion and contraction for a tetrahedron

and the two reference surfaces represented by the height functions

$$h_1(x, y) = 0.2 \sin(x) + \cos(y) + 1.5 \quad (6.4.1)$$

$$h_2(x, y) = 0.3 \sin(x) + 0.5 \cos(y + 0.6) + 1.2 \quad (6.4.2)$$

The lower surface is represented by h_2 and the upper surface by h_1 . Figure 6.8 shows the result of the Medial Axis Transform for these reference surfaces under the assumption that only those points (x, y, z) of the lower surface are involved where $|x|, |y| \leq 1$.

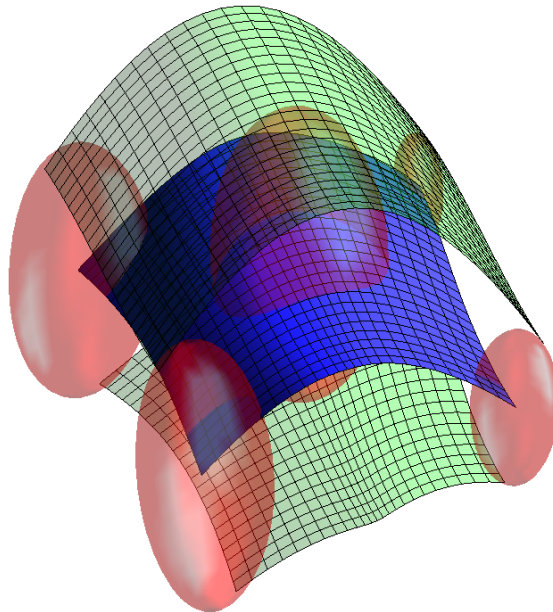


Figure 6.8: Medial Axis Transform of two reference surfaces

7 Geodesic Voronoi Diagrams

To the authors best knowledge the main concepts of the Voronoi diagram were first described by George Voronoi in the journal [Vor07] though its history can be traced back to Descartes 1644. The applications are wide spreading. In Geophysics and Meteorology for example it was named after the American meteorologist Alfred H. Thiessen, in condensed matter Physics it is often called Wigner-Seitz unit cells. In arbitrary metric spaces they are sometimes called metric fundamental polygons though their shape is rather far from being a polygon. A nice overview over comprising calculation techniques can be found in [OBS00] or in condensed form in the *Handbook of Computational Geometry* ([GR04]).

We assume that we have been given a length space $(M, d) = (\mathbb{R}^3, d_1)$, which means that every two distinct points p and q in M can be joined by a length minimal smooth geodesic curve. This length can be regarded as the distance $d_1(p, q)$ of the points p and q . Let $S = \{p_1, \dots, p_n\} \in M$ be a set of sites. Every site p_i can be related to its Voronoi region $VR(p_i, S)$ containing all points p that are closer to p_i than to any other site $p_j, j \neq i$.

We will introduce some local methods that for the first time make the precise computation of Voronoi diagrams of discrete point sets in 3-dimensional length spaces feasible in case the points fulfil a general position assumption and every Voronoi region is contained in a geodesically convex set. This means that any two distinct points can be joined by a unique geodesic being contained in the convex set.

The natural distance function d that makes M a metric space is essential for this definition of Voronoi regions. The Voronoi diagram that is defined to be the complement of these regions, thus consists of faces, edges and vertices under some regularity assumptions.

From Euclidean Voronoi diagrams we already know that the **circumsphere condition** must hold for every vertex v . The same condition is true in this more sophisticated situation. Every vertex v is at least adjacent to three nearest sites p_i, p_j and p_k with

$$d(c, p_i) = d(c, p_j) = d(c, p_k) = r$$

such that

$$B(c, r) = \{x \in M; d(c, x) < r\}$$

contains no site $p \in S$.

The **R**andomised **I**ncremental **C**onstruction **S**cheme tries to compute the Voronoi diagram inside a symbolic sphere $\mathcal{S} \subset M$ containing all relevant features of the Voronoi diagram. \mathcal{S} can be seen as the bisector of every point p_i and the additional site ∞ . Therefore, the RICS begins with five sites $R = \{p, q, r, s, \infty\}$ and introduces the remaining sites $u \in S \setminus R$ step by step. It maintains a history graph and a directed acyclic graph. To reduce time complexity it only computes the skeleton of the updated Voronoi diagram in every step. The update of the skeleton leads to an intersection problem of the old Voronoi edges and the new Voronoi region $VR(u, R \cup \{u\})$, where R represents the set of sites that have already been introduced and u being introduced next.

One main goal of the subsequent explanations is to introduce algorithms for the determination of geodesic joins and the vertices v of the Voronoi diagram. An excellent candidate $v = (x, y, z)$ for a vertex satisfies the equations

$$\begin{aligned} d_p(x, y, z) - d_q(x, y, z) &= 0, \\ d_q(x, y, z) - d_r(x, y, z) &= 0, \\ d_r(x, y, z) - d_s(x, y, z) &= 0, \end{aligned}$$

where p, q, r, s represent four different sites. The solution is a cut locus point if the set

$$\{q \in M; d(v, q) < d_p(v)\} \cap S$$

is empty.

The geodesic polar coordinates can be seen as a natural generalisation of the Euclidean polar coordinates. These polar coordinates involve the geodesic differential equations. As long as the sphere \mathcal{S} is a convex neighbourhood of the sites S , it can be assured that the geodesic polar coordinates of a site provide a diffeomorphism of M inside \mathcal{S} . Under some more assumption we can assure that the geodesic Voronoi diagram has the same topological properties as the Euclidean Voronoi diagram. This will be the fundamental assumption of our approach.

7.1 Definition Of Voronoi Diagrams And Examples

The definition of a Voronoi diagram only involves the existence of a metric space (M, d) . In our case the distance of two points is defined to be the length of the shortest geodesic join of these points.

Definition 7.1.1

Given two points $p, q \in M$, the **bisector** $B(p, q)$ consists of all points $x \in M$ that have the same distance to p as to q , i.e.

$$B(p, q) = \{x \in M | d(p, x) = d(q, x)\}.$$

In addition the metric d makes it possible to define half spaces as in the Euclidean case.

Definition 7.1.2

Let $p, q \in M$. $D(p, q)$ is the set of all points that are closer to p than to q :

$$D(p, q) = \{x \in M \mid d(p, x) < d(q, x)\}.$$

An analogue characterisation can be made for q :

$$D(q, p) = \{x \in M \mid d(p, x) > d(q, x)\}.$$

Note that the order of p and q is crucial for the definition of the sets $D(p, q)$ and $D(q, p)$.

Consider a discrete point set

$$S = \{p_1, \dots, p_n\}.$$

Definition 7.1.3

$$VR(p, S) = \bigcap_{q \in S \setminus \{p\}} D(p, q)$$

is called **Voronoi region** of p with respect to S . Furthermore, the set

$$V(S) = \bigcup_{p \in S} \partial VR(p, S) \tag{7.1.1}$$

is called the **Voronoi diagram** of the reference set S .

In Euclidean spaces it is straightforward to see that each Voronoi cell is convex because it is the intersection of convex half spaces. Moreover, each bounded Voronoi cell consists of piecewise hyperplanes of dimension $n - 1$ in case $M = \mathbb{R}^n$.

Without further restrictions concerning the metric d the bisectors $B(p, q)$ may look strange. Consider e.g. the space $M = \mathbb{R}^2$ and the Manhattan metric

$$d(p, q) = |p_1 - q_1| + |p_2 - q_2|.$$

If for instance the points p and q are diagonal vertices of a square with axis parallel edges, the bisector $B(p, q)$ contains two quadrants of the plane (see figure 7.2).

The reason for the strange behaviour of such bisectors is the fact that the distance unit circle with respect to the metric d contains line segments that are parallel to the segment from p to q . Fortunately, this is not often the case.

In the next section some properties of the Voronoi diagram are given.

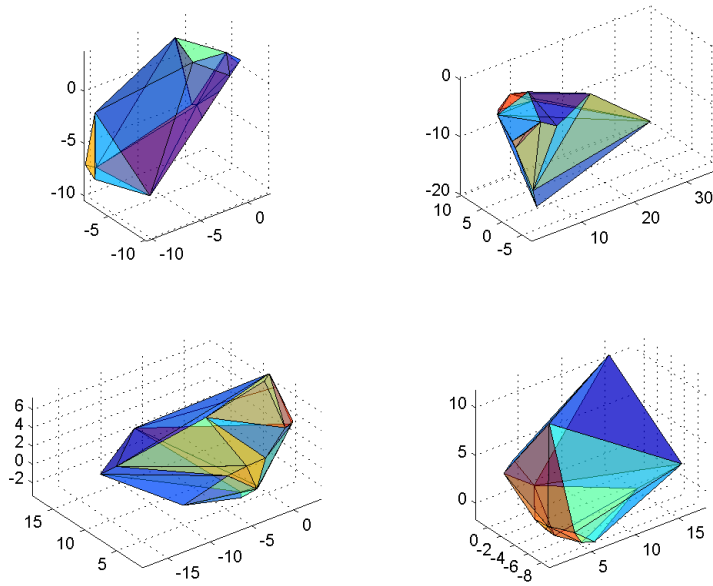


Figure 7.1: Voronoi Cells

7.2 Properties Of Geodesic Voronoi Diagrams

Consider a complete and connected Riemannian manifold M . We will prove some basic properties of the geodesic Voronoi diagram. Therefore, we require some definitions that try to generalise the definitions of convex and star shaped sets being contained in a Riemannian manifold.

Definition 7.2.1

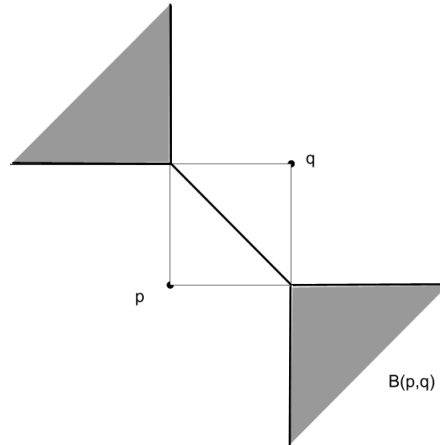
A set $C \subset M$ is called **strongly convex** if and only if for every two points $p, q \in C$ every shortest geodesic between p and q belongs to C . We say that C is **weakly convex** if there exists at least one minimal join of p and q that totally lies in C .

Note that singletons are always strongly convex. The generalisation of star shaped sets is important for some properties of Voronoi regions.

Definition 7.2.2

A set $C \subset M$ is called **strongly star shaped** if and only if there exists a centre point $p \in C$ such that for every point $q \in C$ every minimal join of p and q belongs to C . C is **weakly star shaped** if there is at least one minimal join with the above property.

This yields the following


 Figure 7.2: Bisector of two points p and q
Theorem 7.2.1

Consider a complete and connected Riemannian manifold M with intrinsic distance function d . Every Voronoi region $VR(p, S)$ is strongly star shaped with star centre p .

Proof: Let $x \in VR(p, S)$. Assume there exists a minimal join $\gamma : [0, s] \rightarrow M$ with $\gamma(0) = p$ and $\gamma(s) = x$ and $y = \gamma(t) \notin VR(p, S)$. This means that $q \in S$ exists such that either $y \in VR(q, S)$ or $y \in B(p, q)$ holds. In either cases we have $d(p, y) \geq d(q, y)$. As a result

$$\begin{aligned} d(p, x) &= d(p, y) + d(y, x) \\ &\geq d(q, y) + d(y, x) \\ &\geq d(q, x) \end{aligned}$$

This is a contradiction to the assumption that x belongs to the Voronoi region $VR(p, S)$. Thus, the proof is complete. □

A direct consequence to this theorem is the next corollary.

Corollary 7.2.1

Let M be a complete and connected Riemannian manifold and d be the corresponding intrinsic distance function and S be a discrete finite point set. Then for every point $p \in S$ the Voronoi region $VR(p, S)$ is connected.

Theorem 7.2.2

Let (M, d) be a metric space and $S = \{p_1, \dots, p_n\} \subset M$ be a reference set of sites. Then every Voronoi region $VR(p_i, S)$ is open and $V(S)$ is closed.

Proof: It suffices to show that every half space $D(p, q)$ for distinct p and q is open. Let $x \in D(p, q)$. From the definition of the half space we get $d(p, x) < d(q, x)$. Assume

that for every $r > 0$ there exists an $y_r \in B_r(x)$ such that $d(p, y_r) \geq d(q, y_r)$. Consider the sequence $r_n = 1/n$. Conclude that

$$d(p, y_{r_n}) \geq d(q, y_{r_n}), \quad (7.2.1)$$

$$d(x, y_{r_n}) \rightarrow 0. \quad (7.2.2)$$

Taking the limits it turns out that x did not belong to the half space $D(p, q)$ since $d(p, x) \geq d(q, x)$ as a direct consequence from (7.2.1) and (7.2.2). $V(S)$ is the complement of the open set

$$\bigcup_{i=1}^n VR(p_i, S)$$

and thus closed. □

Let $(M, d_k) = (\mathbb{R}^n, d_k)$ be a length space with d_k being induced by the metric tensor (g_{ij}^k) and S be a set of sites. Let $V^k(S)$ be the Voronoi diagram with respect to the metric d_k . Two Voronoi diagrams V^i and V^j are called **equivalent** if there exists a homoeomorphism $\psi : \mathbb{R}^n \rightarrow \mathbb{R}^n$ such that $V^j = \psi(V^i)$. Even if d is equivalent to the Euclidean metric on \mathbb{R}^2 , i.e.

$$K_1 \|x - y\| \leq d(x, y) \leq K_2 \|x - y\|$$

for some $0 < K_1 \leq K_2$, it cannot be assured that even the bisector of two points is homoeomorphic to a line. Thus, the examination of equivalence classes has no relevancy for the rest of this thesis.

Example 7.2.1

Consider the height function

$$h(x) = \begin{cases} \|x\|^2 & \|x\|^2 \leq 4 \\ 4\|x\| - 4 & \|x\|^2 > 4 \end{cases}$$

that induces a metric d . Choose $p = (0, 0)$ and $q = (q_1, 0)$. To simplify the notations let

$$r_0 = \frac{\sqrt{17} - \frac{1}{4} \ln(4 + \sqrt{17})}{\sqrt{17} - \pi}.$$

We want to show that in case $q_1 > r_0$ the bisector $B(p, q)$ is captured inside the disc $B_p(q_1)$. For $\|x\| = 2$ we have

$$\begin{aligned} d(p, x) &= \int_0^2 \sqrt{1 + 4t^2} dt \\ &= \frac{1}{4} \left[2t\sqrt{4t^2 + 1} + \ln \left(2t + \sqrt{4t^2 + 1} \right) \right]_0^2 \\ &= \sqrt{17} + \frac{1}{4} \ln(4 + \sqrt{17}). \end{aligned}$$

For $\|x\| > 2$ a simple calculation yields

$$d(p, x) = \frac{1}{4} \ln(4 + \sqrt{17}) - \sqrt{17} + \sqrt{17}\|x\|.$$

On the other hand $d(q, x)$ can be bounded by the length of a half circle segment in case $\|q\| = \|x\| > 2$, i.e.

$$d(q, x) \leq \pi\|x\|.$$

Define $F(x) = d(p, x) - d(q, x)$ and deduce $F(x) > 0$ for all $\|x\| = \|q\|$ in case $q_1 > r_0$ as claimed. Obviously, the bisector then must be a closed curve since the corresponding half spaces must be disjoint.

The calculation of the geodesic Voronoi diagram or the cut locus heavily involves the estimation of bisector faces, bisector edges and vertices. There are situations where this calculation can be simplified.

Definition 7.2.3

Let S, M be Riemannian manifolds such that S is a submanifold of M . S is called **totally geodesic**, if every geodesic in S is a geodesic in M . In other words, the second fundamental form of S is zero.

Beem showed the following result for Pseudo-Riemannian manifolds (cf. [Bee75]):

Theorem 7.2.3

Let M be a Pseudo-Riemannian manifold and p, q be two distinct points. $B(p, q)$ is a totally geodesic submanifold if and only if M has constant curvature.

This means that under the circumstance $\dim(M) = 2$ and constant Gaussian curvature every bisector is a geodesic. In fact, these cases are only of theoretical interest in the context of computational geometry. Nevertheless, it is an interesting result for we have a sufficient and necessary condition of bisectors to be totally geodesic submanifolds.

A nice classification of bisectors in a clearly arranged situation was done by Wolter (cf. [Wol85]). It is stated in the following theorem.

Theorem 7.2.4

Let (M, d) be a simply connected complete Riemannian manifold of dimension 2 without conjugate points. Let $p, q \in M$ be two points with $d(p, q) > 0$. The midpoint of p and q is the well defined point m with the property $d(m, p) = d(m, q) = \frac{1}{2}d(p, q)$. Define the half open intervals $I_1 := [0, 1)$ and $I_{-1} = (-1, 0]$.

- Let K be the component of $B(p, q)$ with $m \in K$. Then there exists a C^1 -smooth embedding $\psi : (I_{-1} \cup I_1) \rightarrow M$ with $\psi(0) = m$ and $\psi(I_{-1} \cup I_1) = K$. For every $k \in \{-1, 1\}$ the condition

$$\lim_{t \rightarrow k} d(m, \psi(t)) \rightarrow \infty$$

must hold.

- Moreover, the following identities must be filled:

$$\begin{aligned} B(p, q) &= \overline{\psi(I_{-1})} \cup \overline{\psi(I_1)}, \\ \{m\} &= \overline{\psi(I_{-1})} \cap \overline{\psi(I_1)}. \end{aligned}$$

7.3 Geometric Transformation

Even though the Euclidean Voronoi diagram has been investigated intensively, it has not lost its relevancy during the decades. Edelsbrunner for example introduced in ([Ede87]) a way to compute Voronoi diagrams only by one simple transformation, the so called geometric transformation. He found out that the duality of the Voronoi diagram and the Delaunay triangulation can be used to proof that the computation of a 3D Voronoi diagram has computational and memory complexity (performance) $O(n^2)$. His idea was to reduce the problem to a seemingly easier one, i.e. the computation of convex hulls of a discrete point set in 4D. We will sketch this idea in the following.

Let $S = \{p_1, \dots, p_n\} \subset \mathbb{R}^3$ be a discrete point set. Consider the set

$$P = \{(x, y, z, w) \in \mathbb{R}^4; x^2 + y^2 + z^2 = w\}.$$

P is a hypersurface of revolution. Every point $p \in \mathbb{R}^3$ can be projected onto the hyperparaboloid by

$$p = (x, y, z) \rightarrow p' = (x, y, z, x^2 + y^2 + z^2).$$

The map $p \rightarrow p'$ has some striking properties, e.g.

Theorem 7.3.1

Let

$$K = \{(x, y, z) \in \mathbb{R}^3; (x - m_1)^2 + (y - m_2)^2 + (z - m_3)^2 = r^2\}$$

be a 2-dimensional sphere. The projected set K' is incident to a hyperplane in \mathbb{R}^4

Proof: We have

$$\begin{aligned} K' &= \{(x, y, z, w) \in \mathbb{R}^4 \mid (x - m_1)^2 + (y - m_2)^2 + (z - m_3)^2 = r^2 \\ &\quad \text{and } x^2 + y^2 + z^2 = w\} \\ &= \left\{ (x, y, z, w) \in \mathbb{R}^4; w - 2m_1x - 2m_2y - 2m_3z + \sum_{i=1}^3 m_i^2 = r^2 \right\} \cap P. \end{aligned}$$

It is straightforward that K' is the intersection of P with a hyperplane in \mathbb{R}^4 and the claim follows. □

Now let S' be the projection of S onto the hyperparaboloid P .

Theorem 7.3.2

The Delaunay tetrahedrisation of S is the projection of the lower convex hull of S' onto the xyz -space.

Proof: Four points $p, q, r, s \in S$ build a Delaunay tetrahedron if and only if the circumscribed sphere does not contain any other point from S . Let K be the circumscribed sphere of the tetrahedron $\text{tetra}(p, q, r, s)$. According to the last theorem $K' = E \cap P$ for a hyperplane E of \mathbb{R}^4 . Obviously, the points (x, y, z) inside K correspond to the points on P below the hyperplane E . Thus, the following statements are equivalent:

1. No point in S lies within the sphere K .
2. No point of S' lies below E .

The last property means that p', q', r', s' build a tetrahedron on the boundary of the convex hull of S' . This completes the proof.

□

This nice proof was taken from Klein ([Kle97]), where he showed the same results for the 2D case.

In the sequel we introduce an incremental algorithm with $O(n^2)$ time and space complexity, where n is the number of sites. It is based on some topological results for simple abstract Voronoi diagrams. The presented algorithm makes some assumptions on the structural complexity of the intersection of bisectors. It will be explained, how such intersections can be computed. As we have seen before it is possible that for two points p, q on a Riemannian manifold M the bisector $B(p, q)$ is a compact surface. In addition it can occur that the bisector $B(p, q)$ possesses more than one component. This is the main difference between Euclidean and geodesic Voronoi diagrams.

Since this work only serves as a first step towards the computation of 3D geodesic Voronoi diagrams we will basically focus on the local methods ignoring the topological variety of 3D geodesic Voronoi diagrams. Indeed, our approach presumes that the Voronoi diagrams have the same topological properties like Euclidean Voronoi diagrams. However, there is a big difference in the computational effort since the local shape of Voronoi faces, edges and vertices can only be described by the medial equations that build up a challenging task.

Our approach requires that we can compute geodesic distances between points. The computation of minimal joins between points can be seen as a boundary value problem where the uniqueness of the solution cannot be assured. We will show how to obtain at least one of these solutions by using homotopy methods.

7.4 Minimal Joins

As we have seen earlier it is quite common to use different representation forms of hypersurfaces $M \subset \mathbb{R}^{n+1}$. Two different forms are treated here in the context of the minimal join problem: **implicitly** and **explicitly** given hypersurfaces. Implicitly given hypersurfaces are characterised by the fact that there exists a continuous function

$$h : \mathbb{R}^{n+1} \rightarrow \mathbb{R}$$

such that $h(x) = 0$ if and only if $x \in M$. Without further restrictions concerning h one cannot expect M to be smooth. Therefore, we must assume that

- h is a smooth function.
- 0 is a regular value of h .

Nevertheless, continuous functions h can lead to smooth hypersurfaces. Let us for example take the function

$$h(x) = d_M(x) = \inf_{q \in M} d(x, q).$$

It can be shown immediately that $M = h^{-1}(0)$ for compact and smooth hypersurfaces M and that h is only a continuous function.

In the subsequent sections three methods shall be described for the efficient computation of minimal joins in Riemannian manifolds. Of all these methods the Curve-Tracking-Method is the most universal one. It is simply assumed that for given points p and q an additional point r is known, whose normal coordinates with respect to p can be obtained, as well as a smooth curve α , that joins the points r and q . The main goal is then to parametrise the normal coordinates of the points $\alpha(t)$ by the run length parameter t of the curve α using the aforementioned Predictor-Corrector-Methods. Such a point r can easily be obtained only by starting an arbitrary geodesic from p with any given initial direction. The curve α typically will also not cause any troubles.

The Method Of Single Coordinate Charts assumes that for the computation of a minimal join of two given points with respect to a given homotopy method only one single chart of the manifold M is involved. This is true in many cases.

The Implicit Method however does not know anything about parametrisation functions of the given manifold. It uses a single level function h like in the definition of implicit hypersurfaces.

7.4.1 The Curve-Tracking-Method

Let M be a 2-dimensional complete Riemannian manifold and $p, q \in M$. Suppose $\{e_1, e_2\}$ is an orthonormal basis of the tangent space $T_p M$. Putting

$$g(s, \phi) = \exp_p(s(\cos(\phi)e_1 + \sin(\phi)e_2))$$

we can use g to define the function

$$F(s, \phi, t) = g(s, \phi) - \alpha(t),$$

where $\alpha : [0, 1] \rightarrow M$ is a smooth curve in M with the following properties:

- $\alpha(0) = g(s_0, \phi_0)$,
- $\alpha(1) = q$,
- α does not contain conjugate points with respect to p .

Clearly,

$$\dim DF(s, \phi, t) \leq 2$$

for all tuple (s, ϕ, t) such that $F(s, \phi, t) = 0$ since then g_s, g_ϕ and α' refer to the tangent space $T_{\alpha(t)}M$. With the above prearrangements it is not hard to see that there exist functions

$$s, \phi : [0, 1] \rightarrow \mathbb{R}$$

such that

- $s(0) = s_0$,
- $\phi(0) = \phi_0$ and
- $F(s(t), \phi(t), t) = 0$ for all $t \in [0, 1]$.

Like in 3.4 we get

$$s' = \langle \alpha', g_s \rangle, \tag{7.4.1}$$

$$\phi' = \frac{\langle \alpha', g_\phi \rangle}{\|g_\phi\|^2} \tag{7.4.2}$$

for all $t \in [0, 1]$. (7.4.1) and (7.4.2) have a unique solution and

$$\begin{aligned} F(s(1), \phi(1), 1) &= g(s(1), \phi(1)) - \alpha(1) \\ &= g(s(1), \phi(1)) - q \\ &= 0 \end{aligned}$$

Example 7.4.1

Assume the parametrisation of a bordered surface S is given by

$$f(x, y) = \begin{pmatrix} x \\ y \\ xy - \sin(x) \end{pmatrix}$$

and in addition the points

$$\begin{aligned} p &= (0 \ 1 \ 0)^T, \\ q &= (-1 \ -1 \ 1 + \sin(1))^T. \end{aligned}$$

The right part of figure 7.3 sketches how the Predictor-Corrector-Method works in case of the given black curve α . The point p is encircled by the green offset curve. The red curves only represent a sample of the family of geodesics that join points on the curve α with p . The left part of the figure sketches the curve $t \mapsto (s(t), \phi(t))$. The distance of the points p and q is approximately $d_1(p, q) = 3$.

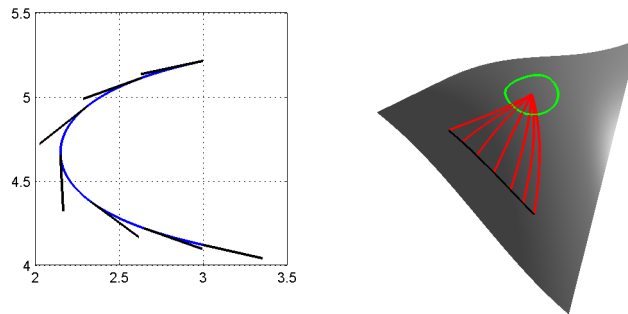


Figure 7.3: The Curve-Tracking-Method

In general one cannot assume that

$$d_1(p, g(s(t), \phi(t))) = s(t)$$

for all $t \in [0, 1]$. This is due to the fact that the curve α may intersect with the cut locus of the point p .

Remark 7.4.1

We have proven that the computation of geodesic joins is feasible on 2-dimensional Riemannian manifolds using Predictor- Corrector-Methods or by solving the system (7.4.1) - (7.4.2). The same is true in case of higher dimensional manifolds with the slight difference that the system that corresponds to (7.4.1) - (7.4.2) will be more difficult to solve. Using spherical coordinates we obtain in case $\dim(M) = 3$ a possible definition of a offset function by

$$g(s, \phi, \psi) = \exp_p(s(\cos(\phi) \cos(\psi)e_1 + \cos(\phi) \sin(\psi)e_2 + \sin(\phi)),$$

assuming that $\{e_1, e_2, e_3\}$ is an orthonormal basis of T_pM .

7.4.2 The Method Of Single Coordinate Charts

Consider the graph M of a smooth function $h : \mathbb{R}^3 \rightarrow \mathbb{R}$ and the homotopy H from example 3.4.1. As we already know $H(M, \lambda)$ is the graph of the smooth function $\lambda \cdot h$.

For the special graph $H(M, 0) = M_0$ we see that every two points $p_0, q_0 \in M_0$ can be joined by the geodesic

$$\gamma_0 : \begin{cases} [0, 1] & \rightarrow & M_0 \\ t & \mapsto & p_0 + t(q_0 - p_0) \end{cases} .$$

Let

$$f : U \subset \mathbb{R}^n \rightarrow M$$

be a local parametrisation of the manifold M . We assume that every point $r \in M$ that is involved in the discussion of the following homotopy method has a representation with respect to f , i.e. there exists a parameter value $u_r \in U$ such that $f(u_r) = r$ holds. As always we will employ the geodesic equations. Not as usual we even deal with a family of parametrisations

$$f_\lambda : U \subset \mathbb{R}^n \rightarrow H(M, \lambda).$$

Moreover, we assume that every involved point $r_\lambda \in M_\lambda$ has a representation with respect to f_λ . The target points will again be denoted by p and q , where $f(u_p) = p$ and $f(u_q) = q$ holds for the distinct values $u_p, u_q \in U$. Let $\gamma_\lambda : \mathbb{R} \times \mathbb{R}^n \rightarrow U$ be solution of the system

$$\gamma_\lambda(0, v) = u_p, \quad (7.4.3)$$

$$\frac{\partial}{\partial s} \gamma_\lambda(0, v) = v, \quad (7.4.4)$$

$$\frac{\partial^2}{\partial s^2} \gamma_\lambda^k(s, v) + {}_\lambda \Gamma_{ij}^k \gamma_\lambda^i(s, v) \gamma_\lambda^j(s, v) = 0. \quad (7.4.5)$$

The ${}_\lambda \Gamma_{ij}^k$ denote the Christoffel symbols of the hypersurface $H(M, \lambda)$ with respect to f_λ . This yields

$${}_\lambda \Gamma_{ij}^k = \frac{\lambda^2 h_{ij} h_k}{1 + \lambda^2 \|\nabla h\|^2}.$$

With γ_λ a new function F can be constructed:

$$F : \begin{cases} \mathbb{R}^n \times [0, 1] & \rightarrow & U \\ (v, \lambda) & \mapsto & \gamma_\lambda(1, v) - u_q(\lambda) \end{cases} ,$$

where $f_\lambda(u_q(\lambda)) = H(q, \lambda)$. The most importance is attached to the function F now. If we want to employ Predictor-Corrector-Methods for the computation of the zeros of F we first need an initial solution of $F(v, \lambda) = 0$ as well as the Jacobian matrix of F at given parameter values (v, λ) . It is not hard to deduce the identity

$$F(u_q - u_p, 0) = 0.$$

Furthermore, we receive

$$DF(v, 0) = \begin{pmatrix} 1 & 0 & \dots & 0 & \star \\ 0 & 1 & \dots & 0 & \star \\ \vdots & \vdots & & \vdots & \vdots \\ 0 & 0 & \dots & 1 & \star \end{pmatrix} ,$$

for all $v \in \mathbb{R}^n$. The last equation already indicates that DF has maximum rank at the beginning of the Predictor-Corrector-Method. This is an important prerequisite. Consequently, a solution of the subsequent system is of special interest:

- $\alpha(0) = (u_q - u_p, 0)$,
- $\alpha'(t) = t(DF(\alpha(t)))$.

The method ends in case we have found a parameter value $t^* \in \mathbb{R}$ such that

$$\alpha(t^*) = (v(t^*), 1)$$

holds, since we are only interested in the solution for $\lambda = 1$.

A big drawback of this method is the costly computation of the Jacobian $DF(v, \lambda)$ for given v and λ . In order to find a remedy to cure this drawback one can employ an approximation of DF using central difference quotients. At the end of the Predictor-Corrector-Method we want to have an approximation of the initial direction v that is as good as possible. This approximation can be improved by simple Newton-Method steps.

Remark 7.4.2

The only difficult in the computation of the Jacobi matrix DF poses the derivative $\frac{\partial}{\partial \lambda} F$. Looking closer at the system (7.4.3) - (7.4.5) one notices that $\frac{\partial}{\partial \lambda} F$ can be obtained by implicit differentiation of (7.4.5) with respect to λ . We will not make a complete discussion of this subject from the aforementioned reasons.

Example 7.4.2

Consider the graph M represented by the height function

$$h(x, y, z) = x^2 + y^2 + \sin(z)$$

as well as the points $p = (0, 0, 1, \sin(1))$ and $q = (-2, 3, 5, 13 + \sin(5))$. For the distance we get

$$d_1(p, q) = 12.6316.$$

Lets consider a compact and complete hypersurface M . This manifold owns a differentiable family of parametrisation functions $A = \{f_i : U_i \rightarrow V_i, i \in I\}$ that makes (M, A) a differentiable manifold. Clearly, the sets V_i are open and cover M and since M is compact one can choose a finite subset $J \subset I$, $|J| < \infty$ such that

$$M \subset \bigcup_{j \in J} V_j.$$

We will now focus on the case $\dim(M) = 2$. However, a generalisation of the subsequent ideas can be performed very easily. Assume we have been given a local parametrisation

of M due to

$$f : \begin{cases} D_f = (-\frac{\pi}{2}, \frac{\pi}{2}) \times (0, 2\pi) & \rightarrow & M \\ (\phi, \psi) & \mapsto & r(\phi, \psi) \begin{pmatrix} \cos(\phi) \cos(\psi) \\ \cos(\phi) \sin(\psi) \\ \sin(\phi) \end{pmatrix} \end{cases} . \quad (7.4.6)$$

with the same assumption as before concerning the points being involved in the Predictor-Corrector-Method.

The first fundamental tensor then can be expressed in the form

$$g_{ij}(\phi, \psi) = \begin{pmatrix} r_\phi^2 + r^2 & r_\phi r_\psi \\ r_\phi r_\psi & r_\psi^2 + r^2 \cos^2(\phi) \end{pmatrix}$$

with the determinant

$$\det(g_{ij}) = r^2(r_\phi^2 \cos^2(\phi) + r_\psi^2 + r^2 \cos^2(\phi)).$$

Note that this determinant can only be zero for $\phi \in \{-\pi/2, \pi/2\}$. We will further assume that $\psi \rightarrow r(-\frac{\pi}{2}, \psi)$ and $\psi \rightarrow r(\frac{\pi}{2}, \psi)$ are both constant functions.

The parametrisation f from (7.4.6) is a **regular parametrisation**, since the Jacobian matrix of f has full rank everywhere. Locally the parametrised surface is the graph of a height function and without going into detail one can deduce that M is locally the graph of a height function $z = z(x, y)$ in case the condition

$$\cos(\phi)(r \sin(\phi) - r_\psi \cos(\phi)) \neq 0 \quad (7.4.7)$$

holds.

To be more concrete let

$$F : \begin{cases} \mathbb{R}^3 \times D_f & \rightarrow & \mathbb{R}^3 \\ (x, y, z, \phi, \psi) & \mapsto & \begin{pmatrix} x - r(\phi, \psi) \cos(\phi) \cos(\psi) \\ y - r(\phi, \psi) \cos(\phi) \sin(\psi) \\ z - r(\phi, \psi) \sin(\phi) \end{pmatrix} \end{cases} .$$

Assume for example $F(x_0, y_0, z_0, \phi_0, \psi_0) = 0$ and let $A = DF_{z, \phi, \psi}$ be the Jacobian matrix of F with respect to the parameter z, ϕ and ψ . If $\det(A) \neq 0$, then there exists a neighbourhood U of (x_0, y_0) and functions $h_1, h_2, h_3 : U \rightarrow \mathbb{R}$ such that

$$F(x, y, h_1(x, y), h_2(x, y), h_3(x, y)) = 0.$$

h_1 is the sought graph function.

There exists a homotopy between M and the unit sphere S^2 , namely

$$H : \begin{cases} \mathbb{R}^3 \times [0, 1] & \rightarrow & \mathbb{R}^3 \\ (x, t) & \mapsto & \frac{x}{(1-t)\|x\| + t} \end{cases} , \quad (7.4.8)$$

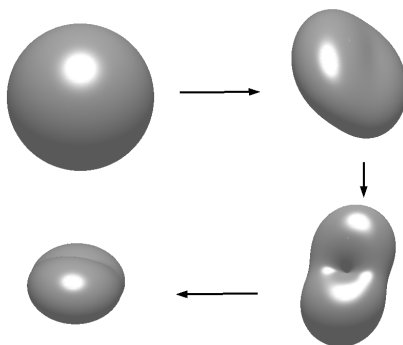


Figure 7.4: Deformation of a sphere ($r(\phi, \psi) = \sin(2\phi) \cos(\psi) + 1.2$)

where $H(M, 0) = S^2$ and $H(M, 1) = M$. Figure 7.4 sketches a sample of the family of manifolds $H(M, t)$ for distinct values t .

For the special surface $S^2 = H(M, 0)$ we see that any two points $p_0, q_0 \in S^2$ can be joined by the geodesic

$$\gamma_0 : \begin{cases} [0, 1] & \rightarrow & S^2 \\ s & \mapsto & p_0 \cos(\alpha s) + w \sin(\alpha s) \end{cases} ,$$

where $w = \frac{1}{\sin(\alpha)}(q_0 - \cos(\alpha)p_0)$ and $\cos(\alpha) = \langle p_0, q_0 \rangle$. The angle α must be chosen such that $0 \leq \sin(\alpha) \leq 1$ to assure that γ_0 is distance minimal. This directly yields $\gamma_0(1) = q_0$. Now it is not hard to see that similar arguments can be employed in case we want to compute minimal joins on the manifold M . This rather technical description will not differ from the last discussion of shortest joins in graphs.

Example 7.4.3

Let $r(\phi, \psi) = \cos(4 \sin(\phi)) + \cos^2(\phi) \sin^2(\psi) + 3$ and

$$p = \begin{pmatrix} -\frac{1}{\sqrt{2}} & 0 & \frac{1}{\sqrt{2}} \end{pmatrix}^T ,$$

$$q = \begin{pmatrix} 0 & \frac{1}{\sqrt{2}} & -\frac{1}{\sqrt{2}} \end{pmatrix}^T .$$

The distance of the points p and q is given by $d_1(p, q) = 7.9602$. Figure 7.5 sketches the geodesic join of p and q .

7.4.3 The Implicit Method

Lets consider a family of implicit given hypersurfaces M_λ that coincide with the zero set of the functions

$$h_\lambda(x) = \sum_{i=1}^3 \frac{x_i^2}{[\lambda a_i^2 + (1 - \lambda)]} - 1.$$

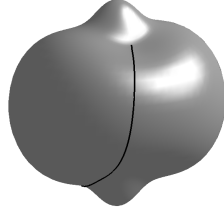


Figure 7.5: Geodesic join on a deformed sphere

For positive numbers a_i the manifold M_λ is an ellipsoid and especially for $\lambda = 0$ the unit sphere S^2 .

Let x^p and x^q be arbitrary points on the unit sphere. These coordinate vectors can be used to define functions $x^p(\lambda)$ and $x^q(\lambda)$ due to

$$\begin{aligned} x_i^p(\lambda) &= x_i^p(0)[\lambda a_i^2 + (1 - \lambda)]^{\frac{1}{2}}, \\ x_i^q(\lambda) &= x_i^q(0)[\lambda a_i^2 + (1 - \lambda)]^{\frac{1}{2}}. \end{aligned}$$

for $i = 1, 2, 3$. Both $x^p(\lambda)$ and $x^q(\lambda)$ are points on the manifold M_λ since

$$h_\lambda(x^p(\lambda)) = h_\lambda(x^q(\lambda)) = 0.$$

Typically, one would try to construct a geodesic join of $x^p(\lambda)$ and $x^q(\lambda)$ as we have done in the past using standard Predictor-Corrector-Methods. For such geodesic joins only the initial directions needs to be computed. Suppose we have been given a geodesic join γ_λ of $x^p(\lambda)$ and $x^q(\lambda)$ for $\lambda \in [0, 1]$. For a natural number $N \in \mathbb{N}_{\geq 1}$ one can chose equidistant points

$$x^p(\lambda) = p_0(\lambda), \dots, p_k(\lambda), \dots, p_N(\lambda) = x^q(\lambda)$$

for which the subsequent conditions approximately hold for sufficiently large values of N :

$$p_{k-1}(\lambda) - 2p_k(\lambda) + p_{k+1}(\lambda) = q_k(\lambda), \quad (7.4.9)$$

$$\left\langle q_k(\lambda), \frac{\nabla h_\lambda(p_k(\lambda))}{\|\nabla h_\lambda(p_k(\lambda))\|} \right\rangle = q_k(\lambda). \quad (7.4.10)$$

The vector

$$\frac{q_k(\lambda)}{\|p_k(\lambda) - p_{k-1}(\lambda)\|}$$

approximates the curvature vector of γ_λ at $p_k(\lambda)$ that should be parallel to the normal vector of the surface M_λ . This is provided by equation (7.4.10).

For $\lambda = 0$ such points can be chosen very easily. For given parameter $\lambda \in [0, 1]$ one can try to obtain the tangent vectors of the curves $p_k(\lambda)$ numerically by differentiation of (7.4.9) and (7.4.10). This is the prediction step. To get the tangent vector $p'_k(\lambda)$ one has to solve a bandwidth-limited linear system, whose coordinate matrix should at least be weakly diagonally dominant.

7.4.4 Remarks On Singular Points

Lets go back to the derivation of the equations (7.4.1) and (7.4.2). What happens if the denominator $\|g_\phi\|^2$ vanishes at a point (s_0, ϕ_0, t_0) ? The following explanations give an answer to this in a more complex situation.

Again we have the graph $M = M_0$ of a function $h_0(x_1, x_2)$ and two points $x^p = (x_1^p, x_2^p)$, $x^q = (x_1^q, x_2^q)$ such that $q = (x_1^q, x_2^q, 0) \in M_0$. Define the function

$$h_1(x_1, x_2) = (x_1 - x_1^q) \frac{\partial}{\partial x_1} h_0(x_1^q, x_2^q) + (x_2 - x_2^q) \frac{\partial}{\partial x_2} h_0(x_1^q, x_2^q).$$

Putting

$$h(x_1, x_2, \epsilon) = \epsilon h_1(x_1, x_2) + (1 - \epsilon) h_0(x_1, x_2)$$

and

$$H(x_1, x_2, \epsilon) = (x_1, x_2, h(x_1, x_2, \epsilon))$$

we obtain the following family of graphs

$$M_\epsilon = H(M_0, \epsilon),$$

where $M_0 = h_0(\mathbb{R}^2)$. Since $h(x_1^q, x_2^q, \epsilon) = 0$, it simply follows that $q \in M_\epsilon$ for all $\epsilon \in \mathbb{R}$. Furthermore, the condition

$$\begin{aligned} \frac{\partial}{\partial x_1} h(x_1^q, x_2^q, \epsilon) &= \epsilon \frac{\partial}{\partial x_1} h_0(x_1^q, x_2^q) + (1 - \epsilon) \frac{\partial}{\partial x_1} h_0(x_1^q, x_2^q) \\ &= \frac{\partial}{\partial x_1} h_0(x_1^q, x_2^q) \end{aligned}$$

assures that every M_ϵ has the same tangent plane at q . Again we consider the solution of the minimal join problem to be a point of the zero set of a function F , namely

$$\begin{aligned} F &= \begin{pmatrix} \langle g(s, \phi, \epsilon) - q, g_s(s_0, \phi_0, \epsilon_0) \rangle \\ \langle g(s, \phi, \epsilon) - q, g_{s\phi}(s_0, \phi_0, \epsilon_0) \rangle \end{pmatrix} \\ &= \begin{pmatrix} f_1(s, \phi, \epsilon) \\ f_2(s, \phi, \epsilon) \end{pmatrix}. \end{aligned}$$

We need the following

Lemma 7.4.1

Let $q(\epsilon_0) = g(s_0, \phi_0, \epsilon_0)$ be conjugate to $p(\epsilon_0)$ such that $g_\phi(s_0, \phi_0, \epsilon_0) = 0$. There exists a neighbourhood $U = U(s_0, \phi_0, \epsilon_0)$ of $(s_0, \phi_0, \epsilon_0)$ such that $F(s, \phi, \epsilon) = 0$ is equivalent to $g(s, \phi, \epsilon) = q$ for all $(s, \phi, \epsilon) \in U$.

Proof: This simply follows from the fact that $g_s(s_0, \phi_0, \epsilon_0)$ and $g_{s\phi}(s_0, \phi_0, \epsilon_0)$ are basis vectors of $T_{q(\epsilon)}M_\epsilon$ for all ϵ .

□

If the conditions of the last lemma hold the Jacobian of F at $(s_0, \phi_0, \epsilon_0)$ is given by

$$DF = \begin{pmatrix} 1 & 0 & \langle g_\epsilon(s_0, \phi_0, \epsilon_0), g_s(s_0, \phi_0, \epsilon_0) \rangle \\ 0 & 0 & \langle g_\epsilon(s_0, \phi_0, \epsilon_0), g_{s\phi}(s_0, \phi_0, \epsilon_0) \rangle \end{pmatrix}.$$

Let us assume that $\frac{\partial}{\partial \epsilon} f_1$ and $\frac{\partial}{\partial \epsilon} f_2$ vanish at $(s_0, \phi_0, \epsilon_0)$, because otherwise we could apply a Predictor-Corrector-Method. From the implicit function theorem deduce that there exists a neighbourhood U of (ϕ_0, ϵ_0) such $f_1(s(\phi, \epsilon), \phi, \epsilon) = 0$ for all $(\phi, \epsilon) \in U$ and $s(\phi_0, \epsilon_0) = s_0$. This yields the identities

$$\begin{aligned} \frac{\partial}{\partial s} f_1 s_\phi + \frac{\partial}{\partial \phi} f_1 &= 0, \\ \frac{\partial}{\partial s} f_1 s_\epsilon + \frac{\partial}{\partial \epsilon} f_1 &= 0. \end{aligned}$$

Consequently,

$$s_\phi(\phi_0, \epsilon_0) = 0 \quad \text{and} \quad s_\epsilon(\phi_0, \epsilon_0) = 0.$$

Putting

$$b(\phi, \epsilon) = f_2(s(\phi, \epsilon), \phi, \epsilon)$$

we obtain

$$b(\phi_0, \epsilon_0) = f_2(s_0, \phi_0, \epsilon_0) = \langle q - q, g_{s\phi}(s_0, \phi_0, \epsilon_0) \rangle = 0.$$

With this it is not hard to show

$$\begin{aligned} \nabla b &= (0, 0), \\ \text{Hess } b &= \begin{pmatrix} \frac{\partial^2}{\partial \phi^2} f_2 & \frac{\partial^2}{\partial \phi \partial \epsilon} f_2 \\ \frac{\partial^2}{\partial \phi \partial \epsilon} f_2 & \frac{\partial^2}{\partial \epsilon^2} f_2 \end{pmatrix}. \end{aligned}$$

Three different cases have to be discussed for a complete description of the zero set of F in U . Using $A = \text{Hess } b$ these are

det(A) > 0:

F has only an isolated solution in a neighbourhood of $(s_0, \phi_0, \epsilon_0)$. This case is not relevant in the study of boundary value problems that we discuss in this thesis.

det(A) < 0:

F has two different solution branches (a **bifurcation**). Details how these branches can be computed can be found in [AG03]. It is quite interesting to see that using a standard Predictor-Corrector-Method one would possibly not even notice that a bifurcation has occurred.

det(A) = 0:

This is indeed the toughest case. Again we must refer to [AG03] and the references therein.

7.5 Distance Spheres, Voronoi Edges And Bisectors

Let M be a 3-dimensional complete Riemannian manifold. We present a generalisation of the property of points to be in general position.

Definition 7.5.1

Let $p_1, \dots, p_4 \in M$ be four sites. The p_i are said to be in **general position** if there exists a unique distance sphere $S(c, r) = \{x \in M; d(x, c) = r\}$ with $p_i \in S(c, r)$ for all $i = 1, \dots, 4$.

The question if there may exist more than one such distance sphere is answered by the next example.

Example 7.5.1

Let $M_a = \{(x, y, z); z = a(x^2 + y^2)\}$ be a paraboloid and $p_1 = (1, \epsilon, a(1 + \epsilon^2))$, $p_2 = (0, 0, 0)$, $p_3 = (1, -\epsilon, a(1 + \epsilon^2))$ for a sufficiently small $\epsilon > 0$. We will show that the Voronoi diagram $V(S)$ of the sites $S = \{p_1, p_2, p_3\}$ for $a \gg 1$ consists of three vertices and four edges.

Proof: This can be seen from different reasons. The closure of the Voronoi region of the point p_2 is a compact set for sufficiently large a , since every point $p = (p_x, p_y, p_z) \in M_a$ with $p_z \geq a(1 + \epsilon^2)$ is closer to p_1 and p_3 respectively. To prove this we build the intersection of the plane $\{z = a(1 + \epsilon^2)\}$ with M_a . It is straightforward to see that this intersection is a circle containing both p_1 and p_3 . The radius of this circle remains constant, in case a increases. The Riemannian distance from p_1 to any of the points on this circle can be bounded by a number $K > 0$. Note that K can be chosen independently from a . The same is true for the point p_3 . The distance from p_2 to any of these points can be bounded from below by $a(1 + \epsilon^2)$, which tends to infinity, if a tends to infinity. Thus, the Voronoi region $VR(p_2, S)$ must be bounded.

Next we must show that the Voronoi diagram has two vertices. Therefore, consider the bisector $B(p_1, p_3)$ of the sites p_1 and p_3 . Simple arguments provide that

$$B(p_1, p_3) = \{(x, 0, ax^2); x \in \mathbb{R}\}.$$

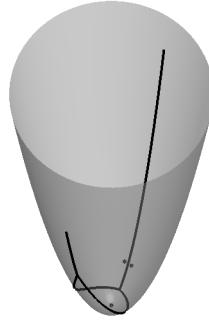


Figure 7.6: Voronoi diagram of three sites containing 2 vertices

Let $f(p) = d(p_2, p) - d(p_1, p)$, $p \in B(p_1, p_3)$. It can be proven that f has exactly two zeros. Every point $p = (p_x, p_y, p_z)$ with $p_y > 0$ is closer to p_1 than to p_2 and hence cannot be a vertex. Similar arguments can be applied for points $p_y < 0$. This completes the proof.

□

The detection of vertices is of major interest for computational Voronoi diagrams. The geometry of the corresponding distance spheres may look strange as one can see by figure 7.7, sketching a distance sphere for a given point $p \in M$ and a radius $r > 0$ in a length space (M, d_1)

Assume there exists a **normal neighbourhood** $U \subset M$ of all the sites p_1, \dots, p_n . A normal neighbourhood U of a point p is characterised by the fact, that the exponential function

$$\exp_p : \exp_p^{-1}(U) \subset T_p M \rightarrow U$$

is invertible. We will even more assume that this neighbourhood contains all important features of the unbounded Voronoi diagram $V(S)$. For the construction of the entire Voronoi diagram it will be important that every bounded Voronoi region is contained in a convex neighbourhood.

Definition 7.5.2

A **convex neighbourhood** U of a point p is an open set $U \subset M$ containing p such that for every $x, y \in U$ there exist an unique geodesic joining x and y in U .

Consider the length space (M, d) and the three sites p_1, p_2, p_3 . Since the edge

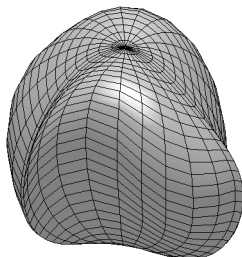


Figure 7.7: Example of a distance sphere

$$B(p_1, p_2, p_3) = B(p_1, p_2) \cap B(p_2, p_3)$$

contributes to the skeleton of the Voronoi diagram one major focus lies in the determination of these edges. We will briefly discuss how a local description of them can be obtained using the distance functions d_i of the sites p_i . Let

$$F(x, y, z) = \begin{pmatrix} d_1(x, y, z) - d_2(x, y, z) \\ d_1(x, y, z) - d_3(x, y, z) \end{pmatrix}.$$

Clearly, $F^{-1}(0, 0) = B(p_1, p_2, p_3)$, which means that the zero set of F coincides with the **triselector** $B(p_1, p_2, p_3)$. Under some regularity assumptions it is possible for a given point $(x_0, y_0, z_0) \in F^{-1}(0, 0)$ to parametrise a curve $\alpha : I \rightarrow M$ such that

- $F(\alpha(t)) = 0$ for all $t \in I$,
- $\alpha(0) = (x_0, y_0, z_0)$.

Remark 7.5.1

1. Typically, one will apply Predictor-Corrector-Methods to parametrise the solution curve α . These methods employ the gradients ∇d_i of the distance functions. If $\mathcal{O}_i(s, \phi_i, \psi_i)$ denotes the offset function of the site p_i , we have that

$$d_i(\mathcal{O}_i(s, \phi_i, \psi_i)) = s$$

and one simply deduces the identity

$$\nabla d_i = (1 \ 0 \ 0) \circ D\mathcal{O}_i^{-1}.$$

2. With the aforementioned method the computation of a bisector $B(p_i, p_j)$ can be achieved similar to the computation of bisectors of bordered surfaces. We will leave out the technical description and the derivation of the corresponding medial equations. Another interesting approach is described in [EH99] which employs the normal form of an implicit parametrisation. It involves the second fundamental form of the implicit surface.

Typically, a trisector $B(p_1, p_2, p_3)$ is not contained in the Voronoi diagram $V(S)$ to the full extent. If there exist two 4-prongs p, q with the property that $\alpha(t_p) = p$ and $\alpha(t_q) = q$, $t_p < t_q$, at least the segment $\alpha([t_p, t_q])$ is considered to be part of the skeleton of $V(S)$ in case

$$d(p_1, \alpha(t)) = d(p_2, \alpha(t)) = d(p_3, \alpha(t)) \leq d(p, \alpha(t))$$

for all $t \in [t_p, t_q]$ and $p \in S$. But how can we find the vertices p and q ? We will demonstrate this for a 4-prong

$$B(p_1, p_2, p_3, p_4) = B(p_1, p_2) \cap B(p_1, p_3) \cap B(p_1, p_4).$$

Define the function

$$F(x, y, z) = \begin{pmatrix} d_1(x, y, z) - d_2(x, y, z) \\ d_1(x, y, z) - d_3(x, y, z) \\ d_1(x, y, z) - d_4(x, y, z) \end{pmatrix}.$$

The convex homotopy of F is defined by

$$H(x, y, z, \lambda) = F(x, y, z) + (\lambda - 1)F(x_0, y_0, z_0).$$

It is not hard to see that $H(x_0, y_0, z_0, 0) = 0$. We seek a curve

$$\beta : J \rightarrow M \times [0, 1]$$

with the properties

- $H(\beta(t)) = 0$ for all $t \in J$,
- $\beta(0) = (x_0, y_0, z_0)$.

For β' the identity

$$DH \circ \beta' = 0$$

must hold and the computation of DH again involves the gradient of the distance functions and the corresponding offset functions. Application of standard Predictor-Corrector-Methods finally yields a point t^* with $H(\beta(t^*)) = F(p) = 0$ under some regularity assumptions.

7.6 Randomised Incremental Construction Of Voronoi Diagrams

Of course problems like the computation of the Euclidean Voronoi diagram are well understood and there exist some paradigms often used in computer science to treat them. These are mainly

- Divide and Conquer
- Incremental Construction
- Sweep

The geometric transformation described in this chapter does not really fit into this list, since it is not really a method that can be used for a larger class of problems. In fact, to the authors best knowledge, no attempts have been made to employ the sweep method for the computation of geodesic Voronoi diagrams.

The aforementioned sweep algorithm is not easy to describe. Consider a discrete static geometrical problem in \mathbb{R}^d . We call a problem static if the prerequisites for the computations will not change during the sweep. The main idea is to transform the static d -dimensional problem into a dynamic $(d - 1)$ -problem.

As in the Euclidean case the geodesic Voronoi diagram typically consists of **vertices**, **edges** and **faces**.

Definition 7.6.1

A face f is a maximally connected subset of $V(S)$ with the property that every $x \in f$ lies on exactly one bisector $B(p_i, p_j)$. A point v is called vertex if it lies on the boundary of k Voronoi regions for $k \geq 4$. An edge is a maximally connected subset of $V(S)$ enclosing all points that lie on the boundary of exactly three Voronoi regions.

In fact, if the Voronoi vertices are known, the entire topology of the Voronoi diagram is determined, but it is highly recommended not to precompute the Voronoi vertices by verifying the circumsphere condition for any four points from S , since this has time complexity $O(n^5)$. There are $\binom{n}{4}$ possibilities for a circumsphere since every combination of four points may lead to such a sphere. For a sphere $S(c, r)$ it has to be checked if no other element of the remaining $n - 4$ sites lies inside the distance sphere. The aforementioned brute force method has been implemented by Hannes Thielhelm in his diploma thesis [HT07] to prove the concepts of the last section. However, we will sketch the RICS method to show that the time complexity of the construction of the Voronoi diagram can be reduced in a wide range of cases.

Following the recommendations from [Le97] the complexity can be reduced in case $V(S)$ is a simple, abstract Voronoi diagram with specialised prerequisites. Therefore, we summarise the results from this paper. It will be shown that this incremental construction technique then has time and space complexity $O(n^2)$. It is postulated that

Voronoi regions have to be homeomorphic to a 3-ball or empty. Let $p, q, r, s, t \in M$ be five sites. Then in addition it is required that the set $B(p, q) \cap B(q, r)$ is a transverse intersection of two bisectors. This set is assumed to have only one single component. Moreover, we assume that the set $B(p, q) \cap B(q, r) \cap B(r, s)$ must be a singleton and $B(p, q) \cap B(q, r) \cap B(r, s) \cap B(s, t)$ must be empty. Finally, we will postulate that every circumsphere exactly contains 4 sites, which means that every vertex of the Voronoi diagram has outdegree 4.

One last restriction must be made to ensure that the resulting Voronoi diagram is simple. Inside a small neighbourhood of a vertex or a point of an edge the restriction of the Voronoi diagram to this neighbourhood must look topologically like a corresponding configuration in the Euclidean space (cf. figure 7.8).

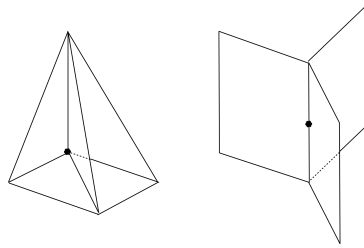


Figure 7.8: Local behaviour of the Voronoi Diagram

All these prerequisites are necessary for the construction process of the simple Voronoi diagrams. They are called simple because they must be topologically equivalent to Euclidean Voronoi diagrams. Although we did not present an axiomatic introduction like it was done in [Le97] the last notes shall be enough for the following considerations.

Definition 7.6.2

For a subset $R \subset S$ we define the respective sets $\text{Edge}(R)$ and $\text{Vert}(R)$, i.e. the set of edges and vertices of $V(R)$.

Definition 7.6.3

The **skeleton** of S is the set

$$\text{Skel}(S) := \text{Edge}(S) \cup \text{Vert}(S).$$

7.6.1 The Algorithm

Let M be a complete Riemannian manifold. From topological point of view the Voronoi diagram has its most important features (vertices) inside a sphere \mathcal{S} that contains at least the set of sites. It is required that this sphere intersects each $B(p_i, p_j)$ transversely. Moreover, the union of all bisectors builds up a cell complex $C(S)$ for which we have the following property. Let $B(p_i, p_j)$ be a bisector. Then the restriction of $C(S)$ to $B(p_i, p_j)$ outside the domain of the sphere \mathcal{S} only consists of halflines and halfplanes.

We add ∞ to the set of sites and define the sets

$$\begin{aligned} B(p_i, \infty) &= B(\infty, p_i) = \mathcal{S}, \\ D(p_i, \infty) &= \text{inner}(\mathcal{S}), \\ D(\infty, p_i) &= \text{outer}(\mathcal{S}). \end{aligned}$$

If \mathcal{S} borders a solid, it is straightforward to define the inner and the outer parts of \mathcal{S} .

The incremental construction process is based on some topological invariants. The skeleton of the Voronoi diagram carries the main topological features of $V(S)$. The first step therefore is to precompute the skeleton and determine the faces afterwards.

As in the Euclidean case we have the following important result for simple Voronoi diagrams

Lemma 7.6.1

The expected size of the structural complexity of the skeleton is at most $O(n)$, where n is the number of sites.

The proof of the lemma can be found in [DRA91].

The incremental construction involves an elementary operation that is assumed to have time complexity $O(1)$. Given five points $R = \{p, q, r, s, t\} \subset S$ assume $V(R)$ contains an edge e that starts at a vertex $B(p, q, r, s)$ and ends at a vertex $B(p, q, r, t)$. In addition a site $u \in S$ is introduced. Depending on whether u is in **conflict** with the edge e , we have several possibilities for the structure of

$$e \cap \overline{VR(u, R \cup \{u\})}.$$

1. The intersection is empty, which means that there is no conflict.
2. The intersection is not empty, simply connected and contains
 - a) the entire edge.
 - b) the part of e that starts at $B(p, q, r, s)$.
 - c) the part of e that starts at $B(p, q, r, t)$.

Remark 7.6.1

e is meant to be in conflict with u , when the circumsphere of one of the endpoints of e (a vertex) contains the new site $u \in S \setminus R$.

The algorithm starts with the sites ∞, p_1, p_2, p_3 . The remaining sites are introduced step by step in a non deterministic order. This can be seen as an application of random sampling to online algorithms in computational geometry (cf. [BDS92]).

Definition 7.6.4

Let $e \in \text{Edge}(\mathbb{R})$. If e joins the points $B(p, q, r, s)$ and $B(q, r, s, t)$, then the **header** $D(e)$ of e is defined by:

$$D(e) = \{p, q, r, s, t\}.$$

Every edge e of a Voronoi diagram can be identified by its header $D(e)$.

Definition 7.6.5

Let e be an edge with header $D(e) = \{p, q, r, s, t\}$ and $u \in S \setminus \{p, q, r, s, t\}$. We say that u **intersects** with $D(e)$, if

$$e \cap VR(u, \{p, q, r, s, t, u\}) \neq \emptyset.$$

Several data structures are maintained during the construction process.

- The topological structure of the Voronoi diagram is entirely described by the skeleton, that can be represented by a **Levi graph** or **incidence graph** (bi-partite graph). A bi-partite graph is a graph that consists of vertices V and edges E such that there exist two disjoint subsets $V_1, V_2 \subset V$ with the following property. Every edge $e \in E$ only joins vertices of different subsets V_i . We call the vertices from V_1 black vertices and the vertices from V_2 white vertices. The black vertices of the Levi graph represent all elements of $\text{Vert}(R)$ and the white vertices symbolise the elements of $\text{Edge}(R)$. There is an edge between a black and a white vertex if and only if there is a corresponding incidence between a Voronoi vertex and a Voronoi edge.
- The history graph $\mathcal{H}(R)$ contains all edges that appeared during the construction process. It is a **directed acyclic graph** (DAG) with a source Q that does not contain any information about the edges.

There are three invariant properties of $\mathcal{H}(R)$:

- The leaves of $\mathcal{H}(R)$ correspond to the actual Voronoi edges of $V(R)$. They do not have outgoing edges, whereas every vertex of $\mathcal{H}(R)$ can not have more than four outgoing edges.
- The header of an edge $e \in \text{Edge}(R)$ is attached to all vertices. It contains the information of all Voronoi vertices that are involved in the genesis of e , for example the points p, q, r, s, t from definition 7.6.4.
- Every time a new site u is introduced, there exist leaves that intersect with u . Let v be an intersecting edge. It must be ensured that there exist a path from Q to v that is only incident to vertices that intersect with u .

For a new site u all intersecting edges $E(u)$ need to be detected. This can be achieved quickly using the history graph $\mathcal{H}(R)$.

Lemma 7.6.2

The time complexity of finding $E(u)$ lies in $O(|A|)$, where A denotes the set of intersecting vertices $v \in \mathcal{H}(R)$.

The proof of this theorem uses mainly the invariance properties.

The update mechanism for the simple Voronoi diagram and the history graph are based on some relevant topological properties and some easy combinatorial results. Note

that some Voronoi vertices are deleted in the next step whereas some new vertices will come into play. In particular, if a vertex v lies outside the new Voronoi region $U = VR(u, R \cup \{u\})$ it stays in the vertex list.

If e is an intersecting edge, i.e. $e \in E(u)$, then new vertices v have to be introduced which correspond to the intersection points. We will denote this by $v \in V_{\text{new}}$. Let $x \in \text{Vert}(R)$ be an old vertex and e be an outgoing Voronoi edge that has to be shortened. If the piece of the intersected edge that becomes part of the new edge list $\text{Edge}(R \cup \{u\})$ is incident to x then x stays in the list, if it is true for every such outgoing edge. We will denote this by $x \in V_{\text{unchanged}}$. It can be shown that only these type of points contribute to the new vertex list $\text{Vertex}(V \cup \{u\})$.

The number of conflicting edges determines the time complexity of the construction of the set $V(R \cup \{u\})$. The major effort lies in the identification of the edges of the new faces f resulting from the introduction of the new site u .

We will try to make this more lucid by an two-dimensional example (cf. figure 7.9). The Voronoi sites are coloured in black and blue, where the blue site is introduced in the current step. The picture shows the final Voronoi diagram. The blue edges correspond to the edges from the Voronoi diagram that only involves the black sites. Some of the old edges from the previous step were shortened (yellow edges) by the conflicting blue site. The new edges of the final Voronoi diagram are coloured in white. Consider for example the edge e . We will describe how the edge e can be constructed. We start from the vertex v_1 along the yellow edge that is an edge of the Voronoi region with respect to the site p . If we follow the subsequent edges that correspond to this region we finally end in the vertex v_2 . Due to the above construction scheme the vertices v_1 and v_2 have to be joined by a bisector segment $e \subset B(\text{blue site}, p)$.

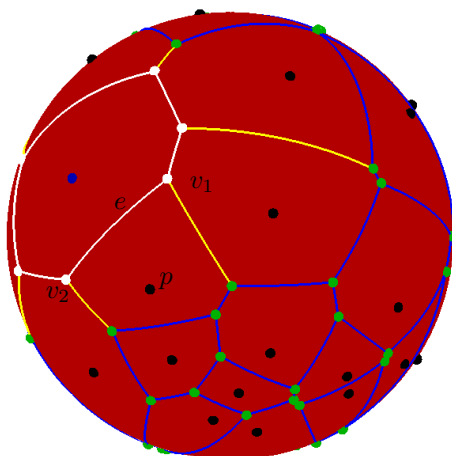


Figure 7.9: Construction of the new Voronoi region

It can be shown that updating the history graph has the same time complexity as the prescribed construction of $V(R \cup \{u\})$. The subsequent steps are necessary for a correct update.

- The edge $e \in \text{Edge}(R \cup \{u\})$ is the son of an edge $e' \in \text{Edge}(R)$, if e is shortened and $e \subset e'$.
- For every new edge e add the edges (e', e) to the history graph for all edges e' that were found during the construction of the new segment (in the example the unshortened yellow edges and the blue edges of the Voronoi region $V(p, R)$).

One can show that no invariance property is harmed by the former construction process. [BDS92] provides the expected values for time and space in relation to the total expenditure. If $f_T(n)$ denotes the time complexity and $f_S(n)$ the space complexity, then $f_T, f_S \in O(n^2)$.

Finally, some examples will be given to illustrate the foregoing results.

7.7 Examples

Example 7.7.1

The first example is rather simple. More sites automatically lead to an arrangements of faces and edges that would overstrain the reader. We consider a manifold that is parametrised by the map

$$f(x, y, z) = \begin{pmatrix} x \\ y \\ z \\ \frac{1}{2}(x^2 - yz) \end{pmatrix}. \quad (7.7.1)$$

The coordinates of the sites with respect to the map f are given by $(0, 0, 0)$, $(0.8, 0, 0)$, $(0.9, 1.1, 0)$, $(1, 1.5, 1)$ and $(0, 1.14, 0.98)$. Figure 7.10 sketches the Voronoi diagram of these site with the metric induced by the parametrisation f .

Example 7.7.2

Up to now we have mainly dealt with geodesic Voronoi diagrams. As an extension of these concepts, that we have evolved so far, we will introduce now the concepts of **geodesic Delaunay triangulations**. Consider the 2-dimensionale hypersurface $M \subset \mathbb{R}^3$ parametrised by the mapping

$$f(x, y) = \begin{pmatrix} x \\ y \\ \sin(x) - \cos\left(\frac{1}{2}y\right) \end{pmatrix}.$$

The Delaunay triangulation $DT(S)$ of a set $S = \{p_1, \dots, p_n\} \subset M$ is **dual** to the Voronoi diagram $V(S)$. It consists of geodesic triangles. The edges of the triangle correspond to minimal joins between two distinct adjacent sites p_i and p_j respectively.

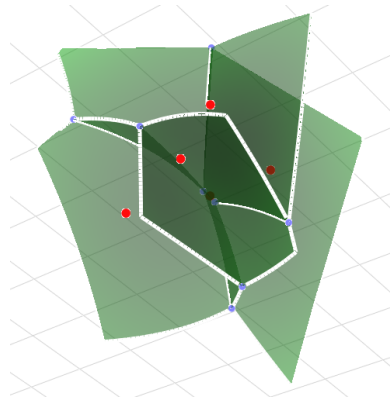


Figure 7.10: Voronoi Diagram of five sites

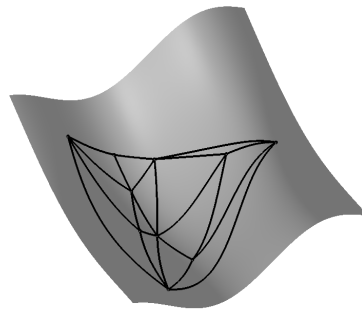


Figure 7.11: Geodesic Delaunay triangulation of 10 sites

Since these joins do not have to be unique, the triangulation $DT(S)$ does not seem to be unique as well. The edges of the triangles have to be chosen such that the corresponding geometric graph does not have self intersections. The uniqueness can however not be ensured. This problem can possibly be solved, when only those triangulations are taken into account where the corresponding sequence of inner triangle angles is maximal with respect to the **lexicographic order**.

Consider for example the points p_i with the coordinates given in table 7.1

| i | 1 | 2 | 3 | 4 | 5 | 6 | 7 | 8 | 9 | 10 |
|-------|-------|-------|-------|-------|-------|-------|-------|------|-------|-------|
| x_i | -2.65 | -0.88 | 1.88 | -2.94 | -2.17 | -1.78 | -1.81 | 0.62 | -1.37 | -1.81 |
| y_i | -2.91 | 1.48 | -0.33 | 2.59 | -0.20 | -0.49 | 2.08 | 0.15 | -1.78 | 1.03 |

Table 7.1: Coordinates of the sites p_i

Figure 7.11 sketches the Delaunay triangulation of the ten sites p_1, \dots, p_{10} .

This Delaunay triangulation of the set of sites S was created in the following way:

- First construct the Delaunay triangulation of the points (x_i, y_i) in the Euclidean plane.
- Join two points $p_i, p_j \in M$ by the shortest geodesic in case their coordinate points are adjacent Voronoi sites in the Euclidean plane.

If the geodesic circumsphere condition is not harmed one can assume that a true Delaunay triangulation has been found.

8 Outlook

This work is intended to serve as a comprehensive overview of some new results in the area of the geodesic medial axis transform and Voronoi diagram computations in 3-Space using medial equations. It has been shown throughout this thesis that some of the numerical problems that one is confronted with during the integration of the medial equations could be solved using the implicit function theorem or Predictor Corrector Methods, assuming that some regularity requirements can be ensured, which is true in most cases.

However, the integration of the medial equations only contributes to the symmetry set, which means that the considered distances are only locally minimal. For the computation of the medial sets it is important to detect situations, where the transition from the global medial axis to the symmetry set occurs. This can for example be achieved by the computation of 3-prongs.

In many places of this work we have assumed that every Voronoi region is contained in a convex neighbourhood. This constraint can be weakened. The exponential map that is defined for a point p might be ambivalent somewhere but without further consequences in case the corresponding Voronoi region is contained in the injectivity region of the exponential map. Nevertheless, the injectivity radius of a point may be of some importance in special situations.

The question if a point q is contained in the cut locus of a point p is indeed a challenging problem, which may be solved, employing the mapping degree of differentiable functions. The mapping degree was explained in the introductory part, yet no comment on the implementation of it was given. Let for example $\Omega \subset \mathbb{R}^n$ be an open bounded set and $f : \Omega \rightarrow \mathbb{R}^n$ a C^1 map. If 0 is a regular value of f relative to the bounded set Ω it can be shown that the mapping degree $d(f, \Omega, 0)$ can be computed in time $O(n)$ using interval arithmetic. This is enough for many applications. The proposed method is a modified version of Aberth's algorithm (cf. [OA94]) that uses interval arithmetic, too. In comparison to Aberth's method the time complexity has been reduced by two further techniques: coordinate transform (preconditioning) and Krawczyk's method (pruning). This method is described in [SM06]. Furthermore, it is possible to determine all zeros of the function f under the above regularity assumptions.

The method suggested for meshing the faces of the Voronoi diagram does not appear to be sophisticated at first glance; practically, we had some very good results. Nevertheless, some weaknesses of our method must be mentioned.

- (i) The usage of spherical coordinates for the construction of geodesic polar coordinates leads to phenomena that arise similarly to the triangulation of spheres. The size of the triangles decreases rapidly in the neighbourhood of the poles.
- (ii) The introduction of an orthonormal basis of T_pM at a point $p \in M$ did not improve this too much. The major reason why we introduced an orthonormal basis was the objective to avoid nasty normalizations that involved differentiation of the square root function.

We will propose some ideas of how a nice mesh of the Voronoi faces can be obtained, using the insights from [TR99]. Assume we have been given a face f and the piecewise differentiable edge curve $\alpha : I \rightarrow \mathbb{R}^3$.

A face f can locally be described by the distance functions d_p and d_q of sites $p, q \in S$ by means of

$$f \subset B(p, q) = \{(x, y, z) \in \mathbb{R}^3; d_p(x, y, z) - d_q(x, y, z) = 0\}.$$

In case f is contained in a small neighbourhood U of the sites p and q it turns out that the distance functions d_p and d_q can be described by the offset functions \mathcal{O}_p and \mathcal{O}_q respectively due to

$$d_p(\mathcal{O}_p(s, \phi, \psi)) = s.$$

If the Jacobi matrix of \mathcal{O} has been given it is straight forward to compute the gradient of d in terms of the Jacobi matrix $D\mathcal{O}$:

$$\nabla d \circ D\mathcal{O} = \begin{pmatrix} 1 \\ 0 \\ 0 \end{pmatrix}^T.$$

The above system is linear and yields a unique solution if $D\mathcal{O}$ is regular in the neighbourhood U of p . In a similar fashion it is possible to find the Hessian matrix of d and also higher order derivatives.

Figure 8.1 sketches the medial axis of the face

$$f = \{(t_1, t_2, \sin(t_1)); t_1 \in [0, 2\pi], t_2 \in [0, 2]\}.$$

Even this simple example is hard enough to solve, since an analytic expression for the medial arcs is not obvious. The medial segment that contains the origin can be expressed as

$$\begin{aligned} s'(t_2) &= 1, \\ t_1'(t_2) &= (G^{-1})'(s(t_2)), \end{aligned}$$

where

$$G(x) = \int_0^x \sqrt{1 + \cos(t)^2} dt.$$

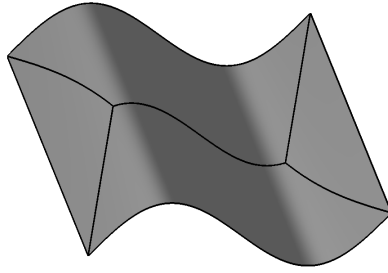


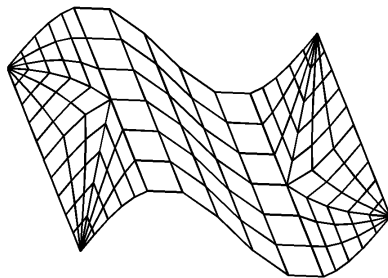
Figure 8.1: Medial Axis of a Face

In chapter 3 we have seen that the implicit geodesic differentiable equations can be used in case we deal with implicit parametrised hypersurfaces. The same is true for the Jacobi equations and variations of it although we have not shown this explicitly.

The next step is evident. The medial axis of the face f consists of segments $\alpha_i : [0, 1] \rightarrow f$, $i = 1, \dots, N$. Let $D, K_1, \dots, K_N \in \mathbb{N}$ be constant integers. We consider the segment α_i . Chosse sample points $0 = t_0 < \dots < t_{K_i} = 1$. Every point $p = \alpha_i(t_k)$ has at least two nearest neighbours on the boundary of the face f except for the case $p \in \partial f$. Let q be one of these neighbours and γ^k the shortest arc length parametrised geodesic that joins p and q . If $d(p, q) = d$ choose real numbers s_i such that

$$s_i = \frac{i-1}{D-1}d$$

for $i = 1, \dots, D$. The points $p_{ik} = \gamma^k(s_i)$ can be seen as points of a quadrilateral mesh that can be singular especially in the vertices of the face f . This mesh is far more complicated to construct but yields some nice advantages for example in industrial applications. Figure 8.2 sketches a coarse mesh of the sinoidal face f from above.

Figure 8.2: Structured Mesh of the Face f

List of Tables

| | | |
|-----|--|-----|
| 7.1 | Coordinates of the sites p_i | 106 |
|-----|--|-----|

List of Figures

| | | |
|-----|--|-----|
| 1.1 | Power Crust Algorithm | 4 |
| 2.1 | Homotopic deformation of a circle | 10 |
| 2.2 | (i) c_1 is tangential to c_2 and (ii) c_1 is not tangential to c_2 | 10 |
| 2.3 | Plot of two solution functions defined by example 2.3.1 | 19 |
| 3.1 | Surface of revolution | 28 |
| 3.2 | Jacobi Fields | 32 |
| 4.1 | Euclidean offset of an arbitrary closed curve | 36 |
| 4.2 | Geodesic offset of a point | 38 |
| 4.3 | Geodesic offset of a curve | 39 |
| 4.4 | Tubular hypersurface | 41 |
| 4.5 | Parabola and its cut locus | 43 |
| 5.1 | Medial axis inverse transform of a surface | 50 |
| 5.2 | Medial axis of an object | 51 |
| 5.3 | Geodesic curvature of the envelope | 57 |
| 5.4 | The sets A_i | 58 |
| 5.5 | Medial Axis Inverse Transform of a paraboloid | 62 |
| 6.1 | Medial axis of a simple domain | 65 |
| 6.2 | The symmetry set and the medial axis of a rectangle | 65 |
| 6.3 | Solution curve of an implicit equation of type $F(x, y) = 0$ | 70 |
| 6.4 | Plot of a perturbed surface $z = \sin(x) \sin(y)$ | 72 |
| 6.5 | Plot of a perturbation function | 73 |
| 6.6 | Plot of the functions ψ , $p_{r,R}$ and $\phi_{r,R}$ | 74 |
| 6.7 | Reflection, expansion and contraction for a tetrahedron | 76 |
| 6.8 | Medial Axis Transform of two reference surfaces | 76 |
| 7.1 | Voronoi Cells | 80 |
| 7.2 | Bisector of two points p and q | 81 |
| 7.3 | The Curve-Tracking-Method | 88 |
| 7.4 | Deformation of a sphere ($r(\phi, \psi) = \sin(2\phi) \cos(\psi) + 1.2$) | 92 |
| 7.5 | Geodesic join on a deformed sphere | 93 |
| 7.6 | Voronoi diagram of three sites containing 2 vertices | 97 |
| 7.7 | Example of a distance sphere | 98 |
| 7.8 | Local behaviour of the Voronoi Diagram | 101 |

| | | |
|------|---|-----|
| 7.9 | Construction of the new Voronoi region | 104 |
| 7.10 | Voronoi Diagram of five sites | 106 |
| 7.11 | Geodesic Delaunay triangulation of 10 sites | 106 |
| 8.1 | Medial Axis of a Face | 110 |
| 8.2 | Structured Mesh of the Face f | 110 |

Bibliography

- [Wol92] Wolter F.-E., *Cut Locus & Medial Axis in Global Shape Interrogation & Representation*, MIT Design Laboratory Memorandum 92-2 and MIT Sea Grant Report, 199
- [Boe04] Guido Böttcher, *Medial Axis and Haptics*, Diploma Thesis, Leibniz Universität Hannover, October 2004
- [GR04] Jacob E. Goodman, Joseph O'Rourke, *Handbook of Discrete and Computational Geometry*, Chapman & Hall/CRC, 2004
- [Lee82] Lee, D.T., *Medial Axis Transformation of a Planar Shape*, IEEE Trans. Patt. Anal. Machine Intell., 4 pp. 363-369, 1982
- [LL92] Leymarie, F. and Levine, M.D., *Simulationg the Grassfire Transform using an active Contour Model*, IEEE Trans. Patt. Anal. Machine Intell., 14, 1, pp. 56-75, 1992
- [Set99] Sethian, J.A., *Level Set Methods and Fast Marching Methods, Evolving Interfaces in Computational Geometry, Fluid Mechanics, Computer Vision, and Material Science*, Cambridge University Press, second ed., 1999
- [RWS97] T. Rausch, F.-E. Wolter, O. Sniehotta, *Computation of Medial Curves on Surfaces*. In T. Goodman and R. Martin, editors, *The Mathematics of Surfaces VII*, pages 43-86. Information Geometers 1997.
- [Alt02] Walter Alt, *Nichtlineare Optimierung, Eine Einführung in Theorie, Verfahren und Anwendung*, vieweg, 2002
- [Mil99] Ronald E. Miller, *Optimization, Foundations and Applications*, Wiley VCH, 1999
- [Vor07] Geogy Voronoi *Nouvelles applications des paramtres continus la thorie des formes quadratiques*, Journal für die Reine und Angewandte Mathematik, 133:97-178, 1907
- [OBS00] Okabe A., Boots B., Sugihara K., *Spatial Tessellations: Concepts and Applications of Voronoi Diagrams*, 2nd ed. New York: Wiley, 2000.
- [Bee75] John K. Beem, *Pseudo-Riemannian Manifolds with Totally Geodesic Bisectors*, Proceedings of the American Mathematical Society, Volume 49, Number 1, May 1975
- [Wol85] F.-E. Wolter, *Cut Loci in Bordered and Unbordered Riemannian Manifolds*, Dissertation, Berlin 1985

-
- [Ede87] H. Edelsbrunner, *Algorithms in Combinatorial Geometry*, volume 10 of *EATCS Monographs on Theoretical Computer Science*. Springer, Heidelberg, 1987
- [Kle97] R. Klein, *Algorithmische Geometrie*, Eddison Wesley Longman Verlag GmbH, 1. Auflage, 1997
- [doC98] Manfredo Perdiago do Carmo, *Differentialgeometrie von Kurven und Flächen*, Vieweg Verlagsgesellschaft, 3. Auflage, 1998
- [Le97] Ngoc-Minh Lê, *Randomized incremental construction of simple abstract Voronoi diagrams in 3-space*, *Computational Geometry* 8 (1997), 279-298
- [Eul52] L. Euler, *Elementa doctrinae solidorum – Demonstratio nonnullarum insignium proprietatum, quibus solida hedris planis inclusa sunt praedita*, *Novi comment acad. sc. imp. Petropol.*, 4, 1752-3, 109-140-160.
- [Poi95] H. Poincaré, *Analysis Situs*, *Jour. cole Polytechnique* 2, 1 (1895).
- [BDS92] Jean-Daniel Boissonat, Olivier Devillers, Rene Schott, Monique Teillaud, Mariette Yvinec, *Applications of Random Sampling to On-Line Algorithms in Computational Geometry*, *Discrete and Computational Geometry* 8, 51-71, 1992
- [Gra04] Alfred Gray, *Tubes*, *Progress in Mathematics*, sec. ed. Birkhäuser, 2004
- [PM02] Nicholas M. Patrikalakis, Takashi Maekawa *Shape Interrogation for Computer Aided Design and Manufacturing*, Springer, Berlin, 1. Edition, 2002
- [HT07] Hannes Thielhelm, *Geodätische Voronoi Diagramme*, Diploma thesis, Leibniz Universität Hannover, 2007
- [TR99] Thomas Rausch *Analysis and Computation of the Geodesic Medial Axis of Bordered Surface Patches*, Doctoral Thesis, Leibniz Universität Hannover, 1999.
- [OA94] Oliver Aberth, *Computation of Topological Degree using Interval Arithmetic, and Applications*, *Mathematics of Computations*, Vol. 62, No. 205, 1994
- [JM65] J. Milnor, *Topology from the differential viewpoint*, University Press of Virginia, Charlottesville 1965
- [BN83] B. O'Neill, *Semi-Riemannian geometry*, Academic Press, New York 1983
- [TS96] T. Sakai, *Riemannian geometry*, AMS, Providence 1996
- [GK04] P. Giblin, B.B. Kimia, *A Formal Classification of 3D Medial Axis Points and Their Local Geometry*, *IEEE Transactions on Pattern Analysis and Machine Intelligence*, Volume 26 , Issue 2,2004
- [BF98] Fornberg B. , *Calculation of Weights in Finite Difference Formulas*, *SIAM Rev.* 40, 685-691, 1998.
- [dC92] Do Carmo, Manfredo, *Riemannian Geometry*, Boston:Birkhäuser, 1992
- [KN63] S. Kobayashi and K. Nomizu, *Foundations of Differential Geometry. I* , New York 1963
- [KWR97] R. Kunze, F.-E. Wolter, T. Rausch, *Geodesic Voronoi Diagrams on Parametric Surfaces*, *CGI '97, IEEE, Computer Society Press Conference Proceedings*, pp. 230-237, June 1997.

- [FEW79] F.-E. Wolter, *Distance Function and Cut Loci on a Complete Riemannian Manifold*, ARCH MATH 32 (1), pp. 92-96, 1979.
- [CD07] Cem Doğan, *Mediale-Achsen-Rücktransformation in Riemannschen Mannigfaltigkeiten* Leibniz Universität Hannover, May 2007
- [DRA91] R. A. Dwyer, *Higher dimensional Voronoi diagrams in linear expected time*, Discrete Comp. Geom., 6:343-367, 1991
- [doC92] Manfredo Perdiago do Carmo, *Riemannian Geometry*. Mathematics: Theory and Applications, Birkhäuser Verlag, Boston, 1992
- [EH99] Erich Hartmann, *Numerical parametrisation of curves and surfaces*, Computer Aided Geometric Design 17 (2000) 251-266
- [BL73] W. Blaschke, K. Leichtweiss, *Elementare Differentialgeometrie*, Springer Verlag, Berlin, 1973
- [SM06] Sunao Murashige, *A Practical Method of Numerical Calculation of the Mapping Degree*, IEICE Transactions on Fundamentals of Electronics, Communications and Computer Sciences 2006 E89-A(6):1813-1819
- [AG03] Eugene L. Allgower, Kurt Georg, *Introduction to Numerical Continuation methods*, SIAM Classics in Applied Mathematics 45, 2003
- [RF94] Rida T. Farouki, John K. *The bisector of a point and a plane parametric curve*, Computer Aided Geometric Design, Volume 11, Issue 2, 1994
- [HH24] Hopf H., *Eine Verallgemeinerung der Poincaréschen Formel*, Nachrichten von der Gesellschaft der Wissenschaften zu Göttingen, Zeitschriftenband 1928, Zeitschriftenheft 2, 1928

Index

- A_k -singularity, 68
- C^∞ -atlas, 24
- D_k -singularity, 68

- Predictor-Corrector-Method, 21
- strongly convex, 80

- barycenter, 75
- bifurcation, 96
- bifurcation point, 21
- bisector, 78
- bitangent, 64

- central difference quotient, 12
- Christoffel symbol, 25
- circumsphere condition, 77
- codimension, 25
- compatible, 35
- conflict, 102
- conjugate point, 42
- convex neighbourhood, 97
- coordinate chart, 23
- covariant derivative, 25
- cut locus, 43

- deformation retract, 51
- differentiable manifold, 24
- differentiable structure, 24
- directed acyclic graph, 103
- downhill-simplex method, 74
- dual, 105

- envelope, 53
- equivalent, 82
- Euler-Newton method, 20
- exponential map, 29

- face, 100

- Fermi Coordinates, 33
- Finite Difference Method, 8
- Finite Element Method, 8
- Finite Volume Methods, 8
- first fundamental form, 64
- first fundamental tensor, 24
- focal point, 42
- focal radius, 48

- general position, 96
- generalized distance function, 47
- geodesic, 28
- geodesic Delaunay triangulation, 105

- header, 102
- homotopy, 20, 51
- hypersurface, 25
- hypersurface of revolution, 26

- implicit function theorem, 17
- implicit geodesic DE, 30
- incidence graph, 103
- induced tangent vector, 20
- intersection, 103

- Jacobi fields, 31

- length space, 63
- Levi graph, 103
- Levi-Civita connection, 25
- lexicographic order, 106

- maximal, 50
- medial axis, 50
- medial axis inverse transformation, 51
- medial axis transformation, 51
- medial equation, 44, 65
- metric complete, 28

- metric tensor, 64
- Moore Penrose inverse, 20
- n-prong, 64
- natural system function, 9
- Nelder-Mead method, 74
- Newton map, 20
- Newton point, 20
- normal coordinates, 33
- normal space, 30
- offset, 36
- parametrisation, 25
- PL Continuation Methods, 49
- polar radius, 3
- pole, 3
- power crust, 3
- power diagram, 4
- progenitor, 37
- reconstruction formula, 55
- rectifiable, 63
- regular, 40, 91
- regular grid, 49
- regular value, 29
- Riemannian curvature tensor, 31
- Riemannian distance, 50
- Riemannian manifold, 24
- Riemannian metric, 24
- second covariant derivative, 31
- simple bifurcation point, 22
- skeleton, 101
- strongly star shaped, 80
- superlinear convergence, 20
- symmetry point, 43
- symmetry points, 44
- symmetry set, 43
- tensor product, 15
- topological manifold, 23
- torsion free, 25
- trisector, 98
- tubular hypersurface, 33
- variation, 29
- Voronoi diagram, 79
- Voronoi edge, 100
- Voronoi region, 79
- Voronoi vertex, 100
- weakly convex, 80
- weakly star shaped, 80
- Weingarten map, 45